STOCKHOLM UNIVERSITY

DEPARTMENT OF PHYSICS

EMITTANCE PRESERVATION FOR THE LARGE HADRON COLLIDER
– correction of static and dynamic blow-up sources between the PS Booster and the CPS Ring

ANDREAS JANSSON

USIP Report 99-06 December 1999

Abstract

To achieve its design luminosity, the Large Hadron Collider, currently under construction at CERN, will demand optimum emittance preservation throughout the injector chain. One expected major source of transverse emittance blow-up is mismatch of the beam optical parameters at the interface between two circular accelerators. This report presents the methods that will be used during LHC operation to minimise the mismatch between the PS Booster and the CPS ring. It is shown that in principle the blow-up due to mismatch can be reduced to the level of the measurement error. A general study of the Booster-CPS transfer line optics is also presented.

This Thesis is Based on the Following Papers

These papers are included in the back of this thesis.

1. **Mismatch Between the PSB and the CPS due to the Present Vertical Recombination Scheme.** *Proceedings of 1997 International Workshop on High Brightness Beams in Hadron Colliders*, Montreux, Switzerland. Published in *Particle Accelerators*, 1997, Vol. 58, pp 201-207.

2. **Emittance Preservation in the PS Complex.** *Proceedings of 1997 International Particle Accelerator Conference*, Vancouver, Canada.

3. **Study of Emittance Blow-up Sources Between the PS Booster and the 26 GeV PS.** *Proceedings of the 1998 European Particle Accelerator Conference*, Stockholm, Sweden.

4. **Simultaneous Matching of Dispersion and Twiss Parameters in a Transfer Line.** *Proceedings of the 1998 Workshop on Automated Beam Steering*, Geneva, Switzerland. Published in *CERN Yellow Report 99-07.*

5. **A Comparative Study of Profile and Scraping Methods for Emittance Measurements in the PS Booster.** Submitted to *Particle Accelerators.*

Other Papers by the Author

These papers (and many of the other papers quoted herein) can be retrieved in electronic form from either the CERN Preprint Server at URL **http://weblib.cern.ch** or the Joint Accelerator Conference Website at URL **http://www.cern.ch/accelconf**.

1. **Generic Automated Beam Steering and Shaping Programs with an Object Oriented Approach.** *Proceedings of the 1997 International Conference on Accelerator and Large Experimental Physics Control Systems*, Beijing, China.

2. **A Magnetic Quadrupole Pick-up for the CERN PS.** *Proceedings of the 1999 International Particle Accelerator Conference*, New York, USA.

3. **Tomographic Reconstruction of Transverse Phase Space from Turn-by-Turn Profile Data.** *Proceedings of the 1999 International Particle Accelerator Conference*, New York, USA.

Contents

- Phase space mismatch and miss-steering at beam transfer between machines, followed by filamentation [9]. In this process, the local phase space density is conserved according to Liouville, but for all practical purposes the emittance has increased since the filamentation can not be inverted.

All effects, except for synchrotron radiation [10], leads to an increase in emittance. But since the energy dissipated due to synchrotron radiation is almost negligible[3] for all other particles than electrons, it is safe to state the emittance can only be constant or grow in proton machines such as the LHC and its injectors.

The smallest achievable emittance is therefore given by the emittance of the source. The difference between the source emittance and the nominal LHC emittance, defines the emittance blow-up margin, and this has been allotted to the different machines in the injection chain according to Tab. 1.2. Between the Booster and the PS, the emittance must not grow more than about 10%. In order to achieve this, among other improvements, the beam has to be carefully steered and matched when it is transfered.

Machine	Energy	Normalised Emittance, ϵ_N	Batches
SPS	450 GeV	3.75 μm	12
PS	26 GeV	3.5 μm	3
PSB	1.4 Gev	3.0 μm	2
LINAC	50 MeV	2.5 μm	
RFQ	750 keV	1.2 μm	
GUN		0.5-1.0 μm	

Table 1.2: Normalised emittances at the exit of each machine in the injector chain, in order to finally reach the nominal LHC emittance. The beam energy and the number of batches required to fill the receiving machine is also shown. Table from [11].

1.2 Emittance Definitions

There are many different definitions of emittance [12]. The one which is used for the LHC beams, and therefore also in this report, is the 1σ emittance, which is defined as

$$\epsilon = \frac{\sigma^2}{\beta} \tag{1.2}$$

where σ is the standard deviation of the beam distribution (corrected for dispersive widening) and β is the Twiss beta function. This definition is equivalent[4] to the definition of statistical emittance due to Lapostolle [13]

$$\epsilon = \sqrt{\langle x^2 \rangle \langle x'^2 \rangle - \langle xx' \rangle^2} \tag{1.3}$$

[3]The damping time due to synchrotron radiation for protons in the LHC is about 40 hours.
[4]Under proper assumptions, such as a linear lattice etc.

where x and x' are the phase space coordinates, and $\langle \cdots \rangle$ denotes average over all particles. Emittance is usually given in the unit mm·mradian, or simply μm.

The emittance as defined above is not a conserved quantity during acceleration. This is because the phase space coordinates x and x', which are generally used in accelerator physics, are not canonical coordinates. The canonical conjugate momentum to x is

$$p_x \approx p\, x' \propto \beta_L \gamma_L\, x' \tag{1.4}$$

but since for a constant beam energy the difference is only a fixed factor, p_x is seldom used. The emittance defined using canonical coordinates

$$\epsilon_N = \beta_L \gamma_L \epsilon, \tag{1.5}$$

containing the relativistic factor $\beta_L \gamma_L$, is a real conserved quantity. This emittance is called the normalised emittance.

1.3 Emittance Increase due to Injection Errors

The increase in the 1σ emittance due to different injection errors can be calculated analytically for a Gaussian beam [9]. For a beam steering error, it is given by

$$\frac{\Delta\epsilon}{\epsilon_0} \approx \frac{1}{2}\left(\frac{\Delta x^2 + (\beta_0 \Delta x' + \alpha_0 \Delta x)^2}{\sigma_0^2}\right) = \frac{1}{2\epsilon_0}\left\| \begin{pmatrix} \dfrac{\Delta x}{\sqrt{\beta_0}} \\ \sqrt{\beta_0}\Delta x' + \alpha_0 \dfrac{\Delta x}{\sqrt{\beta_0}} \end{pmatrix} \right\|^2, \tag{1.6}$$

where the vector to the right gives the normalised injection error.

For a betatron function mismatch

$$\frac{\Delta\epsilon}{\epsilon_0} \approx \frac{1}{2}(\beta\gamma_0 + \beta_0\gamma - 2\alpha_0\alpha - 2) = \frac{1}{2}\frac{\beta_0}{\beta}\left\| \begin{pmatrix} \dfrac{\Delta\beta}{\beta_0} \\ \Delta\alpha_0 - \alpha_0 \dfrac{\Delta\beta}{\beta_0} \end{pmatrix} \right\|^2, \tag{1.7}$$

where the vector to the right is the so-called mismatch vector.

For an error in dispersion function, the emittance increase is given by

$$\frac{\Delta\epsilon}{\epsilon_0} \approx \frac{1}{2}\left(\frac{\Delta D^2 + (\beta_0 \Delta D' + \alpha_0 \Delta D)^2}{\sigma_0^2}\right)\sigma_p^2 = \frac{\sigma_p^2}{2\epsilon_0}\left\| \begin{pmatrix} \dfrac{\Delta D}{\sqrt{\beta_0}} \\ \sqrt{\beta_0}\Delta D' + \alpha_0 \dfrac{\Delta D}{\sqrt{\beta_0}} \end{pmatrix} \right\|^2, \tag{1.8}$$

where σ_p is the standard deviation of the relative momentum distribution (momentum error divided by the reference momentum), and the vector to the right gives the normalised dispersion error.

Chapter 1

Introduction

1.1 The LHC Project

The Large Hadron Collider (LHC), currently under construction at CERN, will become the worlds highest energy accelerator when it starts up in 2005. With its 27 km in circumference, it will also be the worlds largest cryo-installation, since the superconducting magnets will be cooled down to 1.4° K by superfluid helium. Needless to say, this machine poses great technological challenges.

For cost efficiency, very small safety margins have been foreseen in the design, which means that the design parameters has to be strictly met in order for the machine to reach its set performance. This means that all possible problems relevant to the running of the machine has to be identified and eliminated.

Perhaps the most important parameter for a collider like the LHC is the luminosity $\mathcal{L}$, which gives the number of events that will eventually be seen in the experiments. In the LHC it is given by [1],

$$\mathcal{L} = \frac{\gamma_L}{4\pi e} \frac{N_p}{\epsilon_N} \frac{I_p}{\beta_*}, \tag{1.1}$$

where γ_L is the relativistic Lorenz factor, N_p is the number of particles per bunch, ϵ_N is the normalised emittance, I_p is the total beam current and β_* is the optical beta function at the interaction point. The LHC parameters are given in Tab. 1.1. The beam brightness N_p/ϵ_N is the key parameter here, since in principle all the other parameters are fixed by the machine design. In order to achieve a bright beam, the emittance ϵ_N should be small. However, there are also other reasons to keep the emittance small [2], such as:

- The long range beam-beam tune shift, caused by the electro-magnetic interaction between two beams passing close to each other near the interaction region, is getting worse with an increased emittance, since particles in the beam tails pass closer to each other.

	Nominal Parameters	Ultimate Parameters
Particles per bunch, N_p	$1.0 \cdot 10^{11}$	$1.6 \cdot 10^{11}$
Normalised transverse emittance, ϵ_N	3.72 μm	3.72 μm
Beta at IP, β_*	0.5 m	0.5 m
Beam Current I_p	0.5 A	0.8 A
Luminosity, $\mathcal{L}$	$1.0 \cdot 10^{34}$ cm^{-2}s^{-1}	$2.5 \cdot 10^{34}$ cm^{-2}s^{-1}

Table 1.1: LHC beam brightness requirements (Table from [1]).

- The dynamic aperture, which is the region of phase space where particle motion is stable, is relatively small in the LHC due to strong non-linearities. A small emittance gives a larger safety margin.

- The physical aperture, given by the vacuum pipe is even smaller than the dynamic aperture. On top of this, the vacuum pipe is at cryogenic temperature. Due to the very high energy of the particles in the beam, a loss of even a very small fraction of the beam[1] could cause the superconducting magnets to quench, which would be a serious problem. Therefore the beam size has to be kept small to avoid such losses[2].

The beam brightness is limited by the head-on beam-beam tune shift, which can not be greater than the available space between resonances in the tune diagram. The LHC is designed to operate with optimum beam brightness. Further increasing the brightness by decreasing the emittance from the value given in Tab. 1.1 would decrease the luminosity due to the head-on beam-beam effect. Therefore, in order to reach the design luminosity, the emittance has to be kept to the design value.

According to Liouville's theorem [4], the local phase space density is a constant of the motion in a conservative system of non-interacting particles. This implies that the normalised emittance should in general also be constant. However, in a real accelerator there are some effects that can affect the emittance. These are effect as (list not exhaustive):

- Synchrotron radiation, which dissipates energy and therefore is non-conservative. This is mainly a problem in lepton machines.

- Space Charge [5] and Intra Beam Scattering [6], since these are interactions between particles and not with external forces. Space charge effects decrease rapidly with increasing energy and is mainly a problem in low energy machines like the PS Booster.

- The impedance of the machine can excite resonances [7][8], which will result in beam loss or an increased emittance.

[1] A detailed description of the maximum losses allowed in the LHC under different circumstances is given in [3].

[2] A collimation scheme is foreseen for the LHC, where the particles tails are shaved off. A large emittance therefore means intensity loss, which translates into lower luminosity.

It is interesting to note that the relative emittance increase due to beam steering and dispersion function errors are inversely proportional to the beam emittance, whereas the betatron mismatch contribution is independent of the original emittance. Moreover, the emittance increase due to a dispersion function error is quadratic in the momentum spread.

Since the LHC beam will have a small emittance and large momentum spread, this hints that correcting steering and dispersion function errors will be specially important.

1.4 Automatic Beam Steering

Manual trial-and-error optimisation of accelerator performance is time-consuming and slow. One should therefore as much as possible make use of computer power to guide the optimisation procedure. An "Automatic Beam Steering" (ABS) project has been set up in the CERN Proton Synchrotron Division, with the aim to provide such optimisation tools.

The ABS approach consists of three main parts.

- A database [14] that contains all the information about the machine. This information can be extracted in a format suited for beam optics programs, and be used to predict the response of the machine to a certain correction. These predictions are then stored in the database.
- An optimisation algorithm [15] that calculates the optimum corrections given some measured errors.
- A generic correction software [16] that links the measurement program to the database and the correction algorithm, and which can access and control the machine parameters.

The idea is to have a set of generic correction programs for all types of error corrections. They should be data driven in the sense that changes in the database propagate directly to all the programs involved.

Parts of the work presented here deals with the response prediction for different types of errors and the choice of optimisation algorithms.

Chapter 2

The Booster-PS Beam Transfer Line

2.1 The Recombination of the Four Booster Rings

The PS Booster (PBS) consists of four parallel synchrotrons stacked on top of each other. The four rings share major elements but can to some extent be individually controlled using separate correction elements. The filling of the CERN Proton Synchrotron (CPS), the next machine in the chain, is usually done by sequential ejection of the four rings. Following ejection, the particles from the four rings are brought together in a vertical recombination scheme [17] to the level of the CPS (see Fig. 2.1). The bending magnets used for the recombination are rectangular magnets resulting in some edge focusing contributions to the transverse optics. This effect was during the PSB design stage thought to be of no importance, and no elements for compensation were installed. An experimental study of the effect was performed in 1978 [18] and the effect was then considered sufficiently small to be ignored.

However, the tight emittance budget enforced on the injector chain for the LHC beam and the resulting demand on good emittance preservation between the individual machines has triggered a new study of the problem.

The recombination scheme can be divided into three main parts (see Fig. 2.2). In the first part, the beam-lines from the lower two and the upper two rings are joined together. The recombination is done in a symmetrical manner and therefore one would expect the beams from ring one and four to have the same properties after recombination,

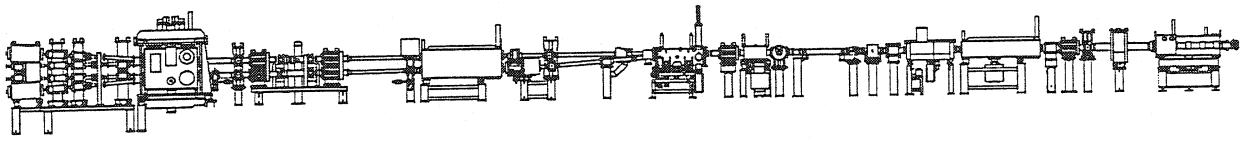

Figure 2.1: Drawing of the vertical recombination scheme in the PS booster. The four beams enter from the left. Note the lack of available space for additional elements.

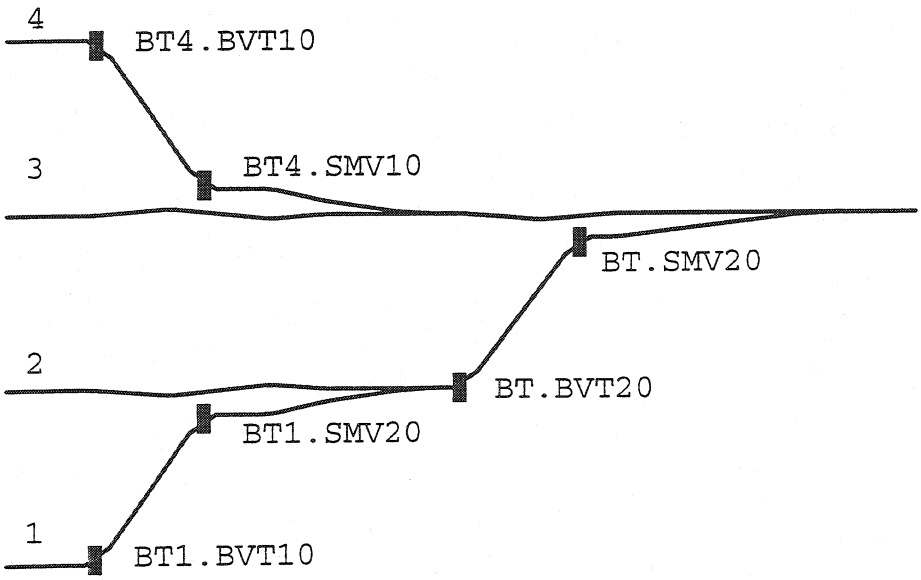

Figure 2.2: Schematic layout of the beam trajectories in the vertical recombination scheme, showing the position of the main bending magnets.

and similarly for ring two and three. This symmetry, however, is broken in the next part of the recombination scheme, where the common beam-line from ring two and one is brought to the level of ring three and recombined. Because of this, the beam-lines from the four rings all have different optics. In the two first parts, the beam-lines are equipped with individual steering dipoles, while all the quadrupoles are common. Since the beams in general do not pass through the centre of the quadrupoles, they have a deflecting as well as a focusing effect. In the last part of the recombination scheme, the beams from the four rings are ideally following the same trajectory and this part can be considered as a standard transfer line. From here the beam is sent to different destinations, either the CPS, ISOLDE, or the Booster measurement line. Depending on the destination, the settings of the quadrupoles in the last part varies, while the settings of the quadrupoles in the first part (recombination) is constant.

2.1.1 Modelling of the Transfer Line

In an attempt to understand the optics of the PSB recombination and transfer region a model have been produced in *Mathematica* [19] using the *BeamOptics* [20] package. In the calculations, a hard edge model of the magnets have been used, taking into account the edge effects of all the dipoles and the off-axis quadrupoles. Also, the fact that the curved beam trajectory inside a bending magnet is slightly longer than the magnetic length of the magnet has been taken into account.

The model was verified qualitatively for ring three by comparison with an independent, and somewhat simpler, model [21] made in an alternative optics program. This simpler

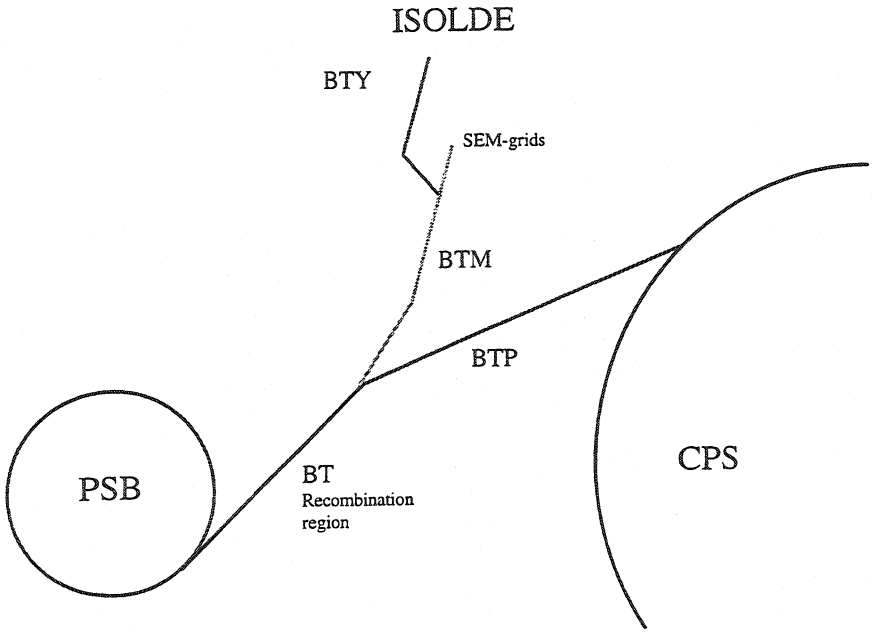

Figure 2.3: General layout of the transfer lines between Booster and CPS, showing the position of the SEM grids in the Booster Measurement Line (BTM).

model was also adapted to the other rings. No major differences between the two models were found. The validity of the *BeamOptics* program has been tested by porting the model to *WinAGILE* [22] and comparing the results.

The resulting Twiss parameters at the first SEM-grid in the Booster measurement line are shown in Tab. 2.1. The large differences observed in the horizontal plane are almost entirely a result of the horizontal edge focusing effect at the entry and exit from the rectangular vertical bending magnets[1].

Plane	Horizontal				Vertical			
Beam from ring	1	2	3	4	1	2	3	4
β_{Twiss}	6.19	6.62	8.44	7.69	5.94	6.00	6.00	5.94
α_{Twiss}	1.77	2.03	2.54	2.22	1.78	1.78	1.79	1.79
Emittance Blow-Up (RMS)	5.4%	3.1%	0%	0.9%	0.0%	0.0%	0%	0.0%

Table 2.1: Theoretical Twiss values deduced with the analytical beam optics program BeamOptics, as well as the corresponding theoretical prediction for the emittance blow-up. The Twiss values are calculated at the first SEM-grid in the Booster measurement line for the actual settings of the quadrupoles.

[1]This was verified by turning off the edge-effect on these magnets in the theoretical model.

2.1.2 Measurements of the Optical Parameters

The Twiss values of the beam from the four Booster rings have been measured using SEM-grids [23] in the Booster measurement line (see Fig. 2.3), and the corresponding RMS emittance blow-up have been calculated using Eq. (1.7), taking the parameters of ring three as a reference. For the measurement, a low intensity proton beam was used. The result is shown in Tab. 2.2.

Plane	Horizontal				Vertical			
Beam from ring	1	2	3	4	1	2	3	4
β_{Twiss}	4.03	3.90	5.75	5.71	5.67	5.51	5.67	5.99
α_{Twiss}	1.19	1.36	1.75	1.59	1.76	1.73	1.74	1.89
Emittance Blow-Up (RMS)	6.5%	9.8%	0%	1.1%	0.0%	0.1%	0%	0.3%

Table 2.2: Measured values at the first SEM-grid in the Booster measurement line, as well as the corresponding theoretical prediction of the emittance blow-up. Since currently no continuous correction of the optics is made, the measured values have differed slightly between measurements (see references [24] [25]), but the relative direction and individual magnitude of the mismatch vectors (see Fig. 2.4), which are independent of drifts in the common quadrupoles, have been stable.

Practical experience shows that the SEM-grids in the measurement line has an absolute accuracy of about 10% in the measurement of the beta function and emittance[2]. Considering this, the measured values for all the four rings in the vertical plane are in agreement with the theoretical values. In the horizontal plane, however, there is a big difference between calculated and measured values. Part of this difference could come from errors in the common part of the recombination line. To study the difference between the line, one should look at the relative mismatch between rings. Fig. 2.4 shows the mismatch vectors of rings one, two and four with respect to the ring three. In both the measured and theoretical case, the mismatch vectors of ring four and two add up approximately to the mismatch vector of ring one (mismatch vectors are approximatively additive). This implies that the source for the differences really is the vertical bending magnets, since ring four is deflected only in the first bending and ring two in the second, while ring four is deflected in both magnets. However, the fact that the vectors does not point in the same direction relative each others in the measured and theoretical case implies that there are effects in the real line which are not accounted for in the model. This is supported by the historical fact that when the optics of the line was first tested, it did not produce the desired Twiss parameters at SEM grids in the measurement line [21]. The effect was empirically corrected by changing some quadrupole settings in the common part of the line in such a way that the effect cancelled for ring three.

[2]According to the conclusions of the 1997 ICFA mini-workshop on emittance preservation, no present emittance measurement device has a better absolute accuracy than about 10% [26].

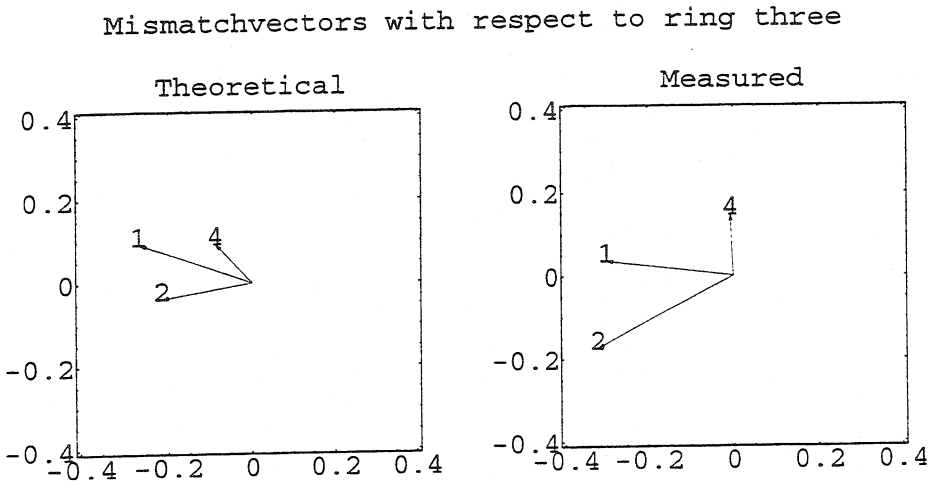

Figure 2.4: Difference between the measured and calculated Twiss values in the horizontal plane. The mismatch vectors for beams from ring one, two and four relative to the Twiss functions of the beam from ring three are plotted in the plane.

2.1.3 Impact on the LHC Beam Emittance

Based on the measured values of the optical differences between the beams from the four different booster rings, the RMS emittance blow-up in the horizontal plane could be as large as 5%, depending on which of the four beams is considered.

This value is half of the allowed emittance blow-up during the Booster-PS beam transfer. It could be argued that this is acceptable, but one should consider that this is just one of many possible blow-up sources which should all sum up less to than the allowed blow-up. If left uncorrected, this effect thus drastically reduces the margin available for other errors.

2.1.4 Suggested Improvements

The first idea of how to compensate optical differences was to attack the problem at its origin. Based on the *BeamOptics* model, it was found that by putting shims[3] on the main bending magnets in the recombination scheme, the optical differences could be efficiently reduced [27]. This approach was however not successful, since the complicated structure of the bending magnets does not allow the simple addition of shims [28].

Therefore, a study of the effects and optimal positions of corrector quadrupoles was made [25]. To find the optimum position for the quadrupole, an analytic approach was taken. Using first order perturbation theory (see Section 3.3), it is possible to derive an

[3] A shim is a wedge-shaped piece of metal that is added to the end of a magnet yoke to change its edge focusing properties.

analytic expression for the residual mismatch vector as a function of correction position, which can be expressed as

$$\mathbf{r} = \mathbf{e} - q\,\mathbf{k}(s) \tag{2.1}$$

where $\mathbf{r}$ is the residual mismatch vector, $\mathbf{e}$ is the original mismatch vector, $\mathbf{k}(s)$ is the first order influence of a quadrupole at position s on the mismatch vector, and q is the strength of the quadrupole. The minimum vector norm of $\mathbf{r}$ is achieved for

$$q = \frac{\mathbf{e}\cdot\mathbf{k}(s)}{\mathbf{k}(s)\cdot\mathbf{k}(s)} \tag{2.2}$$

which gives the minimum residual mismatch vector as a function of position s in the line

$$\mathbf{r} = \mathbf{e} - \frac{\mathbf{e}\cdot\mathbf{k}(s)}{\mathbf{k}(s)\cdot\mathbf{k}(s)}\,\mathbf{k}(s). \tag{2.3}$$

In order to account for the effects of the corrector in both the transverse planes $\mathbf{r}$, $\mathbf{e}$ and $\mathbf{k}$ should be defined as the concatenations of the corresponding horizontal and vertical vectors. Eq. (1.7) then gives a relation between $\mathbf{r}$ and the sum of the relative emittance blow-up in the two planes[4]

$$\mathbf{r}^2 = \mathbf{r}_h^2 + \mathbf{r}_v^2 \propto \frac{\Delta\epsilon_h}{\epsilon_h} + \frac{\Delta\epsilon_v}{\epsilon_v} \tag{2.4}$$

This function can be evaluated for the case of correction for differences between outer and inner rings (caused by the bending magnet BTx.BVT10) and differences between upper and lower rings (caused by BT.BVT20). The relative corrector efficiency, defined as the ratio of the residual error to the original error is shown in Figs. 2.5 and 2.6 for the two cases. It is clear that a single corrector is not a good option for correction between outer and inner rings, whereas it is very efficient for correction between lower and upper rings. Also, fortunately there is space for a correction element just in the optimum position, just after the BT.BVT20 magnet. The fact that the correction is so efficient can be traced back to the large difference in horizontal and vertical beta functions, which means that a single quadrupole can correct efficiently in the horizontal plane without destroying the vertical matching.

A more detailed analysis using a finite length quadrupole verifies the basic result. The corrector quadrupole for the lower rings should have an integrated normalised gradient of about 0.01 m^{-1}. A design for such a quadrupole has been made [29].

[4]Due to linear coupling, the injected beam turns round ($\epsilon_h = \epsilon_v$) in the CPS. Since the sum of the two emittances is ideally conserved in this process, it is proper to minimise the sum of the horizontal and vertical emittance blow-ups.

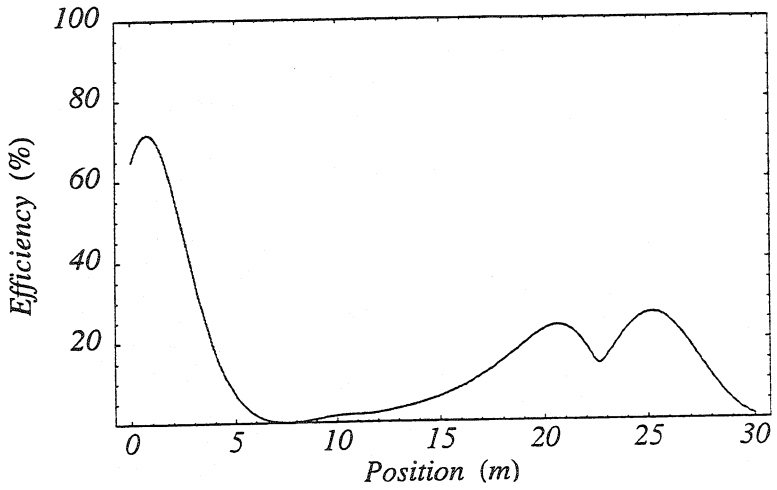

Figure 2.5: Relative corrector efficiency as a function of position in the line for a single corrector quadrupole acting on the outer rings (rings 1 and 4). The reference position is the centre of the Booster ejection septum.

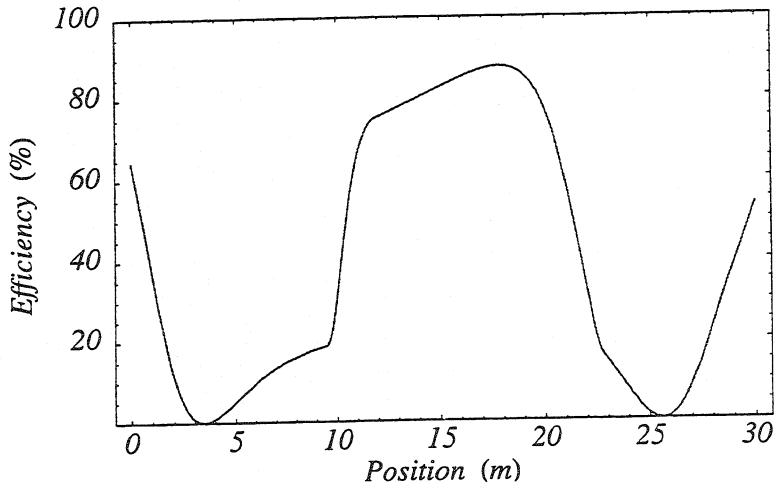

Figure 2.6: Relative corrector efficiency as a function of position in the line for a single corrector quadrupole acting on the lower rings (rings 1 and 2). The reference position is the centre of the Booster ejection septum. The broad peak is roughly centred around the magnet BT.BVT20.

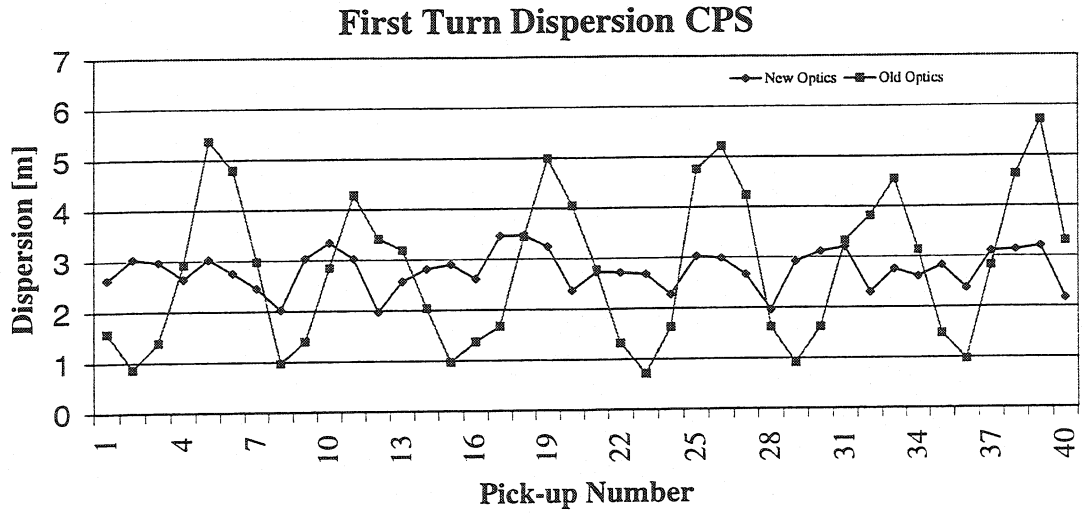

Figure 2.7: Measured transported dispersion for the first turn in the CPS, with the new and old optics. The CPS lattice dispersion is about the same ($\approx 3m$) at all the pick-up locations.

2.2 Dispersion Matching to the CPS

The present transfer line optics PSB-PS leaves a residual dispersion mismatch at the injection point. The mismatch is intentional in the sense that it is not possible to do better with the operational quadrupole magnets. However, there is an additional quadrupole magnet available which is not used because of it's awkward position inside the shielding wall between the two machines. Using this quadrupole, it is possible to match the dispersion. An optics proposal due to Risselada [30] exist since long, but really convincing measurements have not been achieved before, due to different hardware problems.

2.2.1 Measurements of the Effect

Measurements of the transported dispersion from the PSB to the PS, using the PS as a transfer line have been performed. The results show a significant improvement in the dispersion matching between the two machines when applying the new optics (see Fig. 2.7). The betatron matching has also been verified for the new optics, using the SEM harps in the PS ring.

The beam size after filamentation have been measured with the new and old optics, using the wire-scanner in the PS ring. This measurement is very difficult, since all other blow-up sources have to be eliminated, and the effect of the coupling between the transverse planes in the CPS has to taken into account. The results have so far shown no significant difference between the two optics.

2.2.2 Impact on the LHC Beam Emittance

Taking the standard formula in Eq. (1.8) for the RMS emittance blow-up due to dispersion mismatch with the parameters for the LHC beam and the current dispersion mismatch, gives a RMS blow-up of about 30%. The large number is because the LHC beam is very small and has a large momentum spread. Some comparative measurements between the PS SEM-grids and the wire-scanner have indicated a blow-up of the order of 40%, but the measurements are not conclusive. However, an optics change seems necessary to meet the LHC requirements.

Chapter 3

Response Matrices

3.1 Definition of the Response Matrix

In order to find the optimum correction given a measured error, one needs to be able to predict the response of the machine to different corrections. The first order response in a number of observables ξ, such as beam positions, due to some given perturbations δ can be expressed in terms of a response matrix M.

$$\begin{pmatrix} \xi_1 \\ \xi_2 \\ \vdots \\ \xi_i \end{pmatrix} = \begin{pmatrix} m_{11} & m_{12} & \cdots & m_{1j} \\ m_{21} & m_{22} & \cdots & m_{2j} \\ \vdots & \vdots & \ddots & \\ m_{i1} & m_{i2} & & m_{ij} \end{pmatrix} \cdot \begin{pmatrix} \delta_1 \\ \delta_2 \\ \vdots \\ \delta_j \end{pmatrix} \tag{3.1}$$

This response matrix can be obtained in two different ways

- By direct measurement, changing machine parameters and recording the response.
- Through first order perturbation theory, given an accurate model of the machine.

The first method will always work, but brings little knowledge about the machine. The second method is more cumbersome, since a model of the machine has to be produced. However, the machine model is an important spin-off of the procedure. If the calculated response matrix does not work, this shows that the model is insufficient. Eventually, this will lead to a better understanding of the machine.

3.2 Beam Steering

The idea of an Automatic Beam Steering program was first tested in the PS complex [31] for beam steering in transfer lines and closed orbit correction in circular machines. The response matrix elements for this type of corrections can be expressed in terms of the

betatron function β and the phase advance μ as

$$\Delta x_m = \begin{cases} \sqrt{\beta_m \beta_c} \sin(\mu_m - \mu_c)\ \Delta\phi_c & \text{if } \mu_m > \mu_c \\ 0 & \text{if } \mu_m < \mu_c \end{cases} \tag{3.2}$$

for beam steering, and

$$\Delta x_m = \frac{\sqrt{\beta_m \beta_c}}{\sin 2\pi q} \cos(|\mu_m - \mu_c| - 2\pi q)\ \Delta\phi_c \tag{3.3}$$

for closed orbit correction. Here $\Delta\phi_c$ is the increments in angle for corrector magnet c, Δx_m is the corresponding beam displacement at monitor m.

3.3 Response Matrix for Betatron Matching

The beta function evolve between two sections of beam line according to [32]

$$\beta_{\rm m} = C^2\beta_{\rm c} - 2CS\alpha_{\rm c} + S^2\gamma_{\rm c} \tag{3.4}$$

Here, the transfer matrix between corrector and monitor is given in terms of the so-called cosine-like C and sine-like S functions and their derivatives

$$T_{c\to m} = \begin{pmatrix} C & S \\ C' & S' \end{pmatrix}, \tag{3.5}$$

If a small quadrupole perturbation is applied at the corrector location, the transfer matrix between the corrector and the monitor can be obtained from Eq. (3.5) by multiplying by the thin quadrupole transfer matrix. This gives

$$\tilde{T}_{\rm c\to m} = \begin{pmatrix} C & S \\ C' & S' \end{pmatrix} \begin{pmatrix} 1 & 0 \\ \Delta kl & 1 \end{pmatrix} = \begin{pmatrix} C + S\,\Delta kl & S \\ C' + S'\Delta kl & S' \end{pmatrix}, \tag{3.6}$$

where Δkl is the integrated gradient of the error. By using the matrix (3.6), one can find the resulting beta function at the monitor location, namely

$$\tilde{\beta}_{\rm m} = C^2\beta_{\rm c} - 2CS\alpha_{\rm c} + S^2\gamma_{\rm c} + 2\ S(C\beta_{\rm c} - S\alpha_{\rm c})\Delta kl + S^2\beta_{\rm c}(\Delta kl)^2 \tag{3.7}$$

which can be rewritten, using Eq. (3.4), as

$$\Delta\beta_m = \tilde{\beta}_{\rm m} - \beta_{\rm m} = 2\ S(C\beta_{\rm c} - S\alpha_{\rm c})\Delta kl + S^2\beta_{\rm c}(\Delta kl)^2 \tag{3.8}$$

Now, in the standard parametrisation [32] of the transfer matrix $T_{\rm c\to m}$, the sine-like function S is given by

$$S = \sqrt{\beta_{\rm m}\beta_{\rm c}} \sin(\mu_{\rm m} - \mu_{\rm c}) \tag{3.9}$$

and the cosine-like function C

$$C = \sqrt{\frac{\beta_{\rm m}}{\beta_{\rm c}}}\cos(\mu_{\rm m} - \mu_{\rm c}) + \alpha_{\rm c}\sqrt{\frac{\beta_{\rm m}}{\beta_{\rm c}}}\sin(\mu_{\rm m} - \mu_{\rm c}) \tag{3.10}$$

which allows to write the relative error perturbation in the beta function at the monitor as

$$\frac{\Delta\beta_{\rm m}}{\beta_{\rm m}} = \beta_{\rm c}\sin 2(\mu_{\rm m} - \mu_{\rm c})\ \Delta kl + \frac{{\beta_{\rm c}}^2}{2}(1 - \cos 2(\mu_{\rm m} - \mu_{\rm c}))\ (\Delta kl)^2 \tag{3.11}$$

Taking the derivative with respect to $\mu_{\rm m}$ yields

$$\alpha_{\rm m}\frac{\Delta\beta_{\rm m}}{\beta_{\rm m}} - \Delta\alpha_{\rm m} = \beta_{\rm c}\cos 2(\mu_{\rm m} - \mu_{\rm c})\ \Delta kl + \frac{{\beta_{\rm c}}^2}{2}\sin 2(\mu_{\rm m} - \mu_{\rm c})\ (\Delta kl)^2 \tag{3.12}$$

If many perturbations are present in the line, the perturbed transfer matrix from the first corrector to the monitor is

$$\overline{T}_{\rm c\to m} = \prod_{i=1}^{N_c}\begin{pmatrix} C_i + S_i\,\Delta kl_i & S_i \\ C_i' + S_i'\Delta kl_i & S_i' \end{pmatrix} = \prod_{i=1}^{N_c}\begin{pmatrix} C_i & S_i \\ C_i' & S_i' \end{pmatrix} + \Delta k_i\begin{pmatrix} S_i & 0 \\ S_i' & 0 \end{pmatrix}, \tag{3.13}$$

where N_c is the number of correctors between the beginning of the beam line and the monitor m.

This matrix product can be splitted up in a polynomial with matrix coefficients. To calculate the cross terms of second order in $\Delta kl_{\rm i}$, one has only to evaluate the general second order term

$$\begin{aligned} \overline{T}_{\rm c\to m} &= \begin{pmatrix} C_2 & S_2 \\ C_2' & S_2' \end{pmatrix}\begin{pmatrix} 1 & 0 \\ \Delta kl_2 & 1 \end{pmatrix}\begin{pmatrix} C_1 & S_1 \\ C_1' & S_1' \end{pmatrix}\begin{pmatrix} 1 & 0 \\ \Delta kl_1 & 1 \end{pmatrix} \\ &= \begin{pmatrix} C_2 & S_2 \\ C_2' & S_2' \end{pmatrix}\begin{pmatrix} C_1 & S_1 \\ C_1' & S_1' \end{pmatrix} + \begin{pmatrix} C_2 & S_2 \\ C_2' & S_2' \end{pmatrix}\begin{pmatrix} 0 & 0 \\ \Delta kl_2 & 0 \end{pmatrix}\begin{pmatrix} C_1 & S_1 \\ C_1' & S_1' \end{pmatrix} + \cdots \end{aligned} \tag{3.14}$$

Going through the exercise of grouping terms of different orders gives

$$\begin{aligned} \frac{\Delta\beta_{\rm m}}{\beta_{\rm m}} &= \beta_1\sin 2(\mu_{\rm m} - \mu_1)\ \Delta kl_1 + \beta_2\sin 2(\mu_{\rm m} - \mu_2)\ \Delta kl_2 + \\ &+ \frac{1}{2}\beta_1^2(1 - \cos 2(\mu_{\rm m} - \mu_1))\ (\Delta kl_1)^2 + \frac{1}{2}\beta_2^2(1 - \cos 2(\mu_{\rm m} - \mu_2))\ (\Delta kl_2)^2 + \\ &+ \beta_1\beta_2(\cos 2(\mu_2 - \mu_1) - \cos 2(\mu_{\rm m} - \mu_1)\ \Delta kl_1\ \Delta kl_2 \end{aligned} \tag{3.15}$$

where the first terms are just the linear and second order terms already computed, and the last term is the lowest order cross term between perturbations. Again, taking the

derivative with respect to μ_m yields

$$\begin{aligned}\alpha_m \frac{\Delta\beta_m}{\beta_m} - \Delta\alpha_m &= \beta_1 \cos 2(\mu_m - \mu_1)\, \Delta kl_1 + \beta_2 \cos 2(\mu_m - \mu_2)\, \Delta kl_2 + \\ &+ \frac{{\beta_1}^2}{2} \sin 2(\mu_m - \mu_1)\, (\Delta kl_1)^2 + \frac{{\beta_2}^2}{2} \sin 2(\mu_m - \mu_2)\, (\Delta kl_2)^2 + \\ &+ \beta_1\beta_2 \sin 2(\mu_m - \mu_1)\, \Delta kl_1\, \Delta kl_2\end{aligned} \tag{3.16}$$

3.4 Dispersion Matching

If there is dispersion in the transfer line, the evolution of the dispersion function should be included in the formalism used to correct a mismatch in the optical parameters. The approach to calculate the response matrix for dispersion matching can be based on 3×3 transfer matrices [9]. The propagation of the dispersion function from a corrector location to a monitor placed downstream can be written using the matrix

$$\mathcal{T}_{c\to m} = \begin{pmatrix} C & S & \xi \\ C' & S' & \xi' \\ 0 & 0 & 1 \end{pmatrix}. \tag{3.17}$$

The upper left 2×2 sub-matrix represents the transfer matrix for the betatronic motion between corrector and monitor. The quantities ξ, ξ' are different from zero only when bending magnets are present in the transfer line. A quantity

$$\mathcal{W} = \frac{1}{\beta}[D^2 + (\alpha D + \beta D')^2], \tag{3.18}$$

similar to the Courant-Snyder invariant can be defined. In a bending-free region of a transfer line, $\mathcal{W}$ is an invariant and is called the *Dispersion invariant* [32].

The dispersion at a given monitor is linked to the value at the location of an upstream corrector (a normal quadrupole) by the transfer matrix of the section in between. The presence of a quadrupolar error, simulated by a thin lens element, modifies the transfer matrix, according to the following

$$\overline{\mathcal{T}}_{c\to m} = \begin{pmatrix} C & S & \xi \\ C' & S' & \xi' \\ 0 & 0 & 1 \end{pmatrix} \begin{pmatrix} 1 & 0 & 0 \\ \Delta kl & 1 & 0 \\ 0 & 0 & 1 \end{pmatrix} = \begin{pmatrix} C + S\,\Delta kl & S & \xi \\ C' + S'\Delta kl & S' & \xi' \\ 0 & 0 & 1 \end{pmatrix}. \tag{3.19}$$

The modified dispersion at the monitor location is then given by

$$\bar{D}_m = D_m + S\ D_c\ \Delta kl \tag{3.20}$$

$$\bar{D}'_m = D'_m + S'\ D_c\ \Delta kl, \tag{3.21}$$

where

$$D_{\mathrm{m}} = C\ D_{\mathrm{c}} + S\ D'_{\mathrm{c}} + \xi \tag{3.22}$$

$$D'_{\mathrm{m}} = C'\ D_{\mathrm{c}} + S'\ D'_{\mathrm{c}} + \xi'. \tag{3.23}$$

In this case, Eq. (1.8) and the existence of the dispersion invariant suggests to define a dispersion mismatch vector as

$$\begin{pmatrix} \dfrac{\Delta D_{\mathrm{m}}}{\sqrt{\beta_{\mathrm{m}}}} \\ \alpha_{\mathrm{m}} \dfrac{\Delta D_{\mathrm{m}}}{\sqrt{\beta_{\mathrm{m}}}} + \sqrt{\beta_{\mathrm{m}}} \Delta D'_{\mathrm{m}} \end{pmatrix}, \tag{3.24}$$

where $\Delta D_{\mathrm{m}} = \bar{D}_{\mathrm{m}} - D_{\mathrm{m}}$ and $\Delta D'_{\mathrm{m}} = \bar{D}'_{\mathrm{m}} - D'_{\mathrm{m}}$.
Again, by using the standard parametrisation of the transfer matrix between the corrector and the monitor, it is possible to obtain the expression of the dispersion mismatch vector

$$\frac{\Delta D_{\mathrm{m}}}{\sqrt{\beta_{\mathrm{m}}}} = \sqrt{\beta_{\mathrm{c}}} D_{\mathrm{c}} \sin \Delta\mu\ \ \Delta kl \tag{3.25}$$

$$\alpha_{\mathrm{m}} \frac{\Delta D_{\mathrm{m}}}{\sqrt{\beta_{\mathrm{m}}}} + \sqrt{\beta_{\mathrm{m}}} \Delta D'_{\mathrm{m}} = \sqrt{\beta_{\mathrm{c}}} D_{\mathrm{c}} \cos \Delta\mu\ \ \Delta kl. \tag{3.26}$$

3.5 Combined Betatron and Dispersion Matching

As mentioned before, when correcting the dispersion using quadrupole correctors, the betatron matching will be affected as well. Therefore, the response matrix used for the correction should include both effects. In this case, the matrix can be defined as

$$\begin{pmatrix} \dfrac{\Delta\beta_{H_m}}{\beta_{H_m}} \\ \alpha_{H_m} \dfrac{\Delta\beta_{H_m}}{\beta_{H_m}} - \Delta\alpha_{H_m} \\ \dfrac{\Delta\beta_{V_m}}{\beta_{V_m}} \\ \alpha_{V_m} \dfrac{\Delta\beta_{V_m}}{\beta_{V_m}} - \Delta\alpha_{V_m} \\ \dfrac{\Delta D_{H_m}}{\sqrt{\beta_{H_m}}} \\ \alpha_{H_m} \dfrac{\Delta D_{H_m}}{\sqrt{\beta_{H_m}}} + \sqrt{\beta_{H_m}} \Delta D'_{H_m} \\ \dfrac{\Delta D_{V_m}}{\sqrt{\beta_{V_m}}} \\ \alpha_{V_m} \dfrac{\Delta D_{V_m}}{\sqrt{\beta_{V_m}}} + \sqrt{\beta_{V_m}} \Delta D'_{V_m} \end{pmatrix} = \begin{pmatrix} \beta_{H_1} \sin 2\Delta\mu_{H_1} & \cdots \\ \beta_{H_1} \cos 2\Delta\mu_{H_1} & \cdots \\ \beta_{V_1} \sin 2\Delta\mu_{V_1} & \cdots \\ \beta_{V_1} \cos 2\Delta\mu_{V_1} & \cdots \\ \sqrt{\beta_{H_1}} D_{H_1} \sin \Delta\mu_{H_1} & \cdots \\ \sqrt{\beta_{H_1}} D_{H_1} \cos \Delta\mu_{H_1} & \cdots \\ \sqrt{\beta_{V_1}} D_{V_1} \sin \Delta\mu_{V_1} & \cdots \\ \sqrt{\beta_{V_1}} D_{V_1} \cos \Delta\mu_{V_1} & \cdots \end{pmatrix} \cdot \begin{pmatrix} \Delta kl_1 \\ \Delta kl_2 \\ \vdots \\ \\ \\ \\ \\ \\ \vdots \\ \Delta kl_N \end{pmatrix}, \tag{3.27}$$

Here, N_c is the number of correctors. Note that one should in general include a weight factor between the betatronic part of the matrix and the dispersion part. This since the betatron-matching matrix elements has unit m, while the dispersion part has unit $m^{3/2}$. Eqs. (1.7) and (1.8) suggest that the dispersion part of the matrix should be multiplied by a weight factor of $\sigma_p/\sqrt{\epsilon}$, which of order unity for the LHC beam. Therefore, for all the measurements and simulations presented here, the weight factor was set to one.

Chapter 4

Optimisation Schemes

4.1 Problem Formulation

The optimisation problems encountered in accelerator fine tuning are either already linear or can be linearised since only small corrections are considered. Thus the optimisation algorithms should solve a linear problem of the type

$$\min ||\mathbf{b} + A \cdot \mathbf{x}|| \tag{4.1}$$

where $||\cdots||$ denotes a suitable norm. In this work, the standard vector norm was used.

If the number of free parameters N_c (correctors) equals the number of constraints N_m (monitors), A is a $n \times n$ matrix, and could in principle be inverted. If the system is over-constrained or singular, it could be solved using the classical least square fit, which is

$$x = (A^T A)^{-1} A^T \mathbf{b} \tag{4.2}$$

The direct inversion of A often poses numerical problems, since the matrices are often singular or numerically ill-conditioned. If a response matrix is singular, it means that parts of the solution space is inaccessible. In other words, there are correction vectors $\mathbf{x}$ that when multiplied with A give zero. Also, there are error vectors $\mathbf{b}$ that can not be corrected using the available correctors.

The inaccessible solution space is called the null-space of the matrix. The least square method solves this problem by projecting it into the available solution space and solving the restricted problem. However, if the matrix is ill-conditioned, there are parts of this restricted solution space that can still only be reached by applying very large corrections $\mathbf{x}$. This is not good for the stability of the correction, since noise in the in-data is strongly amplified. These kind of corrections could be called near-to-null-space corrections.

Another important point is that each corrector can only be controlled with a finite accuracy. Thus with every corrector that is changed, an error is introduced. Therefore, it is favourable to use as few correctors as possible.

A good correction algorithm should thus:

- Avoid null-space corrections.
- Avoid near-to-null-space corrections.
- Use as few correctors as possible.

4.2 Singular Value Decomposition

The Singular Value Decomposition method is a general method of solving ill-conditioned matrix equations. The idea is that any matrix can be decomposed as

$$M = L^T \cdot D \cdot R, \tag{4.3}$$

where where L and R is a row orthonormal matrices, and D is a diagonal matrix whose diagonal elements d_{nn} are the so called singular values of the matrix M. The decomposition can be done even if M is not a square matrix.

For square matrices, the ratio of the largest singular value to the smallest gives the condition number, or $\mathcal{L}^2$ norm of a matrix, which determines the accuracy of its numerical inverse. The smaller the ratio, the more accurate is the solution.

The pseudo-inverse of M can be defined from the singular value decomposition as

$$M^{-1} = R^T \cdot D^{-1} \cdot L, \tag{4.4}$$

where the inverse of the diagonal matrix D is

$$D^{-1} = \begin{pmatrix} \frac{1}{d_{11}} & 0 & \cdots & 0 \\ 0 & \frac{1}{d_{22}} & 0 & \vdots \\ \vdots & 0 & \ddots & 0 \\ 0 & \cdots & 0 & \frac{1}{d_{kk}} \end{pmatrix} \tag{4.5}$$

and $k = \min(i, j)$. It is clear from Eq. (4.5) that any singular values that are zero will lead to infinities in D^{-1}. Any such infinities are thus simply replaced by zero, which effectively means removing the degrees of freedom associated with those singular values[1]. However, the same way very small singular values will give very large entries in D^{-1}. These large values can also be replaced with zeros in order to get a more stable solution. In this way SVD, trades degrees of freedom for numerical stability.

If M is a non-singular square matrix, the pseudo-inverse is just the normal matrix inverse.

[1]Up to this point, SVD is identical to the Least Square Method

4.3 The Harmonic Correction Method

The Harmonic Correction Method [33] for closed orbit corrections was first conceived for correction of the orbits in the Intersecting Storage Rings (ISR) at CERN. It is based on the idea to make an FFT of the measured data points, and correct the different harmonics separately. Variations of the Harmonic Method are used in some labs around the world, but since it is specific to closed orbit corrections, it will not be discussed here.

4.4 The Micado Algorithm

The *MICADO* algorithm was also first proposed for closed orbit corrections in the ISR machine [34]. Its main advantage is that it uses only a small subset of the of corrector magnets, as opposed to SVD and the harmonic method that uses all available correctors. *MICADO* solves the matrix equation

$$M \cdot \mathbf{a} = \mathbf{b} \tag{4.6}$$

iteratively, by minimising the norm of the residual vector $\mathbf{r}$ defined as

$$\mathbf{r} = \mathbf{b} - M \cdot \mathbf{a}\,. \tag{4.7}$$

The matrix M need not to be rectangular. In the first iteration, *MICADO* finds the column $\mathbf{m}_i$ of M which gives the minimum the residual vector when solving the over-determined system

$$\mathbf{m}_i \cdot a_i = \mathbf{b}\,, \tag{4.8}$$

using the least-square method. This column is then kept to the next iteration, where *MICADO* finds the column of M that, together with the first one, minimises the residual vector when solving

$$M_{\{i,j\}} \cdot \mathbf{a}_{\{i,j\}} = \mathbf{b}\,, \tag{4.9}$$

again using the least-square method. This procedure is repeated N times. The output data for each iteration contains the chosen columns, that in this case correspond to the best correctors, and the vector $\mathbf{a}_{\{i,j\}}$, which gives the corrections to be applied. The error, defined as the norm of the residual vector $\mathbf{r}$, generally decreases much more in the first few iterations than in the later (see Fig. 4.1). Since a measured value is used as input, one can not compensate better than the measurement error. The measurement error comes in already in the calculation of the corrections, and therefore one cannot expect the effect of the correction to be exactly as predicted by *MICADO*. As mentioned before, the corrections can also only be made with a finite accuracy. One should therefore choose the number of correctors so that all of them give a significant improvement.

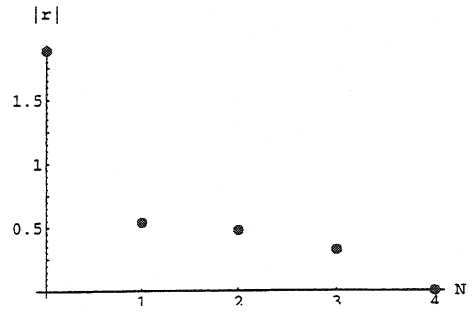

Figure 4.1: Plot of the residual vector norm versus number of correctors from a typical MICADO run.

Also, if the response matrix is a linear approximation, the number of neglected higher-order cross terms grows rapidly with the number of correctors. This is another reason to keep the number of correctors low.

It is unlikely that one will achieve a perfect match directly. However, if the correction results in a smaller error, a new measurement of $\mathbf{k}$ can be done and the procedure repeated until the mismatch is eliminated.

4.5 The Minimo Algorithm

The *MINIMO* algorithm is a modified version of *MICADO* proposed by Risselada [35]. *MICADO* starts out by finding the best single corrector, and then iteratively adds the optimal correctors to the chosen set. In each iteration, one corrector is thus added, and the time to find a correction using a subset of n correctors out of a total of N available is approximately proportional to $N^2n - Nn^2$.

The assumption made in the *MICADO* algorithm is that the optimal set of k correctors is a subset of the optimal set containing $k+1$ correctors This is not always true. It is in fact easy to construct counter-examples. The assumption is however a rather good approximation in most cases, and it significantly speeds up the algorithm.

MINIMO on the other hand, is a brute-force method. It checks all possible solutions, without assumptions. Since the number of possible subsets of a certain number of available correctors can be very large, this method is slow, and in some cases, utterly useless because of the combinatorial growth of computation time. In fact, the time needed to find a correction containing n out of N correctors is approximately proportional to $\binom{n}{N}$. However, in some specific applications the number of available correctors can be rather small. Thus the computation time is acceptable, and *MINIMO* can be considered as an option. For this reason, *MINIMO* has been implemented in *Mathematica* (see Appendix A.1.2).

4.6 A New 'Hybrid' Algorithm

When it comes to the choice of optimisation algorithm, the community of Accelerator Physicists is currently strongly divided. Some prefer *MICADO*, because it effectively limits the number of correctors. Others prefer to use SVD for all corrections, because sometimes *MICADO* proposes unrealistically large corrections on individual magnets. However, it is possible to combine the best of the two algorithms.

The main advantage of the *MICADO* algorithm is that it solves the problem using only correctors that give a significant effect. On the other hand, as mentioned above, in some cases *MICADO* proposes very large corrections. This is most probably due to small singular values in the response matrix, which the least square method does not suppress. By simply replacing the least square method in *MICADO* with an SVD-based matrix inversion (as previously described), these problems can be avoided. An implementation of such an algorithm has been made (see Appendix A.1.1). It has the advantages of

- Avoiding null-space corrections (a property of both *MICADO* and SVD).
- Avoiding near-to-null-space corrections (a property of SVD).
- Choosing only a small number of correctors (a property of *MICADO*).

Comparing these properties to the wish list in Section 4.1 shows that this is a good option for a general purpose correction algorithm.

Chapter 5

The Measurement Problem

5.1 Measurement Accuracy

The ultimate limit to what can be corrected is given by what the measurement systems can detect. Most of the measurement systems in the PS complex were built for large, high intensity beams. It is therefore not obvious that they will perform well for the much smaller LHC beam.

As always, both statistic and systematic errors contribute to the total error. When the beam is stable, the statistic errors are usually very small, which can give the false feeling that the total error is also small. However, the systematic errors can be quite large, and are in the case of accelerator diagnostics usually poorly investigated and understood. These errors can be grouped as

- propagated errors due to incorrect input parameters (such as optical parameters).
- errors due to incorrect data treatment (eg. very elaborate fit or data smoothing schemes).
- errors due to software and hardware bugs.

The first group is fairly easy to estimate using standard error propagation formulas, since the errors in the input parameters and the calibration error can be at least roughly estimated. The rest of the errors are more problematic since they are hidden. They can not be easily estimated unless they are detected, and if they are detected they are immediately corrected. Thus, as soon as one gets a handle of the error-bars, the situation changes and the estimation is no longer valid. However, the error should decrease with every bug found.

During the work presented in here, several such errors have been detected and subsequently corrected. Many of the problems encountered has been specific for small beams, and have therefore not been detected with the larger beams mainly used before. However, this calls for caution when interpreting early measurements of small LHC-type beams.

A series of studies have been made to compare different measurement devices for emittance measurements [36]. The idea behind being that if conceptually different measurement techniques gives an overall agreement, some confidence can be put into the result.

Disagreeing result, on the other hand, shows that improvements and further studies are needed.

5.2 SEM Grid Measurement

SEM grids and harps are destructive or semi-destructive depending on beam energy. They are usually used in triplets for emittance measurement purposes. In this way they can provide three independent measurements of the beam width. If there is no dispersion, these widths are connected to the emittance by

$$\sigma_\beta = \sqrt{\epsilon\beta_i}, \qquad i = 1, 2, 3 \tag{5.1}$$

where the relations between the β_is can be derived the propagation formula for Twiss functions given in Eq. (3.4). If the grids are separated only by drifts, the transfer matrix is exactly known, and the accuracy of the measurement is thus limited only by the accuracy measurement of the beam width. If there are magnets present between the monitors, there will be an extra error contribution due to the limited accuracy in the knowledge of the transfer matrix.

5.2.1 Processing of the Raw Data

The parameter which should be derived from the measured profile in order to deduce the emittance is the beam width σ. If the resolution of the measurement is high enough the discrete statistical formula

$$\sigma^2 = \frac{\sum\limits_i x_i^2 \rho_i}{\sum\limits_i \rho_i} - \left(\frac{\sum\limits_i x_i \rho_i}{\sum\limits_i \rho_i} \right)^2 \tag{5.2}$$

can be used. However, the profiles are often noisy, and even small tails can falsify the result due to the high weight they are given in the formula. Therefore, some kind of data treatment is often nessecary. This will involve suppression of baseline and obviously erroneous data points and/or the fitting of some curve to the data.

One should bear in mind that it is very easy to falsify the results by using very elaborate fitting schemes, and the fitting should therefore preferably be based on simple physical principles. If for example there are physical reasons to assume that the beam has a near-Gaussian distribution, it is probably best to restrict the fit to a Gaussian curve. A Gaussian fit reduces the N measured points to three or four parameters (mean position, width, baseline and maybe slope of baseline) and is therefore very over-constrained. This reduces the influence of noise on the profiles.

A spline interpolation on the other hand is under-constrained. For example, a cubic spline on N data points has $3N$ free parameters but only $3N - 4$ constraints. Thus, by

definition a spline matches any data set perfectly. It is therefore not useful for suppressing noise in the profiles.

The default fitting routine for the PS SEM-grids is an approximative spline fit, where the perfect fit to the data points is traded for a small second derivative such that the resulting spline function $y(x)$ minimises.

$$\xi = \sum_i \left(y(x_i) - y_i\right)^2 + \alpha \left(y''(x_i)\right)^2, \tag{5.3}$$

where y_i are the measured values at wire i, and Δx is the wire spacing. With the extra condition that the second derivative should be small, this approximative spline interpolation has $4N - 4$ constraints and is over-determined, thus qualifying for the name "fit".

The approximative spline has a free parameter which gives the relative weight between second derivative and the fit error. It has been found experimentally that the beam width resulting from the fit is very dependent on the parameter choice, especially in the case of small profiles. In fact, for LHC type profiles it was possible to change the measured emittance by a factor 10 just by changing this fitting parameter.

Another problem with the approximative spline is that there is nothing in the routine that suppresses noisy tails. A baseline can be subtracted, but the noisy tails are just smoothed out, and not removed. A Gaussian fit resolves this, since the tails of a Gaussian curve are rapidly approaching zero.

An alternative way to get around the problem with noisy tails is to use the Koziol method[37], where the discrete statistical formula is used only on the core of the distribution, and the this truncated result is corrected assuming Gaussian tails. The core is defined as the part of the profile where the signal is larger than a certain cut-off, which is a free parameter.

5.2.2 Correction for Dispersive Effects

If the measurement is not performed in a non-dispersive region, the dispersive effects have to be accounted for. In the presence of dispersion, the physical beam profile is not only given by the betatron amplitude distribution, but has an extra contribution due to the momentum spread σ_p of the beam.

$$\sigma^2 = \sigma_\beta^2 + D^2\sigma_p^2 \tag{5.4}$$

where σ_p is the momentum spread, D is the dispersion and σ_β is the pure betatronic width of the beam. The formula can easily be inverted to calculate the betatronic width from the measured width, but it is obvious that if the dispersive term is large, it is important to accurately measure both the momentum spread and the dispersion function in order to get an accurate final result.

5.3 Wire-Scanner

A wire scanner is a device that rapidly passes a wire through the beam, while measuring either the Secondary Emission (SEM) signal on the wire itself or the shower of secondary particles produced. The signal as a function of wire position gives the beam profile. The spatial resolution of the measured profile is generally very high, and thus the derivation of the beam width (using Koziol's method) poses no problem. The time it takes for the wire to pass through the beam is of the order of 10^3 machine turns, and thus the beam has to be stable during that time. The main error source is the limited knowledge of the betatron function at the grid which is used to calculate the emittance from the beam. This error is of the order of 10%, and translates to the same error in the emittance.

5.4 BeamScope

The principle of the BeamScope is to scrape off the beam by moving it into an aperture limitation using a closed orbit bump. By recording the current as a function of bump amplitude, the betatron amplitude distribution can be derived. From the betatron amplitude one can then calculate the emittance. The advantage of the method is that the betatron amplitude distribution in fact contains more information than just the beam profile. The main drawbacks are that many parameters influence the measurements, since the bump amplitude is calculated from measured currents on the bumper magnets, which has to be corrected for remanence and magnetic calibration factors. Correction for dispersion is also non-trivial.

5.5 Foreseen Improvements and New Methods

There is a general agreement [38] that no present emittance measurement device has a higher absolute accuracy than about 10%. This is the same level as the allowed increment of emittance at each machine interface in the LHC injector chain. Thus, compliance with the emittance budget can not be verified by comparing two different emittance measurements.

There is a possible way around this, however. By detecting the cause of the emittance blow-up rather than the blow-up itself, a higher accuracy can be achieved. In the case of injection mismatch, this can be done by detecting, and correcting, beam position and width oscillation at injection. The beam position can be measured with a standard pick-up, but the beam width is not easy to measure on a turn-by-turn basis. Two possibilities for this are considered:

- a multi-turn profile monitor and
- a quadrupole pick-up.

The first method consists of putting a profile monitor (eg a SEM grid) in the path of the circulating beam. By reading out the beam size on a turn-by-turn basis, the betatron

mismatch can be deduced. The advantage of this method is that one does not only measure the width of the beam, but the actual beam profile which contains extra information that can be useful. The disadvantage is the the grid itself causes beam blow-up, and therefore the beam has to be dumped after some hundred turns. In addition, in a machine like the PS, which simultaneously serves several users, the presence of the grid blocks all other users. This method can therefore not be used in the production of the LHC beam.

The second method is non-invasive. Quadrupole pick-ups have been tested in several places with varying success, and their major problems and advantages are fairly well known [39][40]. The basic idea is to measure the lowest-order non-linear term in the signal induced on each pick-up electrode, since this term is proportional to

$$s_Q \propto < x^2 > - < y^2 >= \sigma_x^2 + \overline{x}^2 - \sigma_y^2 - \overline{y}^2 \tag{5.5}$$

In particular, if the beam is centred in the pick-up the signal is proportional to the aspect ratio $\sigma_x^2 - \sigma_y^2$ of the beam.

The most attractive thing with such a pick-up is of course that it is totally non-destructive. The main problem is that the non-linear term is extremely small compared the linear (beam position) and constant (beam intensity) terms. Therefore, a very high common mode rejection ratio (CMRR) is required in the signal treatment.

Another problem is the $\overline{x}^2 - \overline{y}^2$ term in the signal. In order to keep this term small, the beam always has to be relatively well centred when using a quadrupole pick-up. This is, however, generally a minor problem since beam steering is a semi-automated procedure.

The third and last of the major problems is that the horizontal and vertical beam widths can not be extracted separately, but only the differences between the two. Therefore, more than one pick-up is needed to disentangle the two moments. In the case of injection mismatch detection, this problem can be circumvented since one is looking for an oscillation in the horizontal and vertical width. The frequency of these oscillations are given by the tune in the respective planes, and since these are generally different the signals can be separated using FFT analysis.

To cope with the first problem, which is the most tricky one, a new quadrupole pick-up design have been made [41]. Using magnetic coupling instead of electrostatic, the pick-up can be built such that the usually dominating constant (intensity) term is no longer present at the output. The development of a detection system built on this idea is well underway and will be the subject of the authors doctoral thesis.

Chapter 6

Tests and Measurements

6.1 Betatron Matching

In order to test the validity of the correction scheme described in the previous section, matching tests have been performed at several occasions[42], using a LHC-type proton beam from the PS Booster.

The Twiss parameters of the beam from the Booster can be measured either using the three SEM-grids in the Booster measurement line, or the three SEM-grids in the CPS ring (see Fig. 6.1). Both measurement systems have advantages and disadvantages. In the measurement line, it is necessary to have different quadrupole settings depending on if the measurement is performed in the vertical or horizontal plane. This is to achieve the required 60° phase advance between the grids. In the CPS ring, this is not a problem. However, to be able to do a three-SEM-grid measurement in the CPS ring the beam has to be dumped before it has made a full turn in the machine. The dump used for this is simply a target placed in the beam path. This means that the CPS is blocked during the measurement, and cannot deliver beam to anyone else. Thus, the measurements has to be done on dedicated machine time. This reduces the number of measurements that can be done.

All the tests were carried out by first measuring the Twiss parameters, and calculate the corrections needed to reach the nominal parameters. Then, the calculated corrections were tested using different numbers of correctors. The results were then compared with the prediction.

Most of the measurements have been performed in the Booster measurement line. Because of the different quadrupole settings for horizontal and vertical measurement, the effect could not be measured in both planes. Therefore, only the horizontal plane was measured and the algorithm was restricted to keep the vertical Twiss parameters constant (This was found to give better results than just neglecting the vertical effect). Some of the results of the measurements are shown in Fig. 6.2. In all the tested cases, the mismatch decreased significantly at least for the first few correctors.

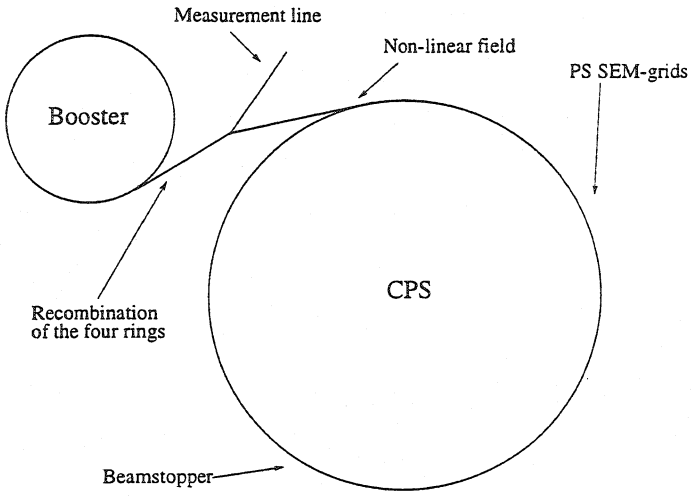

Figure 6.1: Schematic picture of the CPS and the Booster, showing the positions of the measurement equipment.

To be able to measure and correct both planes at the same time, measurements have been performed using three SEM-grids in the CPS ring. These SEM-grids are placed so that the quadrupole settings can be the same for both horizontal and vertical measurement. Here, some problems were encountered in the construction of the correction matrix. At injection to the CPS, the beam from the Booster passes through a rather strong stray field (Fig 6.1), caused by one of the CPS main magnets. This field is non-linear and hard to model, since it has not been thoroughly studied. Thus, some approximations had to be done in order to construct the correction matrix.

The values necessary to calculate the matrix is the β at the quadrupoles, as well as the phase advance from the quadrupoles to the SEM-grids. The β-values could be calculated from the existing model, since all the quadrupoles in the transfer line are upstream of the non-linear region. But the phase advance is affected by the stray-field. A rough estimate was made by neglecting the additional phase advance due to the stray field, since it should be rather small, and assuming that the beam was matched to the CPS after passing through the non-linear section, thus permitting us to use the ring lattice phase advance from the injection point to the SEM-grids. Adding up these partial phase advances gave an estimate of the real phase advance. Direct measurements of some of the columns in this matrix showed that these approximations worked.

The results from one of the matching tests are shown in Fig. 6.3. For one and two correctors, the measured result is almost the same as the linear prediction. There is a big difference at three correctors. The second order-terms predict this to some extent, but that there is also an additional deviation, probably caused by errors in the correction matrix. Even if the agreement prediction-measurement is not total, the result is anyway very useful since the mismatch could be reduced by about two-thirds using two correctors. Also it can be seen that up to five correctors could be used, but that the effect is small and sometimes

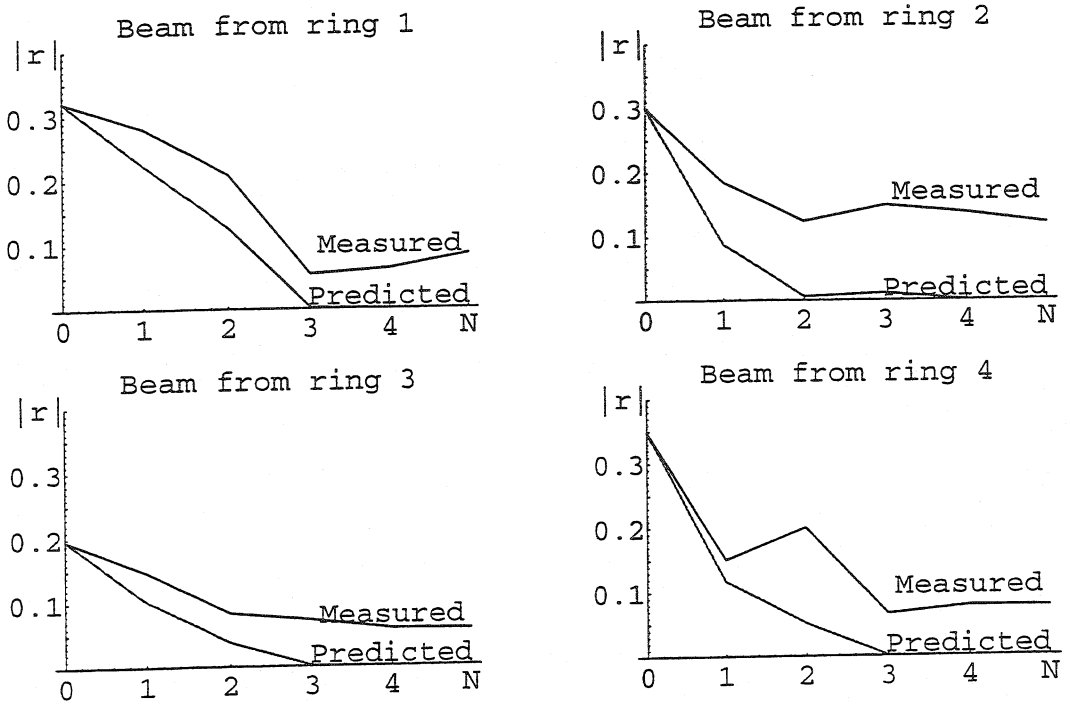

Figure 6.2: Plot of some of the results in the measurement line. Norm of the mismatch vector $\mathbf{k}$*, as a function of of the number of correctors.*

negative after the two first, as expected from the theoretical discussion.

Due to the optical differences between the beams from the four Booster rings[1], one should not match one of the beams perfectly to the CPS, but rather try to distribute the mismatch over the four beams in such a way that the total emittance blow-up is reduced.

Tests have been performed to use a super-matrix, including the effect of all the four beams. This matrix is constructed by stacking individual matrices on top of each other just as the horizontal and vertical effects were added to one matrix. The mismatch vector $\mathbf{k}$ has 16 components in this case. In the tested case this method gave a decreased mismatch for the first corrector only (Fig 6.4). By iterating the correction procedure, the method is expected to work anyway, but to prove this more tests have to be done.

To show that the mismatch could actually be further decreased by an iterative procedure, some tests were performed both in the measurement line and the CPS. It was found in all the tested cases that the mismatch vector could be be reduced to about 0.1, which is in the order of the measurement error. This corresponds to an increase in the RMS emittance of about 0.5%. One of the measurements are shown in Fig. 6.5.

[1]Even if the proposed corrector quadrupole mentioned earlier is installed, there are still small differences between the rings.

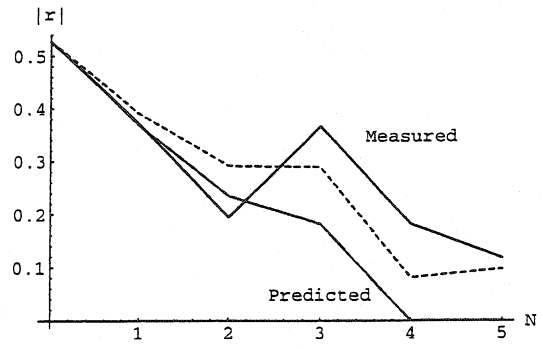

Figure 6.3: Result of measurement in the CPS. Norm of the mismatch vector $\mathbf{k}$*, as a function of of the number of correctors. The dotted line shows the calculated values when the second order terms are taken into account.*

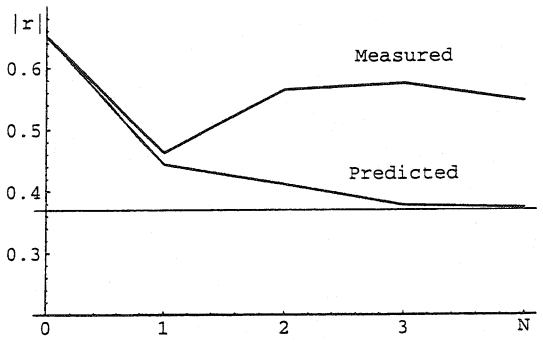

Figure 6.4: Plot of the results using a global matrix. Norm of the mismatch vector $\mathbf{k}$*, as a function of the number of correctors. The horizontal line shows the lower limit of the mismatch due to the differences between the rings*

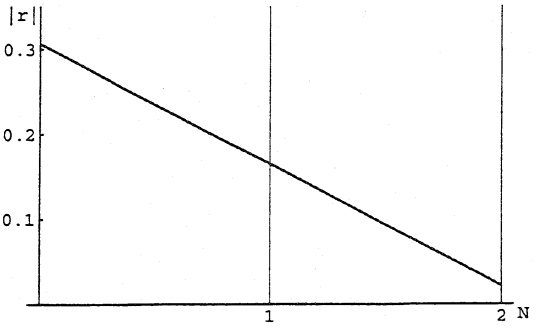

Figure 6.5: Result of iterative MICADO correction. In each iteration, the Twiss parameters are measured and a MICADO correction applied. The norm of the mismatch vector $\mathbf{k}$ *after each iteration is shown. In this case two iterations was enough to bring the mismatch down to practically zero.*

6.2 Combined Betatron and Dispersion Matching

6.2.1 Validation by Simulations

Since the validation measurements are time-consuming and at least semi-destructive, simulations have been performed to test the method for combined dispersion and betatron matching, and to quantify the difference between *MICADO* and *MINIMO*. It is not obvious how to compare the convergence properties of the two algorithms, because in reality an operator would be supervising the minimisation process and controlling it. The chosen strategy consists of making a number of simulations with random initial errors, binning the simulation results according to the size of the initial error and plotting for each bin the average residual error as a function of both the number of correctors used in each iteration, and the number of iterations. All the simulations were carried out on the model of the same transfer line used to perform the real measurements [43]. The results show no significant difference between the two algorithms for small and moderate initial errors (Figs. 6.6 and 6.7).

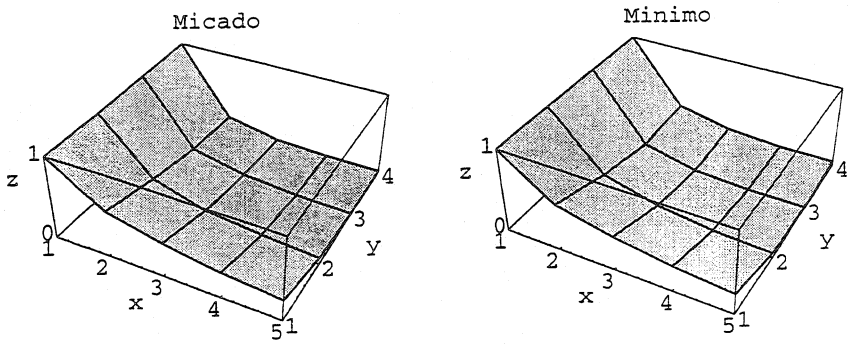

Figure 6.6: Simulation results averaged over 45 seeds. The initial RMS error belongs to the interval [0.2,0.4]. The vertical axes represents the average residual RMS error normalised by the initial RMS error, the x axes the iteration number, the y axes the number of correctors used in each iteration.

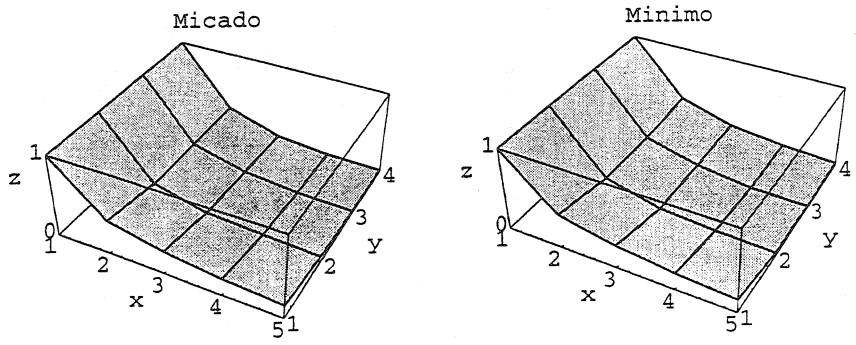

Figure 6.7: Simulation results averaged over 17 seeds. The initial RMS error belongs to the interval [1.0,1.2]. The axes are the same as in Fig. 6.6.

6.2.2 Validation by Measurements

The experimental validation of the optimisation scheme was performed in steps. In all cases the optical parameters was first measured, then an error was introduced on one or several quadrupoles, and *MICADO* or *MINIMO* was used to try to recover the initial values. First, the result of the proposed corrections was measured for different number of correctors, and compared to the linear prediction supplied by *MICADO* and *MINIMO*. The results are shown in Fig. 6.8 and Fig. 6.9 and show a fairly good agreement between measurement and prediction.

Then test were made to iteratively reduce the error down to zero. The results, using one corrector per iteration are shown in Fig. 6.10. In the case of one corrector per iteration, *MICADO* and *MINIMO* always give the same result. A test using three correctors per iteration was made to try to see a difference between the two algorithms, but no significant difference was found (see Figs. 6.11 and 6.12).

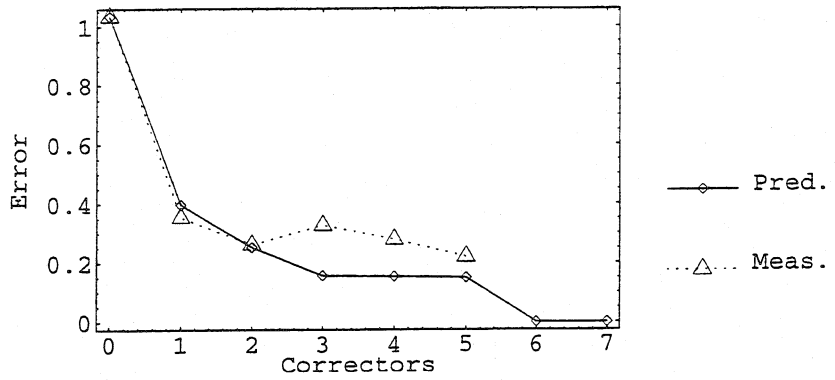

Figure 6.8: The measured correction result and the MICADO prediction for a random initial error are shown as a function of the number of correctors used.

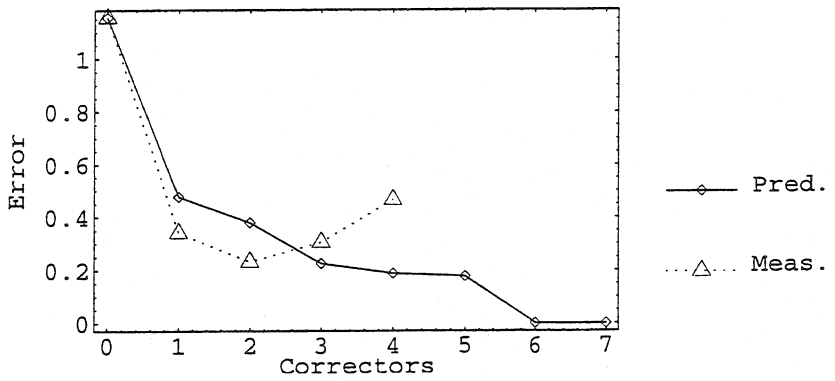

Figure 6.9: The measured correction result and the MINIMO prediction for a random initial error are shown as a function of the number of correctors used.

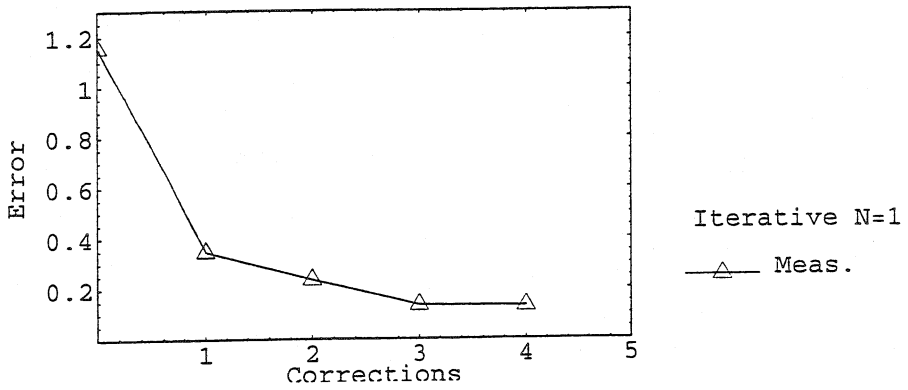

Figure 6.10: The measured correction result and the MICADO prediction for a random initial error are shown as a function of the number of correctors used.

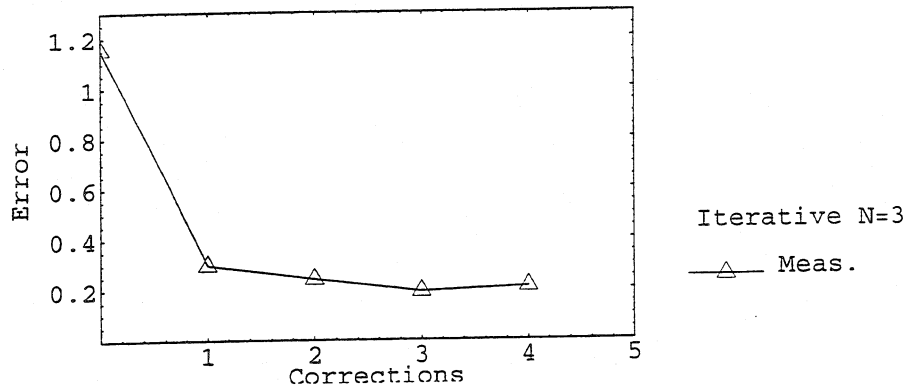

Figure 6.11: The measured correction result and the MICADO prediction for a random initial error are shown as a function of the number of correctors used.

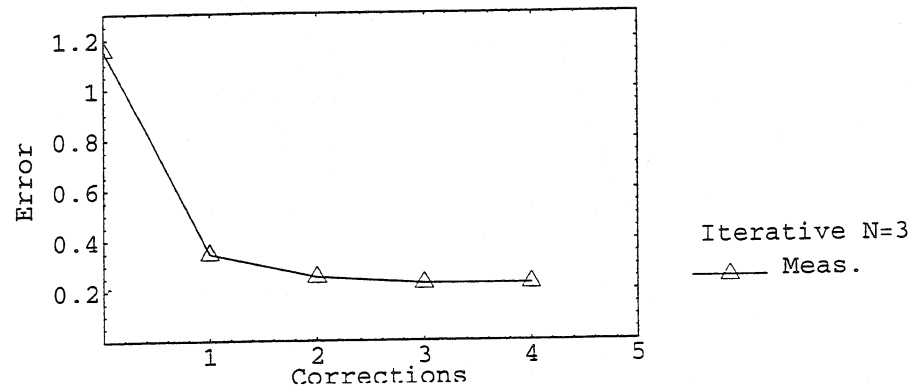

Figure 6.12: The measured correction result and the MINIMO prediction for a random initial error are shown as a function of the number of correctors used.

Chapter 7

Summary

7.1 Transfer Line Optics

A thorough study of the Booster-PS transfer line has pinpointed several emittance blow-up sources. Two of these are static in the sense that they are not due to fluctuations but to the design of the line. The optical differences between the beams from the four Booster rings, which are due to the edge-focusing of the big rectangular bending magnets in the vertical recombination scheme, are expected to cause a emittance increase of up to 5%, depending on which Booster ring is being considered. This can be corrected by adding a corrector quadrupole to the line.

Another static source of emittance blow-up is the dispersion mismatch at injection to the PS. Without correction, this would cause a blow-up of up to 30% to the LHC beam, due to its large momentum spread. To correct this, the optics of the line has to be changed.

7.2 Correction Schemes and Algorithms

The dynamic sources of blow-up, caused by fluctuations in power supplies and other equipment, will be handled by continuously monitoring and correcting. For this, correction schemes based on theoretical response matrices and a linear equations solver will be used.

Response matrices have been derived and verified experimentally for correction of all the injection errors that are expected to be relevant for emittance preservation in view of the LHC beam. For beam steering, this was the case since before, but as a part of the work presented here also betatron and dispersion matching have been developed.

Some new algorithms for solving the resulting linear system have been tested, although it has not been possible to prove that they perform much better than the *MICADO* solver, which is used as standard in the generic application program developed for the the PS control room.

A hybrid algorithm, combining the best of *MICADO* and SVD has been proposed and implemented. It is expected to perform better than *MICADO* alone, although this has not been experimentally proven.

7.3 Conclusions

In this work, correction methods are described to cope with all the different injection errors that are expected to be relevant for the LHC beam. Experimental tests have shown that these methods are able to correct the error down to the accuracy level of the measurement.

However, the absolute accuracy of the present emittance measurement devices are rather poor when seen in the light of the LHC emittance budget. Efforts should therefore be directed towards new and improved methods to measure matching and emittance.

Appendix A

Mathematica Functions

During the work described in this report, a many *Mathematica* functions have been written in order to implement algorithms, facilitate response matrix calculations etc. Most of these have been included in the Mathematica package *BeamOptics*, which is a general tool for accelerator optics calculations. A full manual for *BeamOptics* can be found in [20]. Here, some of the additional functions are described.

A.1 Implementations of Algorithms

A.1.1 Hybrid SVD/Micado Algorithm

A hybrid algorithm combining the best of SVD and *MICADO* has been implemented in *Mathematica*. The implementation of the function is based on the original *MICADO* implementation in the *BeamOptics* package by B. Autin, and the new function has also been incorporated in this package. Only minor changes was necessary to implement the SVD functionality in the existing code. The new function has retained the name *MICADO*, but the extra option `Tolerance` has been added. The value of this option specifies which singular values are to be discarded. Inside the function, the option is passed on to the *Mathematica* internal function `PseudoInverse` which implements the SVD matrix inversion. The default value for `Tolerance` is such that calling *MICADO* without specifying the option gives the standard *MICADO* result. The function call is

```
Micado[matrix, vector, iterations, Tolerance->t]
```

The definition of `Tolerance` is such that singular values smaller than `t` times the larges singular value are suppressed.

The *Mathematica* code is listed below (the functions `Move` and `MoveColumn` are *BeamOptics* functions that have not been modified are included in the listing just for clarity).

```
(* MICADO *)
(* Original version by B. Autin. *)
(* Revised (option Tolerance added) by A. Jansson. *)

Clear[Move]
Move[f_[x__],i1_,i2_]:=
Block[{y,y1},
      y=f[x];
      y1=Drop[y,{i1}];
      Insert[y1,y[[i1]],i2]
     ]

Clear[MoveColumn]
MoveColumn[a_?MatrixQ,i1_,i2_]:=
Block[{a0,a1,a2},
      a0=Transpose[a];
      a1=Drop[a0,{i1}];
      a2=Insert[a1,a0[[i1]],i2];
      Transpose[a2]
     ]

Clear[Residual];
Residual[a_?MatrixQ,b_?VectorQ, opts___Rule]:=
Block[{a1,a2,a3,n,op,r,x},
      a1=PseudoInverse[a, FilterOptions[PseudoInverse,opts]];
      If[Length[a]===1,{a2,a3}=Flatten/@{a,a1};op=Times,
                              {a2,a3}={a,a1};op=Dot];
      x=-a3.b;
      r=op[a2,x]+b;
      n=r.r;
      {x,n,r}
     ];

Options[Residual]=Options[PseudoInverse];

Clear[Micado]
Micado[a_?MatrixQ,b_?VectorQ,iter_Integer,opt___Rule]:=
Block[{a0,a1,cr,df,g,l0,l1,minnorm,n,norm,n0,n1,n2,pos,r,
       sol,sol1,var,x,y},
     df=DisplayFunction/.{opt}/.Options[Graphics];
```

```
    a0=Transpose[a];
    n=Length[a0];
    var=Variables/.{opt}/.Options[Micado];
    l0=If[var===Automatic,Range[n],var];
    a1=a0;
    l1=l0;
    sol=
     Table[
      a2=Table[Transpose[Take[Move[a1,i,k],k]],{i,k,n}];
      r=Residual[#,b, FilterOptions[Residual,opt]]&/@a2;
      norm=Table[r[[i,2]],{i,Length[a2]}];
      minnorm=Min[norm];
      pos= Flatten[Position[norm,minnorm]][[1]] ;
      x=r[[pos,1]];
      y=r[[pos,3]];
      pos=pos+k-1;
      a1=Move[a1,pos,k];
      l1=Move[l1,pos,k];
      cr=Thread[Rule[Take[l1,k],x]];
      {Correction->cr,ResidualVector->y,Norm->minnorm},
     {k,iter}] ;
    If[df===Identity,
    sol,
    n0=Prepend[Range[iter],0];
    n1=Prepend[Norm/.sol,b.b];
    n2=Transpose[{n0,n1}];
    g= ListPlot[n2,FilterOptions[Graphics,opt],
         PlotStyle->{Red,PointSize[.025]},AxesLabel->{"n","norm"},
         Ticks->{n0,Automatic}];
    Append[sol,OpticsPlot->g]
      ]
    ]

Options[Micado]={DisplayFunction->$DisplayFunction, Variables->Automatic,
    Tolerance->Automatic}
```

A.1.2 Minimo

An implementation of *MINIMO* have been made in *Mathematica* to enable comparison with *MICADO*. The function call is

```
Minimo[matrix, vector, iterations, options]
```

which is the same as for the *MICADO* function. The option `Tolerance` has been implemented also for *MINIMO* to enable the suppression of small singular values using SVD.

Since *MINIMO* actually should check all possible sets of correctors consisting of smaller than a given value, the *Mathematica* internal function `KSubsets` is employed, to ensure the correct combinatorics. Also since the computing time rises rapidly with the number of available correctors, an estimation of the computing time is made prior to the actual calculation, and the function returns an error message if the estimated time is too long.

The *Mathematica* code is as follows:

```
(* MINIMO *)
(* Implemented by A. Jansson *)
(* Code based on MICADO by B. Autin *)

Clear[MinimoIterations];
MinimoIterations[corr,iter]:=Sum[Binomial[corr,i],{i,1,iter}];

Clear[Minimo];
Minimo[a_?MatrixQ,b_?VectorQ,iter_Integer,opts___Rule]:=
Module[{df,a0,var,l0,corrn,sol,subc,suba,r,norm,minnorm,x,y,cr,n0,n2,g},
     df=DisplayFunction/.{opts,Sequence@@Options[Graphics]};
     a0=Transpose[a];
     var=Variables/.{opts,Sequence@@Options[Micado]};
     corrn=Range@Last@Dimensions[a];
     l0=If[var===Automatic,Range[Length[corrn]],var];
     If[MinimoIterations[corrn, iter]
       >(MaxIterations/.Join[opts,Options[Minimo]]),
      Message[Minimo::iter];Return[]];
     sol=Table[
      subc=KSubsets[corrn,k];
      suba=Transpose[a0[[#]]]&/@subc;
      r=Residual[#,b, FilterOptions[Residual,opts]]&/@suba;
      norm=#[[2]]&/@r;
      minnorm=Min[norm];
      pos= First@Flatten[Position[norm,minnorm]] ;
      x=r[[pos,1]];
      y=r[[pos,3]];
      cr=Thread[Rule[l0[[subc[[pos]] ]],x]];
```

```
      {Correction->cr,ResidualVector->y,Norm->minnorm},
     {k,1,iter}];
     If[df===Identity,sol,
     n0=Prepend[Range[iter],0];
     n1=Prepend[Norm/.sol,b.b];
     n2=Transpose[{n0,n1}];
     g= ListPlot[n2,FilterOptions[Graphics,opts],
          PlotStyle->{RGBColor[1,0,0],PointSize[.025]},
          AxesLabel->{"n","norm"},Ticks->{n0,Automatic}];
     Append[sol,OpticsPlot->g]]
]
Options[Minimo]=
     {DisplayFunction->$DisplayFunction, Variables->Automatic,
      Tolerance->Automatic, MaxIterations->10000};
```

A.2 Response Matrix Calculation

A.2.1 Response Matrix for Twiss Matching

A function to facilitate the calculation of the response matrix used for Twiss Matching has been implemented and included in *BeamOptics*. The syntax is

```
MatchingMatrix[channel,twisshor,twissver, corr, monhor, monver]
```

where `channel` is the *BeamOptics* model of the line, `twisshor` and `twissver` are the Twiss parameters at the entry and `corr`, `monhor` and `monver` are lists containing the positions of corrector quadrupoles and monitors (horizontal and vertical).

The function returns a response matrix where the columns correspond to the correctors in the list (in order of appearance) and the rows corresponds to the monitors. There are two rows per monitor, corresponding to the two components of the mismatch vector in Eq. (1.7). The horizontal monitors are listed first and the vertical follows.

The *Mathematica* code for the function relies heavily on other *BeamOptics* functions not described here, and is therefore not listed.

A.2.2 Response Matrix for Dispersion Matching

As for the Twiss matching, a function for the calculation of the response matrix used for Dispersion Matching has been implemented and included in *BeamOptics*. The syntax here is

```
DispersionMatrix[channel,twiss,dispersion, corr, mon]
```

where again `channel` is the *BeamOptics* model of the line, `twiss` the Twiss parameters at the entry and `corr` and `mon` are lists containing the positions of corrector quadrupoles and

monitors. Only one plane is considered, since in general dispersion is only present in the horizontal plane.

The function returns a response matrix where the columns correspond to the correctors in the list (in order of appearance) and the rows corresponds to the monitors. Again, there are two rows per monitor, corresponding to the two components of the dispersion error vector in Eq. (1.8).

The *Mathematica* code is not given here for the same reasons as for the case of the `MatchingMatrix` function.

A.2.3 Combined Dispersion and Twiss Parameter Matching

If the same list of correctors is used, the results of `MatchingMatrix` and `DispersionMatrix` can be joined to achieve a matrix that can be used for combined betatron and dispersion matching. The *Mathematica* command for joining two such matrices is simply

```
Join[matchingmatrix, dispersionmatrix]
```

References

[1] F. Willeke. Report on the Working Group on Emittance Preservation. In E. Keil [44].

[2] J. Gareyte. Requirements of the LHC on its injectors. In E. Keil [44].

[3] J.B. Jeanneret, D. Leroy, L. Oberli, and T. Trenkler. Quench levels and transient beam losses in LHC magnets. LHC Project Report 44, CERN, 1996.

[4] H. Goldstein. *Classical mechanics.* Addison-Wesley, 2nd edition, 1980.

[5] K. Schindl. Space charge. In S. Turner, editor, *Proceedings of CERN accelerator school: Beam measurement*, Montreux, Switzerland, 1998.

[6] A. Sorensen. Introduction to intrabeam scattering. In S. Turner, editor, *Proceedings of CERN accelerator school*, CERN Yellow Report, Aarhus, 1986. CERN 87-10.

[7] J.-L. Laclare. Coasting beam longitudinal instabilities. In Turner [45]. CERN 94-01.

[8] J.-L. Laclare. Coasting beam transverse instabilities. In Turner [45]. CERN 94-01.

[9] D.A. Edwards and M.J, Syphers. *An introduction to the physics of high energy accelerators.* Wiley, 1993.

[10] R.P. Walker. Radiation damping. In Turner [45]. CERN 94-01.

[11] K. Schindl. The PS Booster ans pre-injector for the LHC. In E. Keil [44].

[12] M. Martini. Definitions of emittance. In R. Cappi [26]. PS/DI/Note 98-03.

[13] P.M. Lapostolle. Possible emittance increase through filamentation due to space charge in continuous beams. In *Proceedings of the 1971 Particle Accelerator Conference, PAC'71*, volume 18 of *IEEE Trans. Nucl. Sci.*, pages 1101–1014, Chicago, USA, 1971.

[14] B. Autin, F. Di Maio, M. Gourber-Pace, and M. Lindroos. Database for accelerator optics. In *Proceedings of the 1997 International Conference on Accelerator and Large Experimental Physics control systems, ICALEPCS'97* [46].

[15] B. Autin et al. Automated beam optics correction for emittance preservation. In E. Keil [44].

[16] M. Arruat et al. Generic automated beam steering and shaping programs with an object oriented approach. In *Proceedings of the 1997 International Conference on Accelerator and Large Experimental Physics control systems, ICALEPCS'97* [46].

[17] J.P. Delahaye. La recombinasion des faiceaus issus des quatre anneaux du CERN PS Booster. Internal Note, CERN, 1979. PS/BR Note 79-12.

[18] J.P. Delahaye, A. Nicoud, and J.P. Riunaud. Difference d'adaptation entre anneaux Booster a l'injection PS, MD du 22-03-78. Internal Note, CERN, 1978.

[19] S. Wolfram. *Mathematica-a system for doing mathematics by computer.* Addison-Wesley, 1991.

[20] B. Autin et al. BeamOptics: a program for analytical beam optics. Yellow report, CERN, 1998. CERN 98-06.

[21] K. Schindl. Private Communications.

[22] P. Bryant. WinAGILE. http://nicewww.cern.ch/~bryant.

[23] M. Arruat and M. Martini. The new standard method to measure emittances in the PS complex. Internal Report, CERN, 1992. PS/92-59.

[24] A. Jansson and M. Lindroos. Mismatch between the PSB and the CPS due to the present vertical recombination scheme. In E. Keil [44].

[25] A. Jansson, M. Lindroos, and K. Schindl. A study of emittance blow-up sources between the PS Booster and the CPS. In *Proceedings of the 1998 European Particle Accelerator Conference, EPAC'98*, 1998.

[26] R. Cappi, editor. *Proceedings of 4th ICFA beam dynamics mini-workshop on emittance preservation and measurement*, CERN internal note, CERN, Geneva, Switzerland, 1997. PS/DI/Note 98-03.

[27] A. Jansson. A simple way of reducing the PSB-CPS mismatch due to the vertical recombination scheme by using shims. Internal Note, CERN, 1997. PS/DI/Note 97-14.

[28] M.J. Barnes, G.S. Clark, and M. Sassowsky. 3 dimensional field calculations compared to magnetic measurements for CERN PSB-CPS transfer line magnets. In *Proceedings of the 1999 Particle Accelerator Conference, PAC'99* [47].

[29] M. Benedikt, A. Jansson, and M. Sassowsky. Proposal for a quadrupole correction magnet for the PS-Booster recombination section. Internal note, CERN, 1999. PS/OP/Note 99-18.

[30] M. Martini, T. Risselada, and K Schindl. Measurement of betatron and dispersion matching between Booster and PS. Internal Note, CERN, 1991. PS/PA/Note 91-13.

[31] B. Autin, G.H Hemelsoet, M.Martini, and E. Wildner. Automatic beam steering in the CERN PS complex. In *Proceedings of the 1995 Particle Accelerator Conference, PAC'95*, Dallas, USA, 1995.

[32] P. Bryant and K Johnsen. *The principles of circular accelerators and storage rings.* Cambridge University Press, 1993.

[33] Y. Baconnier. Contribution a l'etude de l'orbit fermee. Yellow report, CERN, 1965. CERN 65-95.

[34] B. Autin and Y. Marti. Closed orbit correction of AG machines using a small number of magnets. Internal report, CERN, 1973. ISR-MA/73-17.

[35] T. Risselada. An improved version of the orbit correction program ORBCOR. Internal Report, CERN, 1990. PS (PSR) 87-90.

[36] C. Carli, A. Jansson, M. Lindroos, and H. Schönauer. A comparative study of profiles and scrapings methods for emittance measurements in the PS Booster. *Particle Accelerators*, To be published.

[37] H. Koziol. Evaluation of near-Gaussian distributions with ill-defined tails. Internal Note, LANL, 1974. MP-3-74-1.

[38] H. Koziol and K. Wittenburg. Summary on transverse emittance measurements and instruments. In R. Cappi [26]. PS/DI/Note 98-03.

[39] R.H. Miller, J.E. Clendenin, M.B. James, and J.C. Sheppard. Non-intercepting emittance monitor. In *Proceedings of the XII High Energy Particle Accelerator Conference*, pages 602+, Chicago, USA, 1983.

[40] V. Chohan, F. Pedersen, S. van der Meer, and D.J. Willams. Measurement of coherent quadrupole oscillations at injection into the antiproton accumulator. In *Proceedings of the 1995 European Particle Accelerator Conference, EPAC'90*, Nice, France, 1990.

[41] A. Chapman-Hatchett, A. Jansson, and D.J. Williams. A quadrupole pick-up for the CERN PS. In *Proceedings of the 1999 Particle Accelerator Conference, PAC'99* [47].

[42] B. Autin et al. Emittance preservation in the PS complex. In *Proceedings of the 1997 Particle Accelerator Conference, PAC'97*, 1997.

[43] G. Arduini, M. Giovannozzi, K. Hanke, J.-Y. Hemery, and M. Martini. MAD and BeamOptics description of the TT2/TT10 transfer line - Part I: Optics without emittance exchange. Internal Note, CERN, 1998. PS/CA/Note 98-14.

[44] E. Keil, editor. *Proceedings of the workshop on LHC injectors, LHC'96*, volume 58 of *Particle Accelerators*, Montreux, Switzerland, 1997.

[45] S. Turner, editor. *Proceedings of CERN accelerator school fifth general accelerator physics course*, CERN Yellow Report, Jyväskylä, 1992. CERN 94-01.

[46] *Proceedings of the 1997 International Conference on Accelerator and Large Experimental Physics control systems, ICALEPCS'97*, 1997.

[47] *Proceedings of the 1997 Particle Accelerator Conference, PAC'99*, 1999.

Paper I

Mismatch between the PSB and CPS due to the present vertical recombination scheme

published in Particle Accelerators.

Particle Accelerators, 1997, Vol. 58, pp. 201–207
Reprints available directly from the publisher
Photocopying permitted by license only

MISMATCH BETWEEN THE PSB AND CPS DUE TO THE PRESENT VERTICAL RECOMBINATION SCHEME

A. JANSSON and M. LINDROOS *

CERN PS Division, Geneva 1211 23, Switzerland

(Received in final form 10 January 1997)

The production of the nominal LHC beam will demand optimum emittance preservation between individual machines in the injection chain. The edge effects at the entry and exit of the bending magnets used for the vertical recombination of the four PS booster rings to the level of the CPS results in a small un-compensated, and for each ring, different mismatch. We are here presenting recent measurements of the mismatch done in the PSB measurement line.

Keywords: Emittance preservation; Fringe fields

1 INTRODUCTION

The PS booster consists of four parallel, and on top of each other stacked, synchrotrons. The four rings share major elements but can considering correction, compensation, injection and ejection be individually controlled. The filling of the CPS is for most users done with sequential ejection of the four rings. Following ejection the particles from the four rings are brought together in a vertical recombination scheme (Figure 1) to the level of ring 3. The bending magnets used for the recombination are rectangular magnets resulting in some edge-effect contributions to the transverse optics. As this effect during the PSB design stage was foreseen to be of no importance no

* Corresponding author. Tel.: 41-22-767 3859. Fax: 41-22-767 9145.
E-mail: m.lindroos@cern.c.

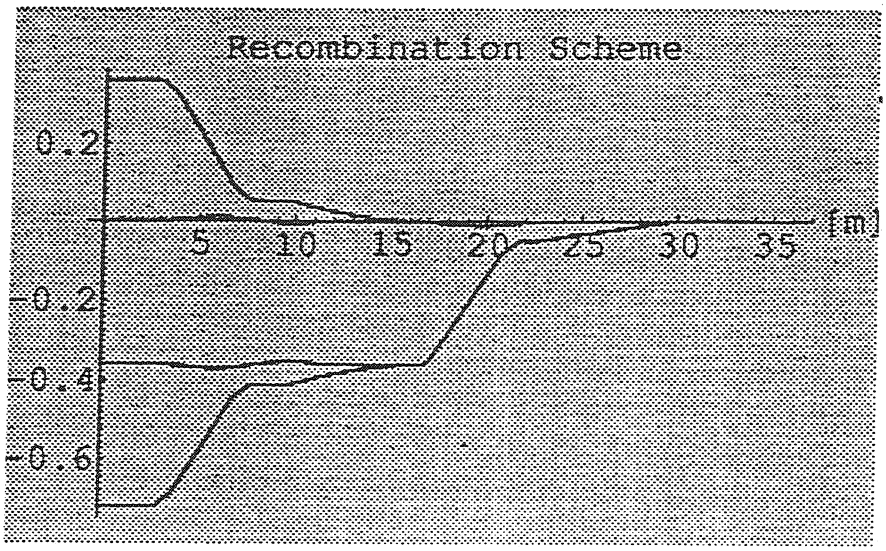

FIGURE 1 General layout of the present vertical recombination scheme in the P booster. The lines are numbered starting from the bottom.

elements for compensation of the differences between the individua rings were installed. An experimental study, in the PSB measuremen line, was performed by Delahaye *et al.*[1] already in 1978 and the effec was then considered sufficiently small to be ignored. However, th tight emittance budget enforced on the injector chain for the Larg Hadron Collider (LHC) beam and the resulting demand on goo emittance preservation between the individual machines has triggere us to take a new look at the problem. We will in this note presen new calculations of the nominal optics based on latest element con figuration. The calculations are compared to measurements done i the PSB measurement line and in the CPS.

2 PRESENT VERTICAL RECOMBINATION SCHEME

The recombination scheme[2] can be divided into three main parts. In the first part, the beam-lines from the lower two and the upper two rings are joined together. The recombination is done in a symmetrical manner and therefore one would expect the beams from ring one and four to have the same properties after recombination, and similarly for ring two and three. This symmetry, however, is broken

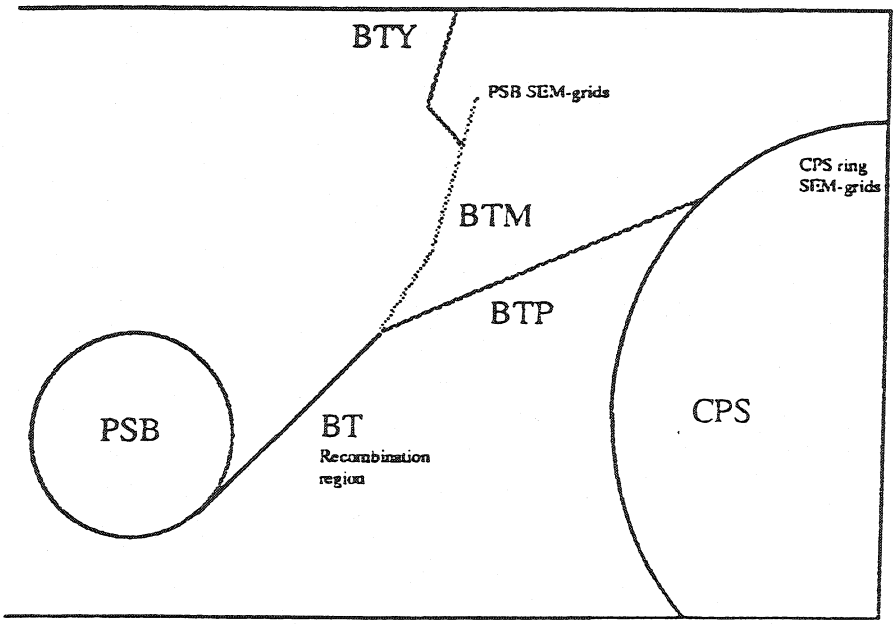

FIGURE 2 General layout of the tranferlines between Booster and CPS

in the next part of the recombination scheme, where the common beam-line from ring two and one is brought to the level of ring three and recombined. Because of this, the beam-lines from the four rings all have different optics. In the two first parts, the beam-lines are equipped with individual steering dipoles, while all the quadrupoles are common. Since the beams in general do not pass through the centre of the quadrupoles, they have a deflecting as well as a focusing effect. In the last part of the recombination scheme, the beams from the four rings are ideally following the same trajectory and this part can be considered as a general transfer line. From here the beam is sent to different destinations, either the CPS, ISOLDE, or the Booster measurement line. Depending on the destination, the settings of the quadrupoles in the last part varies, while the settings of the quadrupoles in the first parts are constant.

An important fact is that the present optics for the transfer line to the Booster measurement line is semi-empirical. To obtain maximum accuracy when measuring the beam with the three secondary emission grids (SEM-grids) in the line, one wants the beam to have a waist at the middle SEM-grid. Hence, the quadrupole settings were calculated in order to achieve this for the beam from ring three. However,

it was found when the new optics was tested, that the waist was slightly off-center. It was also found that this could be compensated for by changing the strength of the quadrupole BT.QNO40, the first quadrupole after the recombination. The change had to be made in different directions in order to compensate the horizontal or the vertical plane, and not in the same direction as would have been the case if the measured value of the integrated gradient versus current *gdl/I* was wrong for this quadrupole. This difference between theoretical prediction and measurements has not yet been properly explained.

2.1 Theoretical Optics

In a first attempt to understand the theoretical optics of the PSB recombination and transfer region we have modelled the recombination scheme using *BeamOptics*,[3] a beam optics package for Mathematica developed by B. Autin *et al.* at CERN. In the calculations, we have used a hard edge model of the magnets, taking into account the edge effects of all the dipoles and the off-axis quadrupoles. Also, we have corrected for the fact that the trajectory inside a bending magnet is slightly longer than the magnetic length of the magnet due to the fact that the beam follows a curved path.

The model has been verified for all beams using an alternative beam optics code. Removing the edge effect from the big bendings in the recombination region results in a very similar optics for the four beams as one would expect. The results using *BeamOptics* for the Twiss parameters at the first SEM-grid in the measurement line are shown in Table I.

The large differences observed in the horizontal plane are almost entirely a result of the horizontal quadrupolar effect at the entry and exit from the rectangular vertical bending magnets.

TABLE I Preliminary theoretical Twiss values deduced with the analytical beam optics program *BeamOptics*. The Twiss values are calculated at the first SEM-grid in the Booster measurement line for the actual settings of the quadrupoles

Plane	*Horizontal*				*Vertical*			
Ring	1	2	3	4	1	2	3	4
β_{Twiss}	6.19	6.62	8.44	7.69	5.94	6.00	6.00	5.94
α_{Twiss}	1.77	2.03	2.54	2.22	1.78	1.78	1.79	1.79

2.2 Mismatch and Beam Blow-up

In a circular accelerator or a storage ring, the Twiss values at all points along the particle trajectory are determined by periodic boundary conditions. Therefore, it is very important that the Twiss values of an injected beam matches the values of the machine at the injection point. Mismatch at injection causes increased betatron oscillations and increase in emittance (emittance blowup). To minimise the emittance blowup, we need to know how much blowup a certain difference in Twiss values will cause. This, of course, will depend on our definition of emittance. If we define the emittance as the area in phase space that contains all particles, the blowup is easy to calculate. Since the phase space ellipse of the injected beam differs from the acceptance ellipse defined by the lattice of the machine, the beam ellipse will start to rotate inside a bigger ellipse, which has the same shape as the acceptance ellipse. After many turns, however, the beam will be smeared out over this new bigger ellipse. A comparison between the area of the injected beam ellipse and this new ellipse gives the blow-up (called mismatch in Table II).

3 MEASUREMENTS

In parallel to the theoretical calculations, measurements have been carried out on the beams in both the Booster measurement line and the CPS. The Twiss parameters have been measured for the beam from all the four rings, and the result has been compared to the theoretical predictions.

3.1 PSB Measurement Line

In the Booster measurement line, the Twiss values of the four beams have been measured using three SEM-grids,[4] and the geometrical mismatch (blowup) with respect to ring three have been calculated. For the measurement, a low intensity proton beam was used. The measurements were repeated at several occasions, well separated in time, to check for long term stability. Possible contributions from (i) beam loss during the transfer and (ii) failed detection of part of the beam at the SEM-grid (in the perpendicular plane to the

TABLE II Measured values at the first SEM-grid in the Booster measurement line

Plane	*Horizontal*				*Vertical*			
Ring	1	2	3	4	1	2	3	4
β_{Twiss}	5.53	4.49	5.52	6.83	5.67	5.51	5.67	5.99
α_{Twiss}	1.63	1.34	1.52	1.94	1.76	1.73	1.74	1.89
Mismatch	11%	26%	0%	24%	2%	5%	0%	7%

measurement plane) were studied without finding any evidence for such contributions. The result is shown in Table II. We see clearly that the beams from the four rings in the horizontal plane are not well matched.

3.2 Comparison between Theory and Measurement

The preliminary theoretical values and the measured values for ring one, two and four in both planes and for ring three in the vertical plane are within reasonable agreement. The much larger deviation for ring three in the horizontal plane could be due to (i) a mistake in the theoretical calculations, (ii) an error in the measurements, (iii) a true difference between the four rings of the local β_{Twiss} value at ejection and (iv) an ejection kicker error in ring three causing an apparent blow-up of the beam. Careful studies of all these possible sources of the observed differences are underway.

3.3 Preliminary Results in CPS Ring

Measurements have also been carried out using three SEM-grids and a beam-stopper in the CPS. However, since the dispersion is large in the CPS, the dispersion effects tends to become significant for the LHC beam with its small transverse beam emittance and introduce systematic errors in the measurement results. Therefore, these measurements have so far been hard to interpret but the preliminary results support qualitatively the PSB measurement line data.

4 CONCLUSIONS

Measurements in the PSB measurement line show that the vertical recombination scheme in the PSB-CPS transfer line introduces a

mismatch between the four PSB rings in the horizontal plane. The result is qualitatively supported by measurements in the CPS ring using the existing three SEM-grids. Theoretical calculations agree qualitatively with the measurements and show that mismatch is due to the edge effects at the vertical recombination bending magnets and septa.

The mismatch will be further studied during the coming operational year 1997 using a quadrupolar pick-up and a turn-by-turn single SEM-grid measurement[5] in the CPS. To further study the exact magnitude of the resulting emittance blow-up there is a need for equivalent emittance measurement instruments in both machines. This is foreseen in the PS for LHC project and will probably be realised with the installation of fast wire scanners in the PSB.

Good agreement between the theoretical optics and the measured optics would help in understanding and possibly curing un-necessarily large mismatch between the PSB rings. Furthermore, such an agreement is necessary for the planned implementation of an automated iterative procedure to reduce the mismatch using e.g. the existing ring independent correction quadrupoles in the PSB rings.

References

[1] J.P. Delahaye, A. Nicoud and J.P. Riunaud, *Difference d'adaption entre anneaux Booster a l'injection PS, MD du 22-03-78*, CERN internal note, not published.

[2] J.P. Delahaye, *La recombinaison des faisceaux issus des quatre anneux du CERN PS Booster, Ameliortions-Evolutions-Mesures*, CERN note CERN/PS/BR 79-12.

[3] B. Autin, V. Ducas, O. Grobner, M. Martini and E. Wildner, *Analytical BeamOptics*, To be published.

[4] M. Arruat and M. Martini, *The new standard method to measure emittances in the PS transfer lines*, CERN note CERN/PS/92-59 (PA).

[5] C. Bovet and R. Jung, *A New Diagnostic for Betatron Phase Space Matching at Injection into a Circular Accelerator* in: *The Proceedings of European Particle Accelerator Conference*, Barcelona, 1996.

Paper II

Emittance preservation in the PS complex
published in Proceedings of the 1997 International Particle Accelerator Conference, Vancouver, Canada.

EMITTANCE PRESERVATION IN THE PS COMPLEX

B. Autin, L. Giulicchi, A. Jansson, M.Lindroos, A. Lombardi, M. Martini, K. Schindl
CERN, CH-1211 Geneva 23, Switzerland

Abstract

As the LHC injectors have to provide bright beams, all the potential sources of emittance blow-up must be eliminated. One such source arises from the mismatch of the betatron focusing at the interface of a transfer line with a circular machine. Measurements and corrections of this effect have been performed in the line downstream of the linac where space charge plays an important role and between the booster and the PS ring where four beams are recombined and have to be matched simultaneously.

1 INTRODUCTION

Emittance preservation is a subject of concern for many high energy machines. In the case of the CERN PS complex, the most severe tolerances are imposed by the LHC beam. A program has therefore been set-up to investigate the sources of beam blow-up and to measure and correct the emittance with the required precision. The LHC injector chain consists of a total of four accelerators: linac, booster, PS and SPS. The tolerance on the beam size blow-up measured at 1 σ is smaller than 20% at the end of each of the accelerators. In a given linear machine and at low space-charge, the normalized emittance is a constant of the motion as far as external fields are concerned and can only be affected by instabilities. At the interface between two machines, the emittance may increase if the injection trajectory is not tangent to the closed orbit and if the focusing of the transfer line does not match the focusing of the accelerator. The first mechanism produces an oscillation of the centre of gravity of the beam; this is the problem of coherent oscillations [1]. The second effect produces a beam envelope oscillation and is the subject of this paper.

2 THEORETICAL BACKGROUND

A focusing error related to a quadrupole field can be treated within the general framework of first order perturbations. The position x and its derivative with respect to the curvilinear abscissa s are replaced by new normalised variables

$$q = \frac{x}{\sqrt{\beta}} \qquad \dot{q} = \frac{dq}{d\mu} \tag{1}$$

where β is the β-function at the point of abscissa s and μ the betatron phase advance at the same point. The betatron motion is thus described by a harmonic oscillator whose motion in phase space is a circle of radius the square root of the emittance, ε.

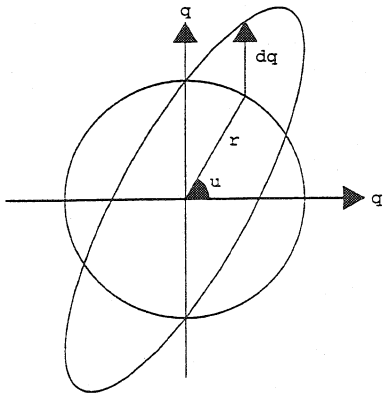

Figure 1: Effect of a quadrupolar error in the normalized phase plane.

A magnet of infinitesimal length ds and of focusing error k at a point of phase μ produces a kick

$$d\dot{q} = k\beta q \, ds \tag{2}$$

This kick changes the betatron emittance, considered not as the area of the ellipse but as a measure of the oscillation amplitude, and the phase of each particle by the quantities

$$d\varepsilon = 2\dot{q} \, d\dot{q} \qquad d\mu = \frac{q \, d\dot{q}}{\varepsilon} \tag{3}$$

whose detailed form can be written

$$\frac{d\varepsilon}{\varepsilon} = \sin 2\mu k\beta \, \mathrm{ds} \qquad \mathrm{d}\mu = \frac{1+\cos 2\mu}{2} \mathrm{k}\beta \, \mathrm{ds} \tag{4}$$

After the kick, the circle is transformed into an ellipse (see Fig. 1). The total focusing error is given by the integral over s of the above expressions. The term independent of μ in the phase perturbation is not relevant in this context because it corresponds to a global rotation of all the particles and does not change the shape of the ellipse which is characterized by the vector:

$$V = \int_0^L \begin{pmatrix} \sin 2\mu \\ \cos 2\mu \end{pmatrix} k\beta \, ds \tag{5}$$

where L is the length of the transfer line. The quadrupoles act in the horizontal and vertical planes simultaneously and the focusing error is corrected by minimizing the norm of

0-7803-4376-X/98/$10.00 © 1998 IEEE

the four-component mismatch vector

$$W = \int_0^L \begin{pmatrix} \beta_h \sin 2\mu_h \\ \beta_h \cos 2\mu_h \\ -\beta_v \sin 2\mu_v \\ -\beta_v \cos 2\mu_v \end{pmatrix} k \, ds \qquad (6)$$

The derivation of the vector W has been based on the classical action-angle perturbation theory. The mismatch can be measured [2] and expressed in terms of the Courant Snyder invariants characterized by β and α functions. The contribution of m discrete and local gradient errors, k_j, in quadrupoles (of length l_j at μ_j) to the α and β functions at a monitor (i) can be written as the sum over the m correctors

$$\begin{pmatrix} \frac{\Delta\beta}{\beta_i} \\ \Delta\alpha_i - \alpha_i \frac{\Delta\beta}{\beta_i} \end{pmatrix} = \sum_{j=1}^{m} \begin{pmatrix} k_j \, l_j \beta_j \sin 2(\mu_i - \mu_j) \\ k_j \, l_j \beta_j \cos 2(\mu_i - \mu_j) \end{pmatrix} \qquad (7)$$

where Eq. (7) can be derived from of Eq. (6).

The correction procedure, called Micado [3], is based on an iterative reduction of the norm of the residual vector. The correction matrix A has as many columns as correctors; each column is the mismatch vector W produced by a unit error; this error can be a focusing strength expressed in m^-2 or a current in Ampere. b is the measured mismatch vector at the interface between the transfer line and the machine. x is the unknown correction vector; at the first iteration, it contains one component attached to the best corrector; at the n-th iteration, the $n-1$ previous correctors are maintained, the best new corrector is chosen and all the corrections are recalculated. The procedure is stopped when the norm is limited by experimental errors.

3 LINAC LINE

The transfer line between linac and booster can be conceptually divided in three parts: the first part (from the output of the linac to the first bending) is space-charge dominated as the beam coming out of the linac is still strongly bunched (some 10 ° at 200 MHz); the second part (between the two bendings) is in a medium space-charge regime, and the third part (up to the last of two emittance measuring lines) is in a low space-charge regime as the beam is almost completely debunched. The matched input ellipse to the booster has been back-traced to the emittance measuring line defining slit where the matching is monitored. The matching is performed by the last four quadrupoles. The purpose of our work, which goes under the name of the Automated Beam Shaping (ABS) project, is the automatic correction of the transverse ellipse parameters at the defining slit.

The application of Micado requires the evaluation of the mismatch vector and correction matrix. The mismatch vector is derived by measuring the emittance of two consecutive cycles to acquire data on the horizontal and vertical planes and comparing it to the target value. The correction matrix represents the sensitivity of the mismatch vector components to small changes in quadrupole input currents.

Considering the limited accuracy introduced by space-charge effects, the evaluation of the quadrupole matrix is one of the most critical points in the application of the ABS procedure.

The evaluation of the matrix has been performed using two methods: the first method is to compute the sensitivity matrix using a beam dynamics model implemented in Trace 3D software tool [4] , the second by experimental measurements.

The matrix has been built by evaluating the mismatch vector components for $\pm 5\%$ change in the quadrupole currents, fitting them with a parabolic function and finally computing the derivative on the reference current value.

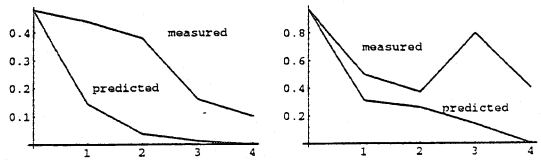

Figure 2: Theoretical and measured norms of the combined total mismatch vector in the linac line after compensation with 1, 2, 3 and 4 correctors.

In Fig. 2 the theoretical and the measured norm of the mismatch vector are shown. The norm has been reduced by a factor of five using four correctors. The correctors may be less efficient if the initial mismatch is big. Tests with a norm of the order of unity, clearly not within the scope of first order perturbations, could be nevertheless reduced by a factor of two using two correctors.

4 TRANSFER BETWEEN BOOSTER AND PS

4.1 Layout of the transfer line

To fill the CPS, the four PS booster beams are ejected sequentially. The present recombination scheme results in non-negligible differences in optical parameters for the four rings at the beginning of the common beam-line section [5]. A solution exists for curing these differences and it is likely to be implemented in the near future.

After the recombination, the beams ideally follow the same trajectory. From here the beam can be sent to different destinations, either ISOLDE, CPS or the PSB measurement line. The latter is equipped with three SEM-grids for transverse optics measurements.

4.2 Theoretical model

As space charge at 1 GeV is negligible for optics calculations an analytical package, *BeamOptics* [6], has been used for the modelling. An advantage with this analytical program is that it can directly generate the the correction matrices.

The inherent difference in the optics between the four booster rings gives a lower limit to the PS injection mismatch. If we try to minimize the mismatch for one of the beams, this will result in increased mismatch in the other beams. A better approach is to try to distribute this effect over the four beams as evenly as possible. This can

be achieved by putting the correction matrices for the individual beams together in a global matrix.

4.3 Experimental results

The correction method has been tested with positive results in the Booster measurement line. The measurements were made in the horizontal plane only, since the quadrupole settings for the line have to be different for horizontal and vertical measurements. The vertical correction was set to zero, i e the vertical mismatch vector was constrained not to change. The results for the correction, Fig. 3, show a significant reduction of the horizontal mismatch.

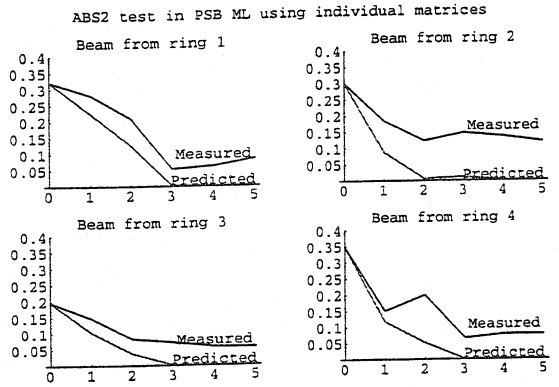

Figure 3: Results in the PSB Measurement line, using individual matrices. The absolute value of the horizontal mismatch vector is plotted as a function of number of correctors used.

Tests have also been performed in the PS ring, using three SEM-grids and a beam stopper. In this case both horizontal and vertical Twiss parameters can be measured with the same optics and it is possible to check if the correction is effective in both planes or not. The results are shown in Fig. 4.

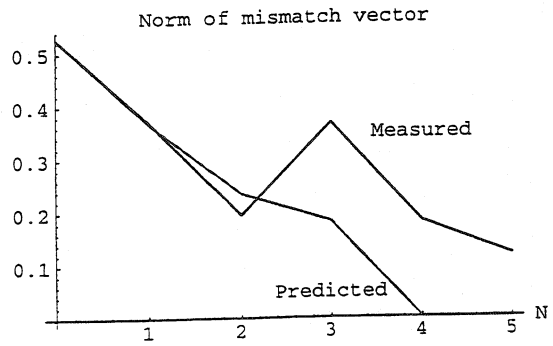

Figure 4: Results in the PS ring using up to 5 corrcetors in the booster-PS transfer line. The measurement was performed using beam from PSB ring three. The absolute value of the total mismatch vector is plotted as a function of number of correctors used.

5 CONCLUSIONS

The good general agreement between theory and measurements in the linac line, the booster measurement line and in the CPS ring confirms the validity of the approach to the problem of mismatch minimization. In the cases tackled, the initial mismatch was rather small, but there are indications that the procedure may diverge for larger values. It is possible to compensate for this by an iterative procedure where the initial mismatch is reduced with one or two correctors. The measurement is then repeated followed by new corrections. First tests of such a procedure show significant improvement of the convergence.

It should be stressed that the results presented here have been achieved using existing measurement software, off-line calculated corrections, which were manually transferred to the quadrupoles. This procedure will be replaced in the near future by a dedicated, but generic software concerning machine part and type of correction. The method can then be made available for the daily work of maintaining the quality of the operational beams. Furthermore, the present very time consuming iterative procedure can be fully tested.

6 ACKNOWLEDGEMENTS

Many thanks to the TRIUMF laboratory for supplying the laminated quadrupoles for the linac line. Many thanks also to Michel Arruat and Olav Tungesvik of our division for prompt and highly reliable software support.

7 REFERENCES

[1] B. Autin, V. Ducas, A. Lombardi, M. Martini, E. Wildner: 'Automated beam optics correction for emittance preservation', Proc. LHC Workshop on LHC Injectors published by Particle Accelerators (1997).

[2] M. Martini, H. Schonauer: 'Emittance measurement', Proc. LHC Workshop on LHC Injectors published by Particle Accelerators (1997).

[3] B. Autin and Y. Marti, 'Closed orbit correction of AG machines using a small number of magnets', CERN ISR-MA/73-17.

[4] K. R. Crandall , 'TRACE 3-D documentation', Los Alamos Accelerator Code Group, LA-UR-90-4146

[5] A. Jansson and M. Lindroos: 'Mismatch between the PSB and CPS due to the present vertical recombination scheme', CERN/PS 97-14, Proc. LHC Workshop on LHC Injectors published by Particle Accelerators (1997).

[6] B. Autin, T. d'Amico, M. Martini, E. Wildner, 'Analytic lattice design with BeamOptics', These Proceedings.

Paper III

Study of emittance blow-up sources between the PS Booster and the 26 GeV PS

published in Proceedings of the 1998 European Particle Accelerator Conference, Stockholm, Sweden.

STUDY OF EMITTANCE BLOW-UP SOURCES BETWEEN THE PS BOOSTER AND THE 26 GEV PS

A. Jansson , M. Lindroos, M. Martini, K.Schindl, CERN, Geneva, Switzerland

Abstract

The tight transverse emittance budget for the bright beams foreseen for the LHC era demands that all sources of emittance blow-up in the injector chain are reduced to a minimum. A critical region is the transfer between the PS Booster (PSB) and the 26 GeV PS. The four rings of the PSB run with RF harmonic one, and for the LHC beam the PS will be filled with eight bunches originating from two consecutive PSB cycles. Thus, each bunch will be different and has to be individually treated. The present recombination scheme introduces an important difference in lattice parameters between the bunches from different rings. The difference between the bunches would, if left uncorrected, result in a substantial emittance blow-up. Several possible improvements of the recombination stage have been studied, including magnet shims, correction quadrupoles and an RF quadrupole magnet. To complement the theoretical studies, the contribution of mismatch and missteering to the emittance blow-up have been measured using a LHC-type beam, measuring the emittance in the PS with a wire-grid and fast wire-scanners. Results of the calculation and the measurements will be discussed and a strategy to minimise the blow-up will be indicated.

1 INTRODUCTION

The production of the relatively low intensity, but very bright beam for LHC will put high demands on efficient emittance conservation in the injector chain. The injector machines were originally, to a large extent, designed for high intensity beams meaning that some sources for possible emittance blow-up were either ignored or considered irrelevant. A systematic review of all such possible sources has therefore been initiated. The results presented here concern the passage of the beam from the 1 GeV PS Booster (PSB) to the 26 GeV PS.

2 THEORETICAL STUDIES

The sources of emittance blow-up during the beam transfer can be separated in two categories; dynamic sources, which originates from fluctuations in power supplies and magnet imperfections, and static sources that are properties of the nominal optics.

2.1 Dynamic sources of blow-up

The dynamic blow-up sources related to the beam transfer PSB-PS are mainly missteering and betatron mismatch. These are treated within the framework of the Automated Beam Steering (ABS) [1] project and have been found to be manageable.

2.2 Static sources of blow-up

The PSB consist of four vertically stacked accelerators from which beam can be ejected in sequence and recombined at the level of the PS during transfer. The vertical recombination scheme introduces a horizontal mismatch in the Twiss values due to edge effects in the rectangular vertical bending magnets. A theoretical study of this process has already been published [2] and in Table 1 the results expressed as Twiss parameters at a common reference point are given. For the sake of convenience this point was chosen at the first SEM-grid in the PSB measurement line, a line to which the beam can be deviated after the vertical recombination is completed.

Table 1: Theoretical lattice parameter values at the first SEM-grid of the PSB measurement line

Horizontal				
Beam from ring	1	2	3	4
β_{Twiss}	4.96	5.46	6.46	6.14
α_{Twiss}	1.47	1.72	2.06	1.77
Relative mismatch	38%	28%	0%	15%
Vertical				
Beam from ring	1	2	3	4
β_{Twiss}	5.21	5.27	5.27	5.21
α_{Twiss}	1.62	1.62	1.63	1.63
Relative mismatch	1.6%	0.7%	0%	2.1%

3 EXPERIMENTAL STUDIES

The measurements were performed partly in the PSB measurement line and partly in the PS using the available instrumentation. The use of the SEM-grids in the measurement line was motivated by the fact that they can be used without interfering with the production beam. For studies of relative differences between the four PSB rings the further transfer and injection of the beam into the PS is irrelevant.

3.1 Difference between PSB rings

The Twiss values of the recombined beam at the first SEM-grid in the PSB have been measured, in Table 2 the results for the horizontal plane is shown.

Table 2: Measured horizontal lattice parameter values at the first SEM-grid of the PSB measurement line

Horizontal				
Beam from ring	1	2	3	4
β_{Twiss}	4.03	3.90	5.75	5.71
α_{Twiss}	1.19	1.63	1.75	1.59

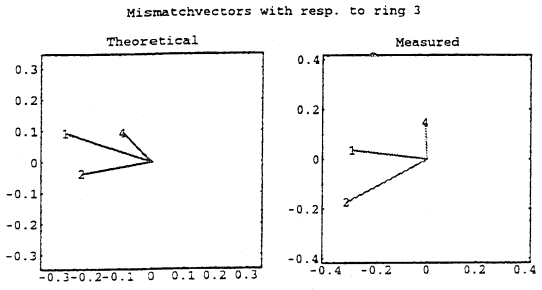

Figure 1: The theoretical and measured mismatch vectors at the first SEM-grid in the PSB measurement line.

The average measured values proved to be within 30% of the theoretical values. However, more interesting is the fact that plotting the experimental and measured mismatch vectors in the same diagram, Figure 1, shows the expected symmetry between the four rings.
Vector addition of the mismatch vector of ring 2 and 4 gives both for the theoretical and experimental values the mismatch vector of ring 1, a symmetry that origins from the symmetry in the used recombination scheme, see figure 2.

3.2 Dispersion mismatch

Measurements have been performed to determine the present dispersion mismatch between the transported beam and the PS lattice. If the momentum spread is σ_p, a dispersion mismatch blows up the rms emittance by [3]

$$\Delta\varepsilon = \frac{\sigma_p^2}{2}\left(\gamma\cdot\Delta D^2 + 2\alpha\cdot\Delta D\Delta D' + \beta\cdot\Delta D'^2\right)$$

It is important to note that the absolute blow-up is independent of the beam emittance, while being proportional to the square of the momentum spread. This means that dispersion mismatch is important for small beams with large momentum spread, such as the LHC beam which will have ε=1.1 μm and σ_p=1.25 10^{-3}. The measured numerical value of the expression in parentheses was found to be 0.4-0.5m in the case of the PSB-PS beam transfer. Using the values for the LHC

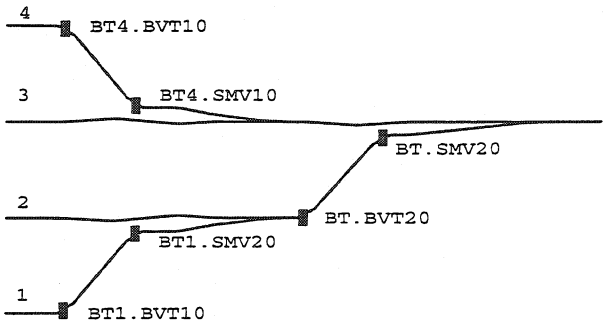

Figure 2: The PSB recombination scheme

beam, this predicts a rms blow-up due to dispersion of 15-25%, which clearly indicates that dispersion matching is important. Therefore, a change of optics is necessary in order to eliminate the dispersion mismatch.

3.3 Measured emittance blow-up in the PS ring

To validate the theoretical formulae for blow-up due to various kinds of misadaptation, a series of measurements have been performed.

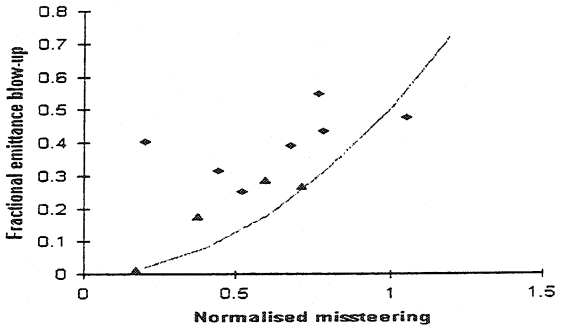

Figure 3: The measured emittance blow-up versus the injection steering error. The line is the theoretical prediction

In the first series, the influence of missteering was studied. The measured values, plotted in Figure 3, shown rather good agreement with the theoretical prediction

In the second series of measurements, the emittance increase due to betatron mismatch was investigated. Here the results (shown in Figure 4) was less obvious to interpret, since a betatron mismatch created by a change in a quadrupole in the transfer line necessarily is accompanied by a dispersion mismatch, if the dispersion is non-zero at the quadrupole as in this case. The measured effect is therefore a combination of the two. However, when this is taken into account, the data followes the theoretical prediction quite well.

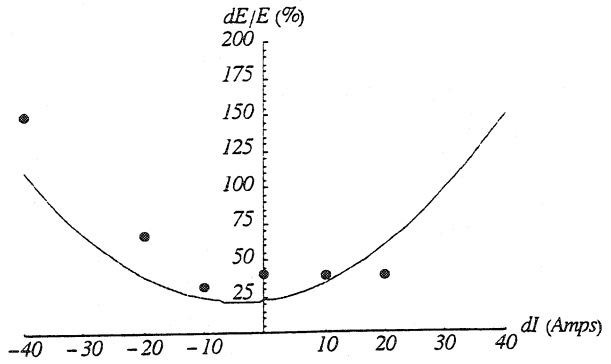

Figure 4: The measured emittance blow-up versus the a quadrupole current. The parabolic curve shows the theoretical prediction.

4 POSSIBLE IMPROVEMENTS

4.1 PSB recombination scheme

The betatron mismatch from the recombination scheme can only be reduced if additional hardware is added to the recombination line. These additions could include: i) magnets shims for vertical bending magnets, ii) individual quadrupoles in the four PSB lines or iii) a set of RF quadrupoles in the PSB-PS transfer line. The different possibilities have all been theoretically studied. The addition of shims proved effective but unrealistic [4] due to the complicated design of the compact vertical dipoles. The addition of a single quadrupole in ring 2 after the recombination of ring 1 and 2 can reduce the mismatch considerably, see table 2. The focal length of this quadrupole should be 125 m. Constrains on the available space in the recombination line leave this as the only possible additional quadrupole. The possible, but maybe not necessary, use of two RF quadrupoles in the following transfer line could probably render the mismatch entirely negligible.

Table 2: The theoretical mismatch values after recombination using one additional quadrupole in ring 2.

Horizontal				
Beam from ring	1	2	3	4
β_{Twiss}	6.18	6.91	6.86	6.14
α_{Twiss}	1.80	2.10	2.06	1.77
Relative mismatch	13%	2.4%	0%	15%
Vertical				
Beam from ring	1	2	3	4
β_{Twiss}	5.39	5.45	5.27	5.21
α_{Twiss}	1.72	1.72	1.63	1.63
Relative mismatch	6.0%	5.1%	0%	2.1%

4.2 Dispersion at PS injection

The dispersion mismatch can be reduced by modifying the optics of the transfer line. The magnet positions in the line are basically fixed due to lack of space, which means that the possible changes in transfer line optics are constrained to changes in quadrupole gradients. With the 10 presently used quadrupoles, it is not possible to match the lattice parameters and the dispersion to the PS at the same time. However, the line has an eleventh quadrupole which has not been used up to now because of its problematic position inside a shielding wall. With this extra degree of freedom, it is theoretically possible to match the dispersion and the Twiss parameters simultaneously [5]. Test of this matched optics has sofar given better, but not yet perfect, results.

5 CONCLUSSIONS

The theoretical study of possible sources of mismatch between the PSB and the PS points towards several possibly critical points: the used recombination scheme, the dispersion mismatch and the possible drift in steering and betatron parameters at PS injection. The most important of them being the dispersion mismatch. The measurements performed shows that all these effects can be observed as a measurable emittance blow-up of a beam similar to the beam for the LHC. A number of possible improvements have been investigated and it has been shown that the emittance blow-up can be kept within the limits of the foreseen emittance budget for the LHC beam. However, it is doubtful whether that can be achieved without the addition of some hardware in the PSB recombination line.

REFERENCES

[1] M. Lindroos, M. Arruat, B. Autin, R. Cappi, L. Giulicchi, A. Jansson, A. Lombardi, M. Martini, M. Gourber-Pace, K. Schindl, O. Tungesvik, D. Williams, "Automated Emittance Preservation in the PS Complex", PAC'97, Vancouver, May 1997.

[2] A. Jansson, M.Lindroos, "Mismatch between the PSB and PS due to the present vertical recombination scheme", Particle Accelerators 58 (1997) p.201

[3] D.A.Edwards, M.J.Syphers,"An introduction to the physics of high energy accelerators", John Wiley & Sons, New York

[4] A. Jansson, "A simple way of reducing the PSB-CPS mismatch due to the vertical recombination scheme by using shims", CERN note: PS/DI/Note 97-14 (Tech.)

[5] M.Martini, T.Risselada, K.Schindl, "Measuremnt of Betatron and Dispersion matching between Booster and PS", Cern note: PS/PA Note 91-13

Paper IV

Simultaneous matching of dispersion and Twiss parameters in a transfer line

published in Proceedings of the 1998 Workshop on Automated Beam Steering, Geneva, Switzerland.

SIMULTANEOUS MATCHING OF DISPERSION FUNCTION AND TWISS PARAMETERS IN A TRANSFER LINE

M. Giovannozzi, A. Jansson, M. Martini
CERN, Geneva, Switzerland

Abstract

Dispersion matching in a beam transfer line is an important issue in order to avoid blow-up and luminosity reduction. This is the case for the LHC beam, due to its small emittance and relatively large momentum spread. The dispersion matching can be performed with quadrupoles, but one has to impose the additional constraint of leaving the Twiss parameters unchanged, to preserve the betatron matching.

A first order pertubative approach, using the *MICADO* solver, has been applied to the problem of simultaneous betatron and dispersion matching. A theoretical derivation of the correction matrix, as well as simulated and experimental results are presented.

1. Introduction

The performance of the new generation of circular machines heavily relies on the injector chain performance. In order to achieve the design luminosity all sources of emittance growth should be avoided. This means that the transfer lines between the various machines should be carefully tuned in order to match the beam parameters at the injection point of the next circular machine.

If one neglects the emittance dilution produced by injection oscillations, which can be cured by properly steering the beam using the injection elements, the other sources of mismatch are the dispersion mismatch and the betatron mismatch.

In the first case the dispersion or its derivative at the end of the transfer line do not match the values for the circular machine due either to dipolar or quadrupolar errors along the transfer line, or wrong initial values at the entrance of the beam line. The resulting emittance growth is quite sensible. This effect is in fact similar to an injection mismatch: particles with different energies enter into the machine at a wrong position and/or angle and perform betatron oscillations. In the second case, the Twiss parameters at the injection point do not agree. The injected beam ellipse will rotate in phase space to match the machine parameters, hence producing beam dilution. Also in this case the source of mismatch can be found in the transfer line quadrupoles, or the initial values.

The correct approach to this problem is to find a strategy to simultaneously correct both dispersion and betatron mismatch. The simple technique of reducing the betatron mismatch without controlling the dispersion is not enough. Such a combined approach is imposed by the large momentum spread foreseen for the LHC.

In the present note, the correction matrix is derived using a perturbative approach and assuming that only quadrupoles can be used to correct the mismatch. A careful analysis of the high order terms is carried out, although the first order is usually enough to achieve good results. Different techniques are applied to the problem of minimising the mismatch: a MICADO

approach and a full minimisation algorithm. These techniques have been bench-marked by using a model of the TT2 transfer line and also by performing some real measurements using the 26 GeV/c LHC-like beam: an overall reduction of the mismatch could be achieved in all the cases considered.

2. Twiss matching

The starting point for the analysis of the Twiss matching is the study of the evolution of the Twiss parameters along a transfer line. It is well-known [1] that the optical parameters between two sections of beam line evolve according to the following rules

$$\beta_{\rm m} = C^2\beta_{\rm c} - 2CS\alpha_{\rm c} + S^2\gamma_{\rm c} \quad (1)$$

$$\alpha_{\rm m} = -C\,C'\beta_{\rm c} + (C\,S' + S\,C')\alpha_{\rm c} - S\,S'\gamma_{\rm c}, \quad (2)$$

Here the transfer matrix between corrector and monitor is given in terms of the so-called cosine-like C and sine-like S functions and their derivatives

$$\mathcal{T}_{c\to m} = \begin{pmatrix} C & S \\ C' & S' \end{pmatrix}. \quad (3)$$

Furthermore, the parameter $\gamma = (1+\alpha^2)/\beta$ has been introduced.

To quantify the effect of a betatron mismatch and to determine the approach to compensate such a mismatch, it is common use to insert a thin lens quadrupolar element at the location of the corrector. This will generate a variation in the optical parameters downstream and such a variation can be measured by using a beam monitor device. In this case the transfer matrix between the corrector and the monitor can be obtained from Eq. (3) by multiplying by the thin quadrupole transfer matrix. The final result is

$$\overline{\mathcal{T}}_{\rm c\to m} = \begin{pmatrix} C & S \\ C' & S' \end{pmatrix}\begin{pmatrix} 1 & 0 \\ \Delta k & 1 \end{pmatrix} = \begin{pmatrix} C + S\,\Delta k & S \\ C' + S'\Delta k & S' \end{pmatrix}, \quad (4)$$

where Δk is the integrated gradient of the error. By using the matrix (4) in Eq. (2), one can find the resulting Twiss parameters at the monitor location, namely

$$\bar{\beta}_{\rm m} = \beta_{\rm m} + 2\,S(C\beta_{\rm c} - S\alpha_{\rm c})\Delta k + S^2\beta_{\rm c}(\Delta k)^2 \quad (5)$$

$$\bar{\alpha}_{\rm m} = \alpha_{\rm m} + [2\,S\,S'\alpha_{\rm c} - (C\,S' + S\,C')\beta_{\rm c}]\Delta k - S\,S'\beta_{\rm c}(\Delta k)^2. \quad (6)$$

It is customary to use the following variables to evaluate the betatron mismatch:

$$\left(\frac{(\Delta\beta)_{\rm m}}{\beta_{\rm m}},\quad \alpha_{\rm m}\frac{(\Delta\beta)_{\rm m}}{\beta_{\rm m}} - (\Delta\alpha)_{\rm m},\right) \quad (7)$$

in which $(\Delta\beta)_{\rm m} = \bar{\beta}_{\rm m} - \beta_{\rm m}$ and $(\Delta\alpha)_{\rm m} = \bar{\alpha}_{\rm m} - \alpha_{\rm m}$. Using the standard parametrisation of the transfer matrix $\mathcal{T}_{\rm c\to m}$

$$\mathcal{T}_{\rm c\to m} = \begin{pmatrix} \sqrt{\frac{\beta_{\rm m}}{\beta_{\rm c}}}(\cos\Delta\mu + \alpha_{\rm c}\sin\Delta\mu) & \sqrt{\beta_{\rm m}\beta_{\rm c}}\sin\Delta\mu \\ \frac{-(1+\alpha_{\rm c}\alpha_{\rm m})\sin\Delta\mu + (\alpha_{\rm c}-\alpha_{\rm m})\cos\Delta\mu}{\sqrt{\beta_{\rm m}\beta_{\rm c}}} & \sqrt{\frac{\beta_{\rm c}}{\beta_{\rm m}}}(\cos\Delta\mu - \alpha_{\rm m}\sin\Delta\mu) \end{pmatrix}, \quad (8)$$

where $\Delta\mu$ represents the phase-advance between the corrector and the monitor, Eq. (8) together with the expression (6), allows to recast the mismatch vector in the following form:

$$\frac{(\Delta\beta)_{\rm m}}{\beta_{\rm m}} = \beta_{\rm c}\sin 2\Delta\mu\ \ \Delta k + \frac{\beta_{\rm c}^{\,2}}{2}(1-\cos 2\Delta\mu)\ \ (\Delta k)^2 \tag{9}$$

$$\alpha_{\rm m}\frac{(\Delta\beta)_{\rm m}}{\beta_{\rm m}} - (\Delta\alpha)_{\rm m} = \beta_{\rm c}\cos 2\Delta\mu\ \ \Delta k + \frac{\beta_{\rm c}^{\,2}}{2}\sin 2\Delta\mu\ \ (\Delta k)^2. \tag{10}$$

The expression (10) of the mismatch vector contains linear and non linear terms in the quadrupolar gradient Δk. The linear part represent the well-know contribution to the β- and α-functions [2]. The same equations hold true also for the other plane, provided the sign of Δk is changed.

The nonlinear terms are usually dropped as the whole approach is based on a linear approximation. In fact, one should compute the transfer matrix from the first quadrupolar corrector to some monitor, including all the correctors in between, namely

$$\overline{\mathcal{T}}_{\rm c\to m} = \prod_{i=1}^{N_m}\begin{pmatrix} C_i + S_i\,\Delta k_i & S_i \\ C_i' + S_i'\Delta k_i & S_i' \end{pmatrix} = \begin{pmatrix} \hat{C} & \hat{S} \\ \hat{C}' & \hat{S}' \end{pmatrix}, \tag{11}$$

or

$$\overline{\mathcal{T}}_{\rm c\to m} = \prod_{i=1}^{N_m}\begin{pmatrix} C_i & S_i \\ C_i' & S_i' \end{pmatrix} + \Delta k_i \begin{pmatrix} S_i & 0 \\ S_i' & 0 \end{pmatrix}, \tag{12}$$

where N_m is the number of correctors between the beginning of the beam line and the monitor m. It is quite easy to prove by induction that the quantities $\hat{C}, \hat{S}, \hat{C}'$ and $\hat{S}'$ are polynomial functions of the gradients Δk_i. More precisely one has:

$$\hat{C} = \hat{C}_{\rm N_m}(\Delta k_1, \Delta k_2, \cdots \Delta k_{\rm N_m}) \qquad \hat{S} = \hat{S}_{\rm N_m-1}(\Delta k_2, \Delta k_3, \cdots \Delta k_{\rm N_m})$$
$$\hat{C}' = \hat{C}'_{\rm N_m}(\Delta k_1, \Delta k_2, \cdots \Delta k_{\rm N_m}) \qquad \hat{S}' = \hat{S}'_{\rm N_m-1}(\Delta k_2, \Delta k_3, \cdots \Delta k_{\rm N_m}),$$

where $\hat{C}_{\rm j}(x_1, x_2, \cdots, x_n)$ is a polynomial of order j in the variables $x_1, x_2, \cdots, x_n$. To obtain the correct expression for the propagation of the β- and α-functions, taking into account the nonlinear terms in the gradients Δk_i, one should evaluate the structure of the polynomials $\hat{C}, \hat{S}, \hat{C}', \hat{S}'$. By using the symbol $\lfloor\cdot\rfloor_i$ to represent the homogeneous polynomial of order i in the quadrupolar gradients, it is possible to recast Eq. (12) in the following form

$$\lfloor\overline{\mathcal{T}}_{\rm c\to m}\rfloor_0 = \prod_{i=1}^{N_m}\begin{pmatrix} C_i & S_i \\ C_i' & S_i' \end{pmatrix}$$

$$\lfloor\overline{\mathcal{T}}_{\rm c\to m}\rfloor_1 = \sum_{i=1}^{N_m}\Delta k_i\ \mathcal{T}_{\rm i+1\to m}\begin{pmatrix} S_i & 0 \\ S_i' & 0 \end{pmatrix}\mathcal{T}_{\rm c\to i}$$

$$\lfloor\overline{\mathcal{T}}_{\rm c\to m}\rfloor_2 = \sum_{i,j=1\ j>i}^{N_m}\Delta k_i\ \Delta k_j\ \mathcal{T}_{\rm j+1\to m}\begin{pmatrix} S_j & 0 \\ S_j' & 0 \end{pmatrix}\mathcal{T}_{\rm i+1\to j}\begin{pmatrix} S_i & 0 \\ S_i' & 0 \end{pmatrix}\mathcal{T}_{\rm c\to i}$$

$$\vdots\ \ \vdots$$

where $\mathcal{T}_{\mathrm{i}\to\mathrm{j}}$ represents the transfer matrix between corrector i and corrector j.

To find out the quantities $\lfloor\beta\rfloor_i$, $\lfloor\alpha\rfloor_i$ it is simply a matter of replacing C, S, C', S' with the quantities $\hat{C}, \hat{S}, \hat{C}', \hat{S}'$ in Eq. (2) and grouping terms of the same order in the gradients Δk_i, namely

$$\begin{aligned}
\lfloor\beta_{\mathrm{m}}\rfloor_i &= \beta_{\mathrm{c}}\sum_{j=0}^{i}\lfloor\hat{C}\rfloor_j\lfloor\hat{C}\rfloor_{i-j} - 2\alpha_{\mathrm{c}}\sum_{j=0}^{i}\lfloor\hat{C}\rfloor_j\lfloor\hat{S}\rfloor_{i-j} + \gamma_{\mathrm{c}}\sum_{j=0}^{i}\lfloor\hat{S}\rfloor_j\lfloor\hat{S}\rfloor_{i-j} \\
\lfloor\alpha_{\mathrm{m}}\rfloor_i &= -\beta_{\mathrm{c}}\sum_{j=0}^{i}\lfloor\hat{C}\rfloor_j\lfloor\hat{C}'\rfloor_{i-j} + \alpha_{\mathrm{c}}\sum_{j=0}^{i}(\lfloor\hat{C}\rfloor_j\lfloor\hat{S}'\rfloor_{i-j} + \lfloor\hat{S}\rfloor_j\lfloor\hat{C}'\rfloor_{i-j}) - \gamma_{\mathrm{c}}\sum_{j=0}^{i}\lfloor\hat{S}\rfloor_j\lfloor\hat{S}'\rfloor_{i-j},
\end{aligned} \tag{13}$$

where it has been used the following expression for the product of homogeneous polynomials $\hat{C}, \hat{S}$ of degree N, M respectively:

$$\hat{C}\hat{S} = \sum_{i=0}^{N}\sum_{j=0}^{M}\lfloor\hat{C}\rfloor_i\lfloor\hat{S}\rfloor_j = \sum_{i=0}^{NM}\sum_{j=0}^{i}\lfloor\hat{C}\rfloor_j\lfloor\hat{S}\rfloor_{i-j}. \tag{14}$$

3. Dispersion matching

When bending magnets are present in the transfer line, the evolution of the dispersion function should be included in the formalism used to correct a mismatch in the optical parameters. The approach is now based on 3×3 transfer matrices [3]. The propagation of the dispersion function from a corrector location to a monitor placed downstream can be written using the matrix

$$\mathcal{T}_{\mathrm{c}\to\mathrm{m}} = \begin{pmatrix} C & S & \xi \\ C' & S' & \xi' \\ 0 & 0 & 1 \end{pmatrix}. \tag{15}$$

The 2×2 sub-matrix represents the transfer matrix for the betatronic motion between corrector and monitor. The quantities ξ, ξ' are different from zero only when bending magnets are present in the transfer line.

It is customary to introduce a quantity $\mathcal{W}$ defined as

$$\mathcal{W} = \frac{1}{\beta}[D^2 + (\alpha D + \beta D')^2], \tag{16}$$

similar to the Courant-Snyder invariant. In a bending-free region of a transfer line $\mathcal{W}$ is invariant and it is called *Dispersion invariant* [1, 4].

It is possible to repeat what was done for the betatron matching. The dispersion at a given monitor is linked to the value at the location of an upstream corrector (a normal quadrupole) and the transfer matrix of the section in between. The presence of a quadrupolar error, simulated by a thin lens element, modifies the transfer matrix, according to the following

$$\overline{\mathcal{T}}_{\mathrm{c}\to\mathrm{m}} = \begin{pmatrix} C & S & \xi \\ C' & S' & \xi' \\ 0 & 0 & 1 \end{pmatrix}\begin{pmatrix} 1 & 0 & 0 \\ \Delta k & 1 & 0 \\ 0 & 0 & 1 \end{pmatrix} = \begin{pmatrix} C + S\,\Delta k & S & \xi \\ C' + S'\Delta k & S' & \xi' \\ 0 & 0 & 1 \end{pmatrix}. \tag{17}$$

The modified dispersion at the monitor location is then given by

$$\bar{D}_{\mathrm{m}} = D_{\mathrm{m}} + S\ D_{\mathrm{c}}\ \Delta k \tag{18}$$

$$\bar{D}'_{\mathrm{m}} = D'_{\mathrm{m}} + S'\ D_{\mathrm{c}}\ \Delta k, \tag{19}$$

where

$$D_{\mathrm{m}} = C\ D_{\mathrm{c}} + S\ D'_{\mathrm{c}} + \xi \tag{20}$$

$$D'_{\mathrm{m}} = C'\ D_{\mathrm{c}} + S'\ D'_{\mathrm{c}} + \xi'. \tag{21}$$

In this case, the existence of the dispersion invariant suggests to define a dispersion mismatch vector as

$$\left(\frac{(\Delta D)_{\mathrm{m}}}{\sqrt{\beta_{\mathrm{m}}}},\ \alpha_{\mathrm{m}} \frac{(\Delta D)_{\mathrm{m}}}{\sqrt{\beta_{\mathrm{m}}}} + \sqrt{\beta_{\mathrm{m}}} (\Delta D')_{\mathrm{m}} \right), \tag{22}$$

where $(\Delta D)_{\mathrm{m}} = \bar{D}_{\mathrm{m}} - D_{\mathrm{m}}$ and $(\Delta D')_{\mathrm{m}} = \bar{D}'_{\mathrm{m}} - D'_{\mathrm{m}}$.

Once again, by using the form (8) for the transfer matrix between the corrector and the monitor, it is possible to obtain the expression of the dispersion mismatch vector

$$\frac{(\Delta D)_{\mathrm{m}}}{\sqrt{\beta_{\mathrm{m}}}} = \sqrt{\beta_{\mathrm{c}}} D_{\mathrm{c}} \sin \Delta\mu\ \ \Delta k \tag{23}$$

$$\alpha_{\mathrm{m}} \frac{(\Delta D)_{\mathrm{m}}}{\sqrt{\beta_{\mathrm{m}}}} + \sqrt{\beta_{\mathrm{m}}} (\Delta D')_{\mathrm{m}} = \sqrt{\beta_{\mathrm{c}}} D_{\mathrm{c}} \cos \Delta\mu\ \ \Delta k. \tag{24}$$

In the case of the dispersion mismatch, the vector is a linear function of the corrector strength. The same expressions hold for a dispersive transfer line.

The approach used in the computation of the nonlinear terms depending on the quadrupolar gradients in the expression of the Twiss parameters can be applied even for the dispersion function. In this case the knowledge of the polynomial functions $\hat{C}, \hat{S}, \hat{C}', \hat{S}'$ allows to derive the development of D, D' as a function of Δk_i, namely

$$\begin{aligned} \lfloor D_{\mathrm{m}} \rfloor_i &= D_{\mathrm{c}} \lfloor \hat{C} \rfloor_i + D'_{\mathrm{c}} \lfloor \hat{S} \rfloor_i + \delta_{i,0} \xi \\ \lfloor D'_{\mathrm{m}} \rfloor_i &= D_{\mathrm{c}} \lfloor \hat{C}' \rfloor_i + D'_{\mathrm{c}} \lfloor \hat{S}' \rfloor_i + \delta_{i,0} \xi', \end{aligned} \tag{25}$$

where $\delta_{i,0}$ is the Kronecker delta.

4. Correction strategy

The first approach consists in dropping the nonlinear terms in the Eqs. (14) and (26). Then one can build up a correction matrix in the standard way (see for instance Ref. [2])

$$\begin{pmatrix} \dfrac{(\Delta\beta)_1^H}{\beta_1^H} \\ \alpha_1^H \dfrac{(\Delta\beta)_1^H}{\beta_1^H} - (\Delta\alpha)_1^H \\ \dfrac{(\Delta D)_1^H}{\sqrt{\beta_1^H}} \\ \alpha_1^H \dfrac{(\Delta D)_1^H}{\sqrt{\beta_1^H}} + \sqrt{\beta_1^H}(\Delta D')_1^H \\ \vdots \\ \vdots \\ \dfrac{(\Delta D)_{\mathrm{N_m}}^V}{\sqrt{\beta_{\mathrm{N_m}}^V}} \\ \alpha_{\mathrm{N_m}}^V \dfrac{(\Delta D)_{\mathrm{N_m}}^V}{\sqrt{\beta_{\mathrm{N_m}}^V}} + \sqrt{\beta_{\mathrm{N_m}}^V}(\Delta D')_{\mathrm{N_m}}^V \end{pmatrix} = C \begin{pmatrix} \Delta k_1 \\ \Delta k_2 \\ \vdots \\ \vdots \\ \Delta k_{\mathrm{N_c}} \end{pmatrix}, \tag{26}$$

where C is an $8\mathrm{N_m} \times \mathrm{N_c}$. Here $\mathrm{N_m}$ stands for the number of monitors, while $\mathrm{N_c}$ is the number of correctors. The matrix elements $C_{i,j}$ can be written as

$$\begin{aligned} C_{i\ \ ,j} &= \beta_{\mathrm{j}}^H \sin 2\Delta\mu_{\mathrm{ij}}^H & C_{i+4,j} &= \beta_{\mathrm{j}}^V \sin 2\Delta\mu_{\mathrm{ij}}^V \\ C_{i+1,j} &= \beta_{\mathrm{j}}^H \cos 2\Delta\mu_{\mathrm{ij}}^H & C_{i+5,j} &= \beta_{\mathrm{j}}^V \cos 2\Delta\mu_{\mathrm{ij}}^V \\ C_{i+2,j} &= \sqrt{\beta_{\mathrm{j}}^H} D_{\mathrm{j}}^H \sin \Delta\mu_{\mathrm{ij}}^H & C_{i+6,j} &= \sqrt{\beta_{\mathrm{j}}^V} D_{\mathrm{j}}^V \sin \Delta\mu_{\mathrm{ij}}^V \\ C_{i+3,j} &= \sqrt{\beta_{\mathrm{j}}^H} D_{\mathrm{j}}^H \cos \Delta\mu_{\mathrm{ij}}^H & C_{i+7,j} &= \sqrt{\beta_{\mathrm{j}}^V} D_{\mathrm{j}}^V \cos \Delta\mu_{\mathrm{ij}}^V, \end{aligned}$$

for $1 \leq j \leq \mathrm{N_c}$ and $i = 8(l-1)+1, 1 \leq l \leq \mathrm{N_m}$. Note that one should in general include a weight factor between the betatronic part of the matrix and the dispersion part. This is obvious since the betatronic matrix elements have unit m^{-2}, while the dispersion part has unit $m^{-3/4}$. For all the measurements and simulations presented in this note this weight factor was set to unity, which was found to work fine, but that is just one possible choice. It is likely that a bad choice of weight factor will cause the minimisation procedure to diverge.

5. MICADO and MINIMO

The corrector strengths can be computed using a number of different algorithms. The algorithms discussed in this note are the well-known *MICADO* [5], and a slower but more general algorithm, which has been named *MINIMO* [6].

In principle, assuming that the response matrix is non-singular the number of free parameters (corrector magnets) have to be the same as the number of constraints (monitors) for the linear problem to be exactly solved. However, in general a very good approximate solution can be achieved by using only a small subset of correctors, provided that the subset is cleverly

chosen. *MICADO* and *MINIMO* are two algorithms that have been developed to choose such a subset.

For a given subset of correctors, the optimal solution can be defined, for example, as the least-square fit or a *SVD* fit with a certain tolerance. The least-square fit suppresses all null-space corrections, that is, linear combinations of individual corrections that in total gives no effect on the monitors. The *SVD* fit also suppresses near-to-null space corrections, which are combinations of individual corrections that give a very small effect on the monitors. The definition of what is a very small correction is given by the tolerance level. The correction is computed using the pseudo-inverse of the response matrix, where all the singular values smaller than the tolerance are set to zero.

MICADO starts out by testing all the possible subsets containing only one corrector and finding the best one. Then it tests all subsets that can be obtained by adding one more corrector to this subset. In each iteration, one corrector is thus added, and the time to find a correction using a subset of n correctors out of a total of N available is approximately proportional to $(N^2n - Nn^2)/2$.

The assumption that is made in the *MICADO* algorithm, that the optimal set containing k correctors is a subset of the optimal set containing $k + 1$ correctors is not true in general. It is in fact easy to construct counter-examples. The assumption is however a rather good approximation in most cases, and it significantly speeds up the algorithm.

MINIMO on the other hand, is a brute-force method. It checks all the possible solutions, without assumptions. Since the number of possible subsets of a certain number of available correctors can be very large, this method is slow, and in some cases, utterly useless because of the combinatorial growth of computation time. In fact, the time needed to find a correction containing n out of N correctors is $N!/(n!(M-n)!)$. However, in the case of transverse matching, the number of available correctors is rather small (typically < 10). Thus the computation time is acceptable, and *MINIMO* can be considered as an option. An implementation of *MINIMO* in *Mathematica* [7] have thus been done for the purposes of these tests.

6. Simulation results

Since the validation measurements are time-consuming and at least semi-destructive, simulations have been performed to test the method, and to quantify the difference between *MICADO* and *MINIMO*. It is not obvious how to compare the convergence properties of the two methods, because in reality an operator would be supervising the minimisation process and change the free parameter (the number of correctors in each iteration) if necessary. The chosen strategy consists of making a relatively large number of simulations with random initial errors, binning the simulation results according to the size of the initial error and plotting for each bin the average residual error as a function of both the number of correctors used in each iteration, and the number of iterations. All the simulations were carried out on the model of the same transfer line used to perform the real measurements [8]. The results show no significant difference between the two algorithms for small and moderate initial errors (Figs. 1 and 2).

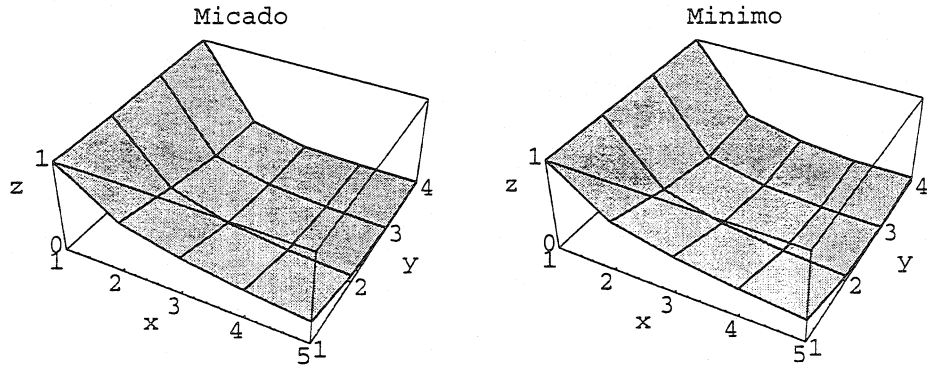

Fig. 1: Simulation results averaged over 45 seeds. The initial rms error belongs to the interval [0.2,0.4]. The vertical axes represents the average error, the x axes the iteration number, the y axes the number of correctors used in each iteration.

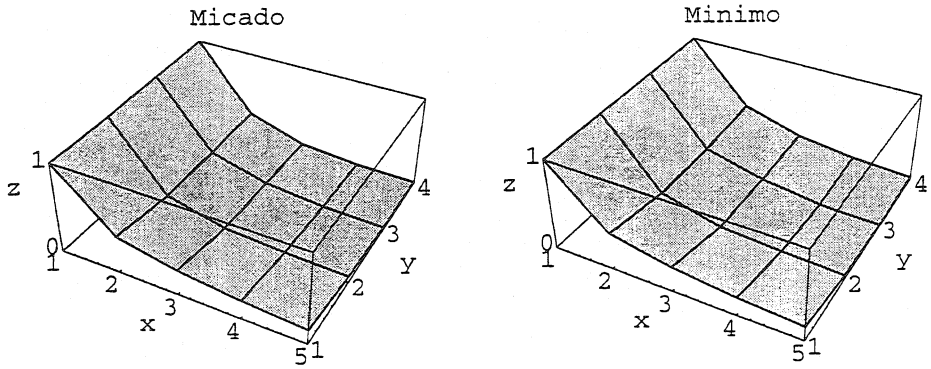

Fig. 2: Simulation results averaged over 17 seeds. The initial rms error belongs to the interval [1.0,1.2]. The axes are the same as in Fig. 1.

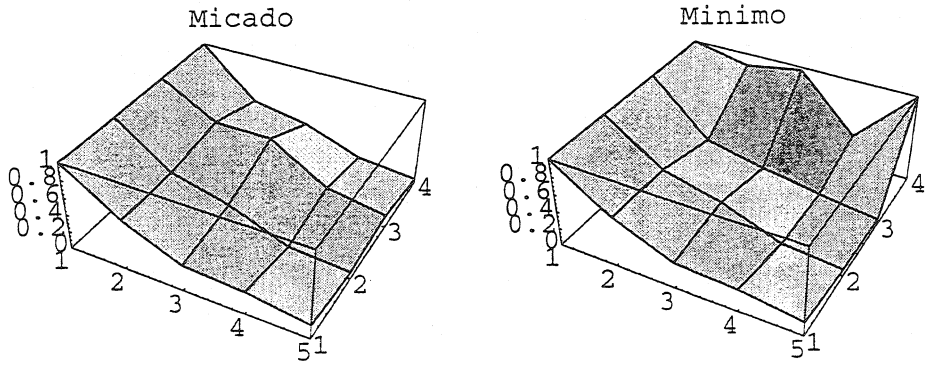

Fig. 3: Simulation results averaged over 2 seeds. The initial rms error belongs to the interval [1.8,2.0]. The axes are the same as in Fig. 1.

7. Experimental results

Tests of the method have been performed in the CPS-SPS transfer line. This line is divided into two parts: the TT2 line and TT10 line. TT2 transports the beam from the extraction point of the PS machine to the TT10 part, which, in turn, connects the transfer line to the SPS injection point. At the junction of the two lines, the beam is deflected about 81 mrad to the right. Due to the difference in height between the PS and SPS, a vertical deflection angle of about 60 mrad is imposed at the entrance of TT10 and then cancelled before injection in the SPS.

Three Secondary Emission Monitors are installed both in TT2 and in TT10 section. These two sets of monitors are routinely used to perform emittance and *Twiss* parameters measurement in both lines. For this purpose, it is used the standard method, with the dispersion measured by performing an energy shift.

A 26 GeV/c proton beam is extracted from the PS machine using a kicker magnet and delivered to the SPS through the TT2/TT10 line. The beam intensity is $\approx 1.1 \times 10^{12}$ ppp, distributed into 16 bunches 15 ns long with a momentum spread δ of about 0.6×10^{-3} at 2σ. The beam is extracted on a flat top in one turn (fast extraction) by the standard scheme based on bumper, septum and kicker. The nominal setting of these elements is reported in Table 1.

Element	Value
PE.KFA71 [kV]	710
PE.SMH16 [A]	28200
PE.BSW16 [A]	1350
PE.QKE16 [A]	1550
PE.DHZ15 [A]	250

Table 1: Nominal setting of the extraction elements for the 26 GeV/c proton beam.

In Table 2 are listed the main parameters of the proton beam used during the matching studies.

p [GeV/c]	26
ε_H [μm] (normalised, rms)	3.0
ε_V [μm] (normalised, rms)	3.0
dp/p	10^{-3}
bunch length [ns] (4σ)	5-7
ε_l [eVs]	0.1

Table 2: Parameters of the proton beam used to study the simultaneous matching of betatron and dispersion functions.

The experimental validation of the optimisation scheme was performed in steps. In all cases the optical parameters was first measured, then an error was introduced on one or several quadrupoles, and *MICADO* or *MINIMO* was used to try to recover the initial values. First, the result of the proposed corrections was measured for different number of correctors, and

compared to the linear prediction supplied by *MICADO* and *MINIMO*. The results are shown in Fig. 4 and Fig. 5 and show a fairly good agreement between measurement and prediction, with an apparent tendency for *MINIMO* to diverge when many correctors are used.

Then test were made to iteratively reduce the error down to zero. These results, using one corrector per iteration are shown in Fig. 6. In the case of one corrector per iteration, *MICADO* and *MINIMO* always give the same result. A test using three correctors per iteration was made to try to see a difference between the two algorithms, but no significant difference was found (see Figs. 7 and 8).

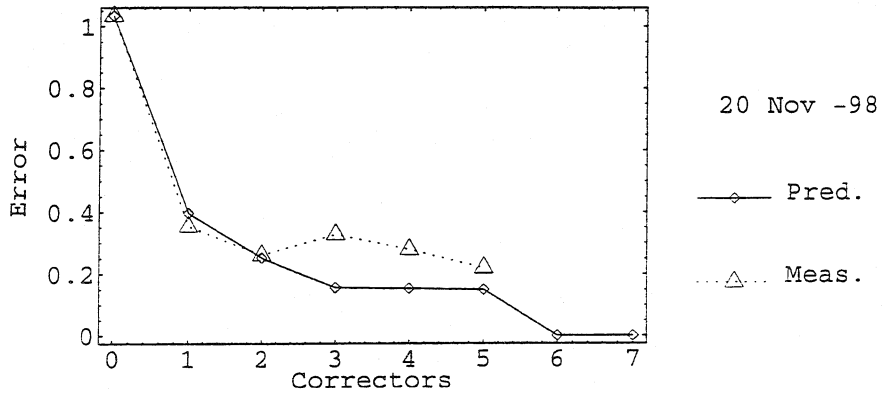

Fig. 4: The measured correction result and the *MICADO* prediction for a random initial error are shown as a function of the number of correctors used.

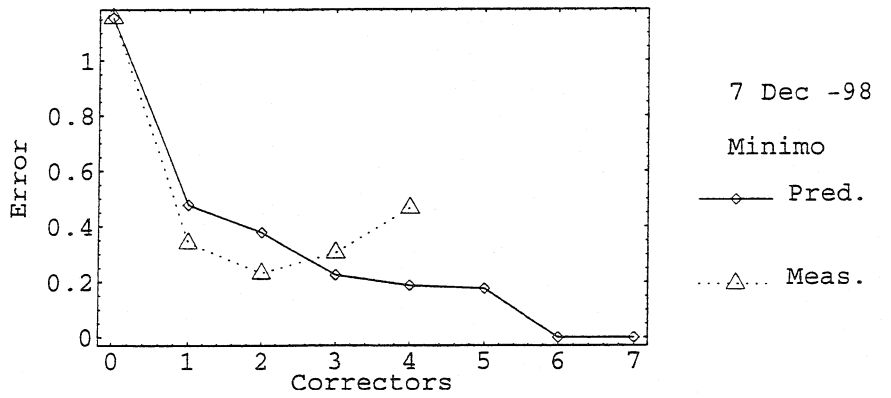

Fig. 5: The measured correction result and the *MINIMO* prediction for a random initial error are shown as a function of the number of correctors used.

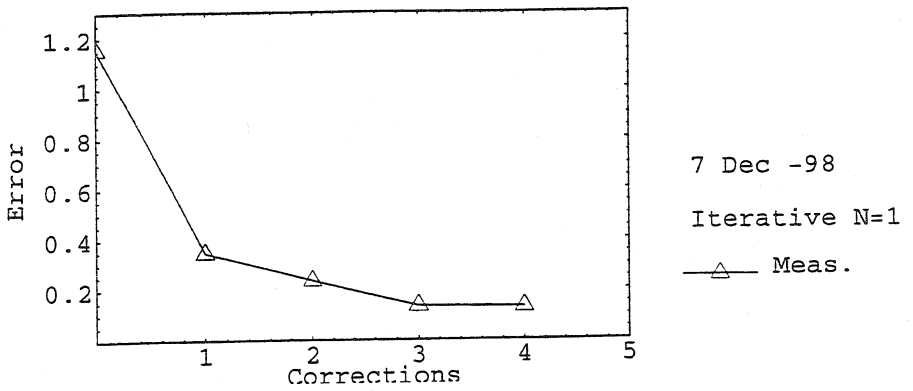

Fig. 6: The measured correction result and the *MICADO* prediction for a random initial error are shown as a function of the number of correctors used.

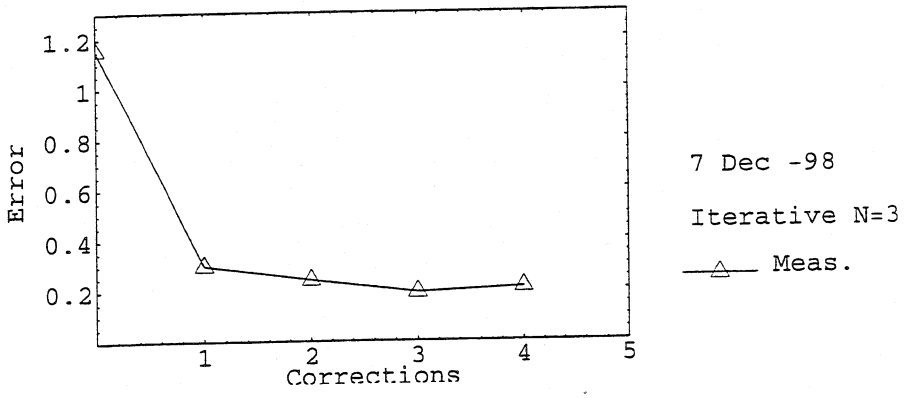

Fig. 7: The measured correction result and the *MICADO* prediction for a random initial error are shown as a function of the number of correctors used.

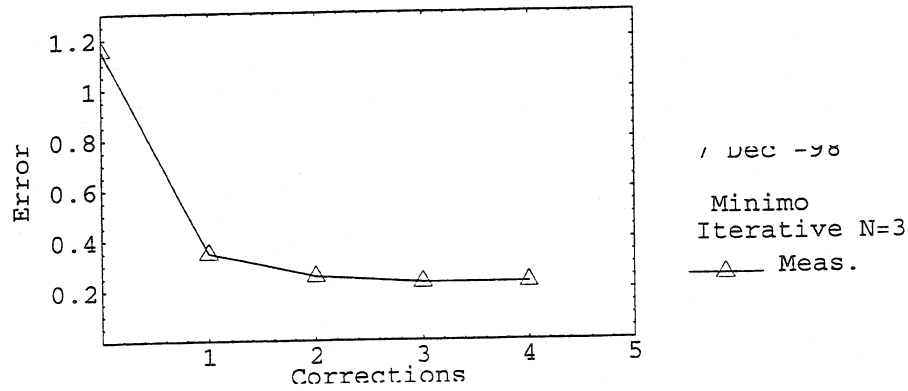

Fig. 8: The measured correction result and the *MINIMO* prediction for a random initial error are shown as a function of the number of correctors used.

8. Conclusions

We have found that both *MICADO* and *MINIMO* works well for combined dispersion and betatron matching, using the correction matrix derived in this note. A comparison between the two algorithms, show no major advantage of using *MINIMO* for this kind of correction, and since *MICADO* is faster it should be natural to choose this algorithm.

References

[1] P. J. Bryant, K. Johnsen, "Circular Accelerators and Storage Rings", (Cambridge University Press, NY, 1993).

[2] B. Autin, C. Carli, T. D'Amico, O. Gröbner, M. Martini and E. Wildner, "*BeamOptics* A Program for Analytical Beam Optics", *CERN* **98-06** (1998).

[3] D. A. Edwards, M. J. Syphers, "An introduction to the phisics of high energy accelerators", (John Wiley & Sons, NY, 1993).

[4] E. Keil, Y. Marti, B. W. Montague, A. Sudbø, "AGS, the ISR computer Program for Synchrotron Design, Orbit analysis and Insertion Matching", *CERN* **75-13** (1975).

[5] B. Autin, Y. Marti, "Closed orbit correction of alternating gradient machines using a small number of magnets", *CERN ISR-MA* **73-17** (1973).

[6] T. Risselada, "An improved version of the orbit correction program ORBCOR", *CERN PS (PSR)* **87-90** (1990).

[7] S. Wolfram, "Mathematica, a system for doing mathematics by computer", (Addison-Wesley, NY, 1993).

[8] G. Arduini, M. Giovannozzi, K. Hanke, J.-Y. Hémery, M. Martini, " *MAD* and *BeamOptics* Description of the TT2/TT10 Transfer Line - Part I: Optics without Emittance Exchange Insertion", *CERN PS Note (CA)* **98-014** and *CERN SL Note (OP)* **98-040** (1998).

Paper V

A comparative study of profile and scraping methods for emittance measurements in the PS Booster

submitted to Particle Accelerators.

A COMPARATIVE STUDY OF PROFILE AND SCRAPING METHODS FOR EMITTANCE MEASUREMENTS IN THE PS BOOSTER

C. CARLI, A. JANSSON, M. LINDROOS*, H. SCHÖNAUER

CERN, Geneva, Switzerland

It is important to have a clear understanding of the transverse emittance in a circular accelerator in order to achieve optimum brilliance. Experience from comparing emittance data from different instruments has shown that systematic errors can be important. In an attempt to detect such errors in the PS Booster the emittance measurements are done according to two different principles: measurement of density distribution and measurement of amplitude distribution. In this paper we i) discuss these two principles and the theory behind them; ii) show how the data can be compared; iii) describe the instrumentation used for these measurements; and iv) present results for typical PS Booster beams.

KEY WORDS: Detectors, Instrumentation

1 INTRODUCTION

In an injector chain consisting of several accelerators and transfer lines, the emittance and the beam optical parameters have to be known to a high degree of precision to prevent transverse beam dilution at beam transfer. In day-to-day operation only the emittance is monitored as any mismatch of optical parameters necessarily will result in an emittance increase. However, experience has shown that systematic errors associated with the instrument and the principle according to which it works make it difficult to compare emittance data, in particular from different machines. In an attempt to unveil systematic errors in the PS Booster instrumentation, the emittance measurements are made according to two different principles: measurement of density distribution ("profile") and measurement of amplitude distribution ("scraping")[1]. The amplitude distribution can be compared to the transverse profile data using an Abel transform.

* Corresponding Author. E-mail: Mats.Lindroos@cern.ch.

In this paper these two principles and the theory behind them are discussed. Furthermore, the instrumentation used for these measurements is presented together with some results for typical PS Booster beams.

2 MEASUREMENT OF AMPLITUDE DISTRIBUTION

2.1 Introduction

Scraping the circulating beam is a conceptually simple method to obtain the distribution of the betatron amplitudes $n(a)$ in a transverse plane. An aperture limitation is moved into the beam (or the beam is moved towards an obstacle) and the resulting relative beam loss is recorded. This can be done on consecutive machine cycles with different positions or by a fast-moving interceptor in the same cycle. One immediately obtains a set of values of the function

$$N(a) = \int_{-\infty}^{a} n(a')da' \tag{1}$$

if one knows the position of the beam centre, i.e. the closed orbit at the location of the aperture limitation. This is one of the practical difficulties of this approach, which is frequently circumvented by consecutive scraping from both sides to determine the centre. Numerical differentiation yields the wanted function $n(a)$. Measurements in a plane with finite dispersion yield a distribution which is a convolution of both betatron amplitude and momentum distributions. In order to obtain the true betatron amplitude distribution, one needs to know the detailed momentum distribution for unfolding. The second moments, $\sigma_a^2 = \int a'^2 n(a')da'$ and $\sigma^2_{\text{scraped}}$ of the measured distribution, however, obey the simple law

$$\sigma^2_{\text{scraped}} = \sigma_a^2 + \sigma_p^2 \tag{2}$$

i.e., the calculation of σ_a^2 requires only the knowledge of the variance

$$\sigma_p^2 = D^2 \int (\Delta p/p)^2 n_p(\Delta p/p) d(\Delta p/p)$$

of the momentum dispersion. In order to obtain the projected density, one would need to apply an Abel type transform. However, the projected density itself is of little interest as it shows less detail and conveys less physical insight than the amplitude distribution. Thus it suffices to know the variance of the amplitude distribution to compare emittance measurements from a scraping method with those from a device measuring the projected density, which is simply

$$\sigma_\beta^2 = \sigma_a^2/2 \tag{3}$$

2.2 *Resolution of Scraping Methods*

All particles of a given betatron amplitude are located on a circle in normalised phase space. An intercepting obstacle penetrating by an increment d per turn into this circle, cuts arc segments. At simple fractional tunes, corresponding to resonances like 1/2, 1/3, etc., these segments superpose exactly, and one realises immediately, that it takes many turns to scrape the whole circle away. This is of minor importance as the particles locked in low-order resonances would be unstable anyway. But even at irrational fractional tunes, complete scraping takes a certain number of turns, n_{scraped}, depending on the amplitude a and the increment d. A detailed account of the resolution limit and the following approximation for n_{scraped} can be found in Schönauer et al. [2], where it is shown that n_{scraped} can be written as

$$n_{\text{scraped}} = \frac{1}{2}\left(\frac{9\pi^2 a}{d}\right)^{1/3} \tag{4}$$

To give an example, for a target speed of 6 μm/turn, the particles of amplitude 5 mm appear smeared out over 0.125 mm or 2.5% of their amplitude. For beams of this size, scraping speeds of the order of $3-6\,\mu$m/turn are thus a good compromise between the duration of the measurement and its intrinsic accuracy limits.

2.3 *The BeamScope*

The full name behind the acronym, "BEtatron AMplitude Scraping by Closed-Orbit PErturbation"[3], describes the principle, which is illustrated in Fig. 1. A local orbit bump, produced by three pulsed dipoles, drives the beam progressively into a fixed aperture limitation, while the beam current and its numerically or electronically produced derivative are recorded by sampling-ADCs, together with the shunt signals of the bumper dipoles. The amplitude distribution can then be calculated from these signals. A typical output from the BeamScope in the PS booster can be seen in Fig. 2.

For a machine like the PS booster with its four rings, this was a more economic solution than moving an aperture limitation into the beam, since the (orbit correction) dipoles were already installed and only three multiplexed bumper power supplies were required. The price to pay is, however, an elaborate processing of the dipole signals in order to get the beam orbit position as precisely as possible. The processing includes, beyond the usual calibrations, a representation of the bench-measured magnetisation curves of the 24 correction dipoles involved, and a lattice code using the off-line measured and stored individual coherent tunes. Corrections for eddy current effects and electronic delays also have to be included.

The instrument displays the betatron amplitude distribution, the so-called 95% amplitude emittances and the emittance of the projected distribution. Projections are found by Abel transforms in the vertical plane and by polynomial fits in the horizontal plane, where the Abel transform is not directly applicable because of the

effect of dispersion[4]. The latter entails a change in the circumference of the closed orbit due to the bump, which induces a counter-reaction from the radio frequency system that interferes with the measurement in a non-reproducible and fluctuating way.

A crucial issue is the determination of the beam centre. Looking at the derivative of the recorded beam current, called the raw profile (see Fig. 3), the final collapse of this signal indicates that the beam centre has been scraped and all particles are lost. For the reasonable assumption of a locally uniform phase space density in the vicinity of the origin, the final slope of the derivative should theoretically be constant, with a sharp discontinuity at zero amplitude. The round-off and tails observed in reality stem from non-vanishing dispersion, limited electronic bandwidth and finite resolution. Putting a tangent on the turning point of the slope, its foot point represents the beams centre of a bunched beam even with finite dispersion and constitutes a good approximation for the other cases.

2.4 The "Beam Guillotine"

A fast mechanical scraper named "Beam Guillotine" has been built at TRIUMF for the PS Booster. This device will cross the aperture at speeds up to 10 m/s and will produce amplitude distributions directly, avoiding many of the complications of the BeamScope. The "Beam Guillotine" is scheduled for installation in spring 2000.

3 MEASUREMENT OF DENSITY DISTRIBUTION

3.1 Introduction

Several instruments measure the beam profile in real space, rather than the phase space particle density. These are instruments like secondary emission monitors, screens, wire-scanners and ionisation monitors. All these methods measure the density distribution, but differ widely in other respects, such as the spatial resolution.

The natural emittance definitions to use with these measurement methods are the σ-emittances, defined as

$$\epsilon_{x,1\sigma} = \frac{\sigma_\beta^2}{\beta_x} \tag{5}$$

and

$$\epsilon_{x,2\sigma} = \frac{4\sigma_\beta^2}{\beta_x}, \tag{6}$$

in terms of the standard deviation σ_β of the betatronic beam width and the optics parameter β_x. It might seem strange to have two definitions differing only by a

fixed factor, but historically the 1σ emittance has been used for electron machines and the 2σ emittance for proton machines. The 2σ emittance is used in this paper.

The parameter which should be derived from the measured profile in order to deduce the emittance is the RMS beam width σ_{profile}. If the resolution of the measurement is high enough the discrete statistical formula

$$\sigma^2_{\text{profile}} = \left(\sum_i x_i^2 \rho_i \Big/ \sum_k \rho_k \right) - \left(\sum_j x_j \rho_j \Big/ \sum_k \rho_k \right)^2 \tag{7}$$

can be used. However, the profiles are often noisy, and even small tails can falsify the result due to the high weight they are given in the formula. Therefore, some kind of extra data treatment is often necessary. This will involve suppression of baseline and obviously erroneous data points and/or the fitting of a curve to the data. One should bear in mind that it is very easy to falsify the results by using very elaborate fitting schemes, and the fitting should therefore preferably be based on simple physical principles.

The most commonly used fit function is a Gaussian curve. A Gaussian fit reduces the N measured points to three or four parameters (mean position, width, baseline and maybe slope of baseline) and is therefore very over-constrained. This reduces the influence of noise on the profiles.

A spline interpolation on the other hand is under-constrained. For example, a cubic spline interpolation on N data points has $3N$ free parameters but only $3N - 4$ constraints. Thus, a spline fits any data set perfectly. It is therefore not useful for suppressing noise in the profiles. An approximate spline fit, where the perfect fit to the data points is traded for a small second derivative, is used for the Booster secondary emission monitors. The fitting routine has a free parameter which gives the relative weight between second derivative and the fit error. It has been found that the beam width resulting from the fit is very dependent on the parameter choice, especially in the case of small profiles.

An alternative way to get around the problem with noisy tails is to use Koziol's method[5], where the discrete statistical formula is used only on the core of the distribution, and the truncated result is corrected assuming e.g. Gaussian tails. The core is defined as the part of the profile where the signal is larger than a certain cut-off, which is a free parameter.

Whenever the discrete statistical formula is used, missing data points have to be accounted for. This can be done by replacing the missing point with an interpolation based on the surrounding points.

As in the case of scraping methods, the dispersive effects have to be accounted for. In the presence of dispersion, the physical beam profile is not only given by the betatron amplitude distribution, but has an extra contribution due to the

momentum spread σ_p of the beam.

$$\sigma^2_{\text{profile}} = \sigma^2_\beta + \sigma^2_p \tag{8}$$

where σ_p is the dispersive spread and σ_β is the pure betatronic width of the beam. The formula can easily be inverted to calculate the betatronic width from the measured width, but it is obvious that if the dispersive term is large, it is important to measure this with the same accuracy as the beam width in order to get an accurate final result.

3.2 Wire Scanner

The fast wire scanner method for measuring beam profiles is based on the simple fact that an energetic particle beam passing any obstacle, which in this case is a thin carbon wire, will cause secondary emission and a secondary particle shower which is proportional to the primary beam intensity at the wire location. The beam profile is either recorded by detecting the secondary particles or by measuring the generated current as a function of the wire position. In a circular accelerator, such as the PS Booster, the wire is swept fast (> 10 m/s) through the circulating beam and consequently the recorded beam profile is the sum of all bunch profiles over many turns. Evidently it is important that the closed orbit and the local Twiss β-value stays constant through the duration of the sweep. A detailed discussion of the fast wire scanners in low energy accelerators can be found in Elmfors et al.[6]. The main results are summarised here for convenience.

The geometry of the PS Booster wire scanners are shown in Fig. 4. The figure depicts an instant in the process of the wire sweeping through the beam. The wire scanner mechanism consists of three parts: i) an electric motor with a crankshaft and a connecting rod, ii) a push- pull device connecting the motor via bellows to the fork inside the vacuum and iii) the U- shaped fork with the wire strung between the prongs. A decoder is connected to the motor, measuring its angular position from which the linear position of the wire is derived by geometrical considerations. The spatial resolution is much greater than that of secondary emission monitors due to a high sampling rate for the resolver (< 0.1 mm). The beam density can either be obtained through secondary emission from the wire (SE mode), or by observation of secondary particles with a scintillation detector (scintillator mode). Again, the baseline is determined and the variance extracted from the profile.

At very low energies, problems can be encountered using the scintillator mode as the secondary particles produced are few and have low energy. Since the detector is positioned outside the wire scanner vacuum chamber, low energy particles are filtered out by the chamber wall. In Fig. 5 the total number of detected particles is plotted against energy. At approximately 150 MeV a sudden decrease in the number of particles can be observed. This corresponds to the threshold for pion production.

If the physical beam size is of the order of tens of millimetres, which is common in low-energy synchrotrons, several difficulties are encountered detecting the secondary particles. Firstly, the big change in angle between the detector and the wire during such a long sweep will falsify the deduced beam profile as the secondary particle shower is highly anisotropic [6]. Secondly, at very large angles, the solid angle covered by the detector can change to such an extent that that an additional deformation of the beam profile is acquired. A simple way of avoiding these geometrical problems is to use the SE mode rather than the scintillator mode. In Fig. 6 the profiles measured with a wire scanner at 50 MeV in the PS Booster with 4×10^{12} protons can be seen. The lower profile is from the scintillator and the upper one from the SE mode. The measurements were made on consecutive machine cycles. The asymmetry caused by the geometrical effects discussed above in the case of secondary particle detection are clearly visible.

The emittance of the beam will increase due to the passage of the wire. To calculate this increase, the wire is pictured as a virtual foil, the thickness of which depends on the velocity and shape of the wire and the velocity of the beam. For the case of a wire with a circular cross section in a synchrotron with a revolution time of τ_0 (at $\beta_L = 1$) the virtual foil thickness (vft) can be written as

$$z_{\mathrm{vft}} = \frac{(2r)^2 \pi \beta_L}{4 v \tau_0} \quad . \tag{9}$$

Consequently, the emittance blow up due to the wire scanner device can be evaluated using the the well-known formula [7]

$$\epsilon = \epsilon_0 + \Delta\epsilon = \epsilon_0 + \frac{\pi}{2} \beta_T \langle \theta^2 \rangle. \tag{10}$$

Here ϵ_0 is the initial emittance and β_T the Twiss value at the wire scanner position. The average square scattering angle will depend on the characteristics of the foil and the beam and is usually derived using formulas based on the Molière theory for multiple Coulomb scattering [8]. For small deflection angles a good approximation for the average root mean square scattering angle is given by [9, 10]

$$\theta_0 = \frac{13.6 \text{ MeV}}{\beta p c} Q \sqrt{\frac{z}{X_0}} \left(1 + 0.038 \ln \left(\frac{z}{X_0} \right) \right), \tag{11}$$

where $p, \beta_L c$ and Q are momentum, velocity and charge number of the incident particles and $\frac{z}{X_0}$ is the thickness of the scattering medium in radiation lengths (z being the coordinate along the beam-line). However, the formula is only accurate to about 11% or better for $1 \times 10^{-3} < \frac{z}{X_0} < 100$. For a typical wire scanner with z_{vft} according to Eq. (9), $\frac{z_{\mathrm{vft}}}{X_0}$ is much smaller than 1×10^{-3}. Consequently, we are for the PS Booster wire scanners left in a situation in between single Coulomb scattering and multiple scattering. However, we can use the multiple scattering approximation to get an upper limit for the blow-up. Typically in the PS booster at 50 MeV the upper limit is a few π mm mrad of emittance increase. This is to be compared to typically 100 π mm mrad of physical beam emittance at this

energy. Already at 300 MeV, the blow-up is insignificant compared to other sources of errors in the measurement.

3.3 Secondary Emission Monitors

Secondary Emission Monitors (SEM) are destructive or semi-destructive depending on the beam energy. They can either be made of thin ribbons (grid) or thin wires (harp). They are usually used in groups of three for emittance measurement purposes. In this way they can provide three independent measurements of the beam width. The optimum positioning is such that the phase advance is 60° between the individual grids. The measured widths are related to the emittance by

$$\sigma_\beta = \sqrt{\epsilon\beta_i}, \qquad i = 1, 2, 3 \tag{12}$$

where the relations between the β_is can be derived from the transfer matrix T_{ij} between the grids, knowing that the Courant-Snyder invariant

$$A = \beta x'^2 + 2\alpha x x' + \gamma x^2 \tag{13}$$

is a conserved quantity. From these equations, the emittance and Twiss parameters can be derived. If the grids are separated only by drifts, the transfer matrix is unambiguously known, and one can expect a relatively high accuracy limited only by the accuracy of the width measurement. In cases where magnets are present between the monitors, there will be an extra error contribution due to the limited accuracy in the knowledge of the transfer matrix.

It should be stressed that any coupling between the transverse phase planes before or in between the SEM-grids will render this kind of measurement meaningless. Coupling introduces a correlation between the phase planes, which will make it impossible to extract the emittance from three width measurements.

The emittance can in principle be measured using only one SEM-grid or harp, if the preceding optics can be changed sufficiently in order to produce at least three independent width measurements.

If more than three harps are available, the extra data can be used either to make a χ^2-fit and get an error estimation, or to derive[12] the additional parameters D, D' and $\Delta p/p$ directly from the profiles instead of measuring them separately. This is, however, only possible if there is at least one bending magnet between the monitors, since otherwise the measurements are not independent. The accuracy that can be expected in measuring the dispersion in this way is naturally lower than in a direct measurement when the beam energy is changed, but it can still be an interesting alternative, for example when the energy cannot be easily changed.

4 THE ABEL TRANSFORM

When one wishes to compare not only the emittances, obtained with scraping methods and profile measurements, but also the detailed shape of the distribution, one has to transform the amplitude distribution into a profile or vice versa. The difference between two particle distributions is more clearly visible in amplitude distributions - profiles tend to be smoother than the underlying densities in phase space or oscillation amplitudes and thus differences are more difficult to visualise.

To compare the shape of the distributions resulting from the two measurement methods, a profile has to be converted to an amplitude density by means of the Abel type integral transformation[13, 14]:

$$\rho(A) = -2\frac{d}{dA}\int_A^R d\eta \frac{g(\eta)\,\eta}{\sqrt{\eta^2 - A^2}} = -2A\int_A^R d\eta \frac{g'(\eta)}{\sqrt{\eta^2 - A^2}} \qquad (14)$$

where ρ means the density in normalised amplitudes $A = a/\sqrt{\beta}$ and g is the profile in normalised $\eta = x/\sqrt{\beta}$.

One should note, that the Equation 14 only applies, if the measured profile is exclusively determined by the transverse betatron motion of the beam particles. If there is dispersion - which is not the case for the application of the formula in Section 5.1, because the vertical phase space is investigated - the profile is modified due to a contribution from the momentum uncertainty and the above Abel type transform will not give a correct result[a].

5 MEASUREMENTS

The final emittances of the proton beams at CERN are determined by the multiturn injection process in the PS Booster. As emittance control is of primordial importance for future LHC performance, the measurement of the emittances of the PS Booster beam prior to extraction must be possible with an adequate accuracy and confidence in the measurement device. Confidence can only be established if comparisons of measurements can be made with different devices, preferably of different type to avoid systematic shortcomings of a particular method. Their results should agree to the wanted accuracy, or differences should at least be explained in order to apply the appropriate corrections during data processing. Comparisons should extend over all the available range of beam emittances and intensities.

In the PS Booster, wire scanners have been chosen as the future main instrument for operational emittance measurements. A prototype wire scanner, installed for

[a] However, if the momentum distribution is known and uncorrelated with the transverse phase, one could still apply formula 14 to the profile after unfolding the contribution due to momentum width.

vertical measurements, has been compared with the existing BeamScope and, for measurement at extraction energy, with a triplet of SEM grids in the dedicated measurement beam line.

Results for intensity scans at 1 GeV (PS Booster extraction energy in 1998) and at 200 MeV (roughly the lower limit for quantitative wire scanner measurements) are presented in Fig. 7 and Fig. 8, respectively. The general trend that wire scanner emittances are larger than those measured with BeamScope would be expected at 200 MeV, because the evaluation of the variance is extended over the whole wire scanner profile, which is asymmetric due to multiple scattering in the wire (cf. Fig. 9). This argument fails at 1 GeV (cf. Fig. 10) where the emittances obtained with the two instruments differ even more. Part, but certainly not all of the difference could be explained by deviations of the local beta function from its theoretical value. In fact, such an error at the location of the BeamScope precision aperture should be detected and compensated by the calibration by aperture re-computation possible with BeamScope[2].

Wire scanner measurements at 50 MeV, the injection energy of the PS Booster, should not be compared directly with BeamScope. Multiple scattering is so pronounced at this energy that there is considerable emittance blow-up during the passage of the wire. Those particles that have gained large amplitudes will be hit again when the wire moves out from the centre and will attain even larger amplitudes until they eventually hit the walls. This loss is indeed observed and clearly visible in Fig. 11. This mechanism, by which the particles with a large amplitude are removed by the outgoing wire explains that a subsequent BeamScope measurement on the same beam pulse will not "see" them and shows only a modest blow-up as in Table 2. Depending on the beam size and the scanning speed there might even be an apparent emittance reduction after the wire has passed. The wire scanner however measures these particles before they are lost and thus records very large emittances. At this energy the very noisy and highly anisotropic scintillator signal, see Fig. 6, gives unreliable results.

Fig. 12 shows an interesting application of the wire scanner. It is very simple to track the normalised emittance through an acceleration cycle. It reveals a linear emittance blow-up of a high-intensity beam during the early acceleration which is absent at low intensities. A series of BeamScope measurements (not exactly on the same beam) confirmed this fact.

5.1 Comparisons of Amplitude Densities

The detailed shape of the amplitude densities measured directly with the BeamScope and the one obtained applying an Abel type integral transform to a profile measured with a wire scanner are compared in Fig. 9 and Fig. 10. Since the Twiss β function is not the same at the location of the two devices, the amplitudes (and positions of the profile) are given in normalised space, i.e. the amplitude divided by the square root of the β function is plotted rather than the amplitude.

The measured data points of the profile are smoothed applying a Savitzky-Golay filter (of order 3, taking typically 20 to 40 points on either side) and then interpolated by a spline of order 3.

Since the Abel assumes rotational symmetry in normalised phase space, the profile should ideally be symmetric around the beam centre. In reality the two half-profiles are slightly different. Both half-profiles can be introduced into Equation 14, giving two approximations of the amplitude distributions.

The limits of the half-profile are defined by the beam centre and the closest point where the signal has fallen below a certain threshold.

On of the reasons why the profiles is not exactly symmetric is scattering in the wire. The leading edge of the profile, which is passed first is not yet affected by the scattering and thus generally steeper resulting in a steeper fall-off of the amplitude density. The amplitude distribution computed with the second half profile has a fall-off which is less sharp than the one of the original distribution.

In Fig. 9 amplitude densities are compared at 200 MeV. The profile obtained applying the Abel type transform to the first half profile (solid curve with the steeper fall-off) agrees well with the BeamScope measurement (dashed curve). Both vary significantly from a Gaussian beam, which is plotted as a dot-dashed line for comparison. It is typical for the PS Booster that the amplitude distribution is close to constant in the centre of the beam and falls off rapidly at the edge. If the Abel type transform is applied to the second half profile (solid curve with flatter fall-off) scattering systematically alters the result.

In Fig. 10 the amplitude densities obtained from a wire scanner profile measurement via the Abel transform is compared with the direct measurement by the BeamScope for a beam of 1 GeV. At higher energies the blow-up and the smoothing of the profile due to scattering is less important. Thus it is not surprising that the amplitude distribution obtained with the second half-profile also agrees well with the BeamScope result.

6 CONCLUSIONS

Although the BeamScope and the wire scanner agree well for small LHC-type beams, where confidence in the measurements is most important, the differences for larger emittances raises doubts. At the time of writing there is no convincing explanation for the observed systematic divergence, which makes it particularly difficult to determine which of the two devices gives the more accurate result. The SEM grid results equally plotted in Fig. 7 are not trustworthy. Due to the large step of the grid, the applied spline fit turns out to be strongly dependent on the fitting parameters. In fact, a subsequent comparison study revealed that a Gaussian fit yields better results, despite the fact that the real betatron amplitude distribution is far from Gaussian (see Fig. 10).

With the installation of wire scanners in the PS Booster the emittance in the LHC injector chain can be measured in all machines, including the LINAC, using profile methods, which allows direct comparisons. The role of the scraping methods will be detailed studies of e.g. amplitude distributions, in particular at the lowest energies and calibration of the profile devices. The SEM-grids in the PS Booster measurement line will be replaced by wire harps with smaller wire spacing. This should allow reliable profile measurements even for the small emittance LHC beam. The use of wire scanners in lower energy machines, like the PS Booster, is new. This has been made possible by the mechanical improvements of the instrument, the use of multi-fibre carbon wires and careful calibration of the wire movement. The use of the SEM-current for signal detection has proved superior, providing better signal quality and less dependence on secondary particle cascade anisotropy.

ACKNOWLEDGEMENTS

We would like to thank all our colleagues at the PS Division for their support, in particular C. Carter, H. Koziol, J-M. Nonglaton, J. Olsfors and U. Raich.

REFERENCES

1. M.Arruat, C.Carli, H.Koziol, M.Lindroos, J.Olsfors, U.Raich, H.Schönauer, "A Comparative Study of Fats Wire Scanners, BeamScope and SEM-Grids for Emittance Measurements at the PS Booster", Proc. 3rd DIPAC, Frascati (Rome), p. 129, 1997
2. H. Schönauer, "Beamscope: Physics considerations, implementation and results of tests", CERN internal note: CERN/PS/BR/82-2
3. H.Schönauer, "Beamscope – a Novel Device for Measuring Emittances and Betatron Amplitude Distributions", IEEE Trans. Nucl.Sci. NS-26, p. 3294, 1979
4. M.Martini, H.Schönauer, "Methods to Compare and to Obtain Representative Emittance Values from Fundamentally Different Measurement Devices", Proc. 1st DIPAC, Montreux, p. 146, 1993.
5. H.Koziol, "Evaluation of Near-Gaussian Distributions with Ill-Defined Tails", Note: MP-3-74-1
6. P.Elmfors, A.Fasso, M.Huhtinen, M.Lindroos, J.Olsfors and U.Raich, "Wire scanners in Low energy accelerators", Nuclear Instruments and Methods in Physics Research A396 (1997) 13-22
7. P. J. Bryant, "Beam transfer lines" in: Proceedings of the CERN Accelerator school, Fifth general accelerator physics course, Editor: S. Turner, Jyväskylä, Finland, 1992.
8. H. A. Bethe, Phys. Rev. **89**, 1256 (1953).
9. V. L. Highland, Nucl. Instr. and Meth. **129**, 497 (1979).
10. G.R. Lynch and O.I. Dahl, Nucl. Instr. and Meth. **B58**, 6 (1991).
11. P.L.Walden, "Meson Production Reactions by p, d, ? ... on Nuclei", Nuclear Physics A 374, p.277, 1982.
12. G.Arduini, M.Giovannozzi, D.Manglunki, M.Martini, "Multigrid Measurements in a Transfer Line", CERN internal note: CERN/PS/DI/Note 98-03
13. P.W. Krempl, "The Abel-type Integral Transformation with the Kernel $(t^2 - x^2)^{-1/2}$ and its Application to Density Distributions of Particle Beams", CERN internal note: CERN - Note MPS/Int. BR/74-1

14. C. Carli, M. Lindroos and H. Schönauer, "Comparision of amplitude Profiles from BeamScope and Wire Scanner measurements for the vertical Plane in the PSB", CERN internal note: PS/CA Note 99-11

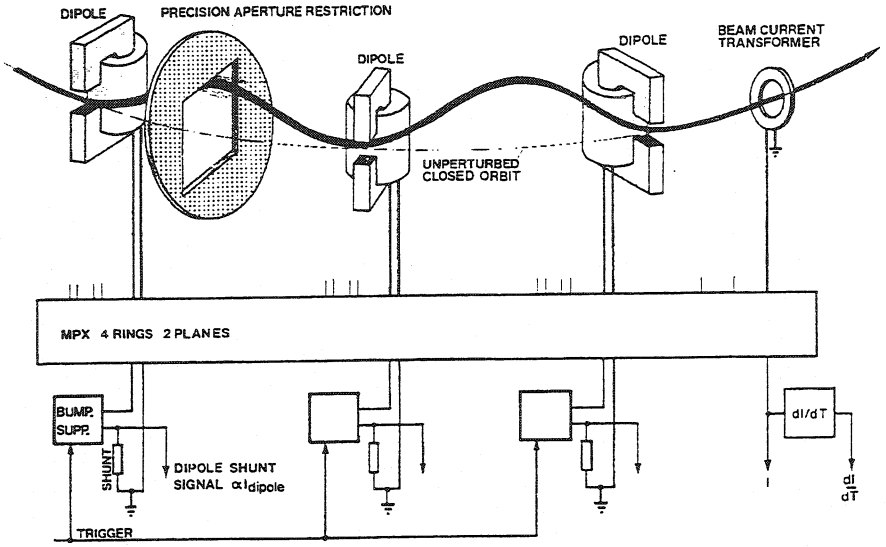

FIGURE 1: Artists view of the BeamScope.

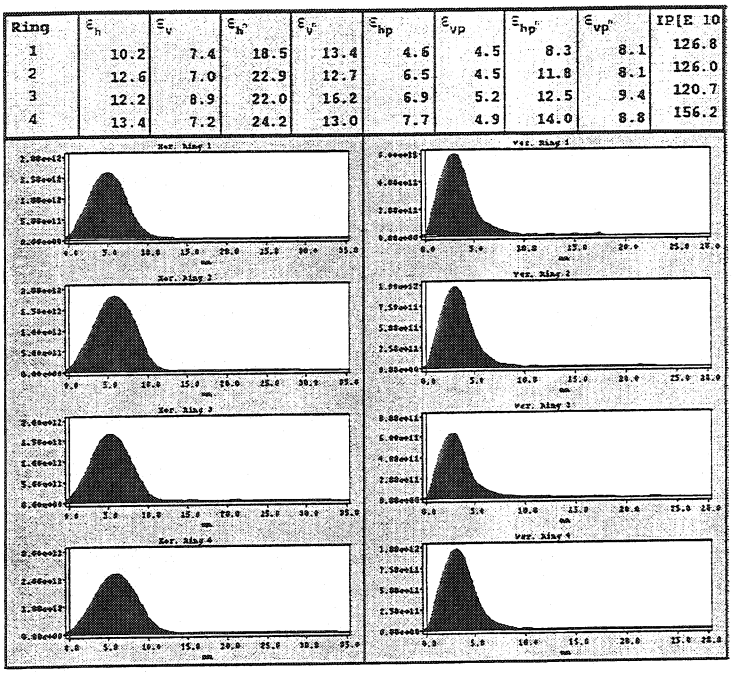

Ring	ϵ_h	ϵ_v	ϵ_h^n	ϵ_v^n	ϵ_{hp}	ϵ_{vp}	ϵ_{hp}^n	ϵ_{vp}^n	IP[E 10
1	10.2	7.4	18.5	13.4	4.6	4.5	8.3	8.1	126.8
2	12.6	7.0	22.9	12.7	6.5	4.5	11.8	8.1	126.0
3	12.2	8.9	22.0	16.2	6.9	5.2	12.5	9.4	120.7
4	13.4	7.2	24.2	13.0	7.7	4.9	14.0	8.8	156.2

FIGURE 2: BeamScope Measurements on a LHC type beam in all four PS Booster rings. $\epsilon_{h,v}$ denote the emittances encompassing 95% of the scraped amplitudes, subscript p the 2σ emittances of the projected profiles, $n$indicates normalised values.

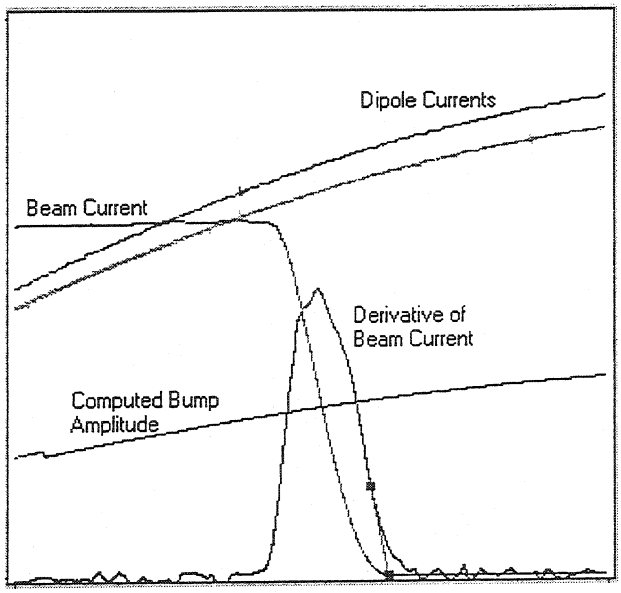

FIGURE 3: The five raw signals used by BeamScope: the shunt signals from the three bumper dipoles (two of them are equal and appear as a single trace), the beam current and its electronically produced derivative. Also displayed is the computed bump amplitude. Its discontinuity indicates the numerical delay applied to this signal to compensate for the real delay due to eddy currents in the vacuum chamber. One may also notice the noise on the raw signals. While the high-frequency component can be easily smoothed out, the lower frequency perturbations of the derivative present a problem and can compromise the tangent fit, which is always shown for verification. The horizontal axis spans 6 ms and the vertical one 1024 bits, or 102.4 mm for the computed bump.

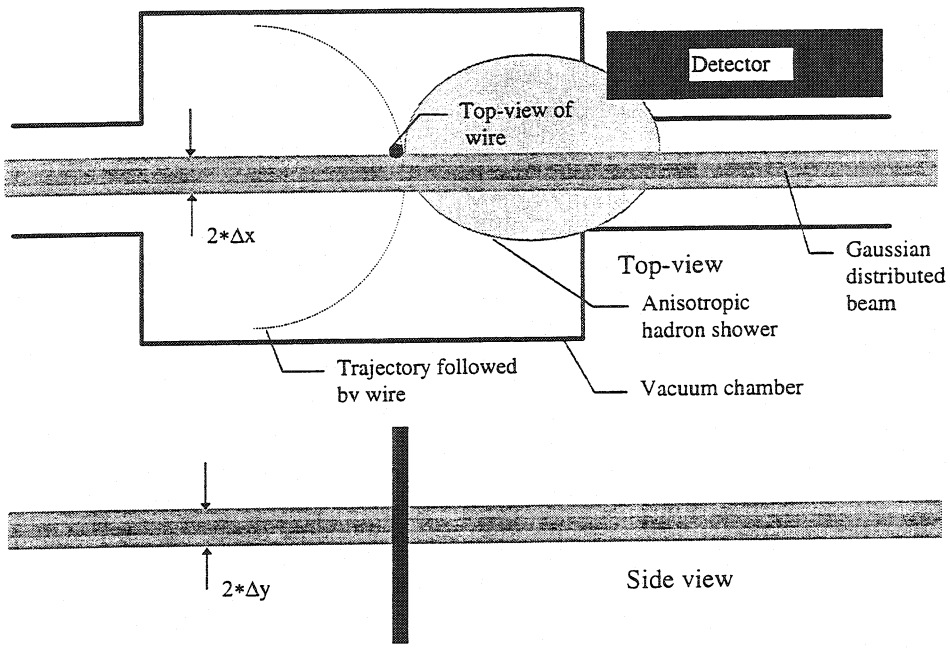

FIGURE 4: Geometry of beam and wire for a horizontal measurement ($\Delta x = 1\sigma_x$ and $\Delta y = \sigma_y$).

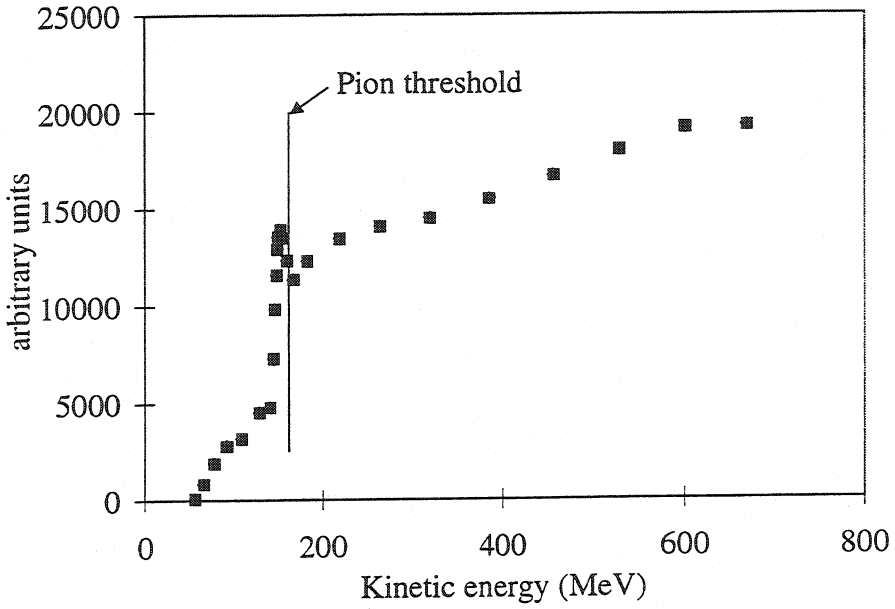

FIGURE 5: Integral over profile for constant photo-multiplier voltage, as a function of the beam energy. At 150 MeV the pion threshold is clearly visible. The peak in intensity just above this threshold is probably due to nuclear effects, see e.g. Walden[11]. All measurements were made with 5×10^{11} protons.

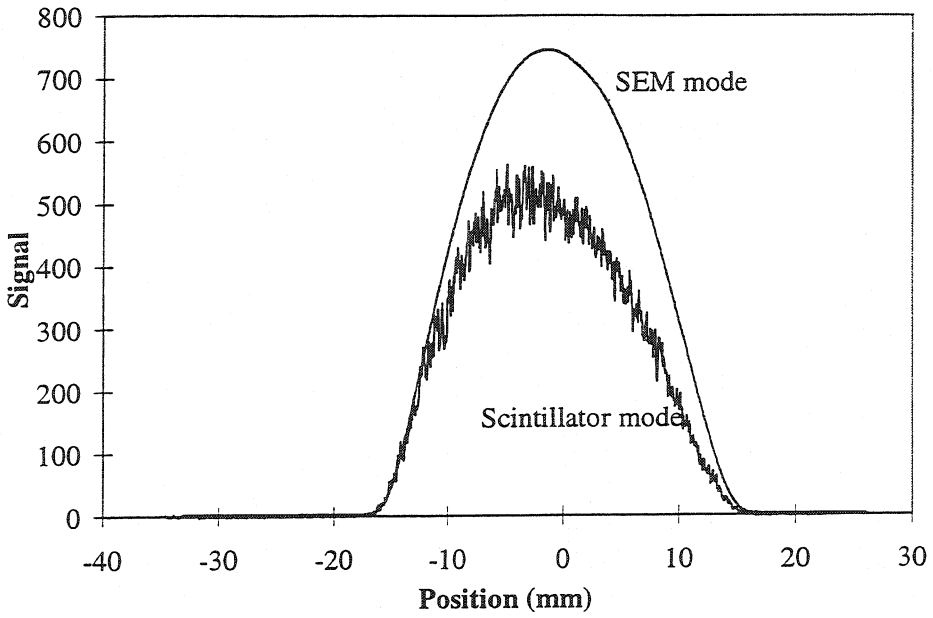

FIGURE 6: Profiles measured with the wire scanner at 50 MeV in the PS Booster with 4×10^{12} protons. The lower profile is from the scintillator signal and the upper one from the secondary electron emission. The measurements were made on consecutive machine cycles. It has been shown [6] that the asymmetry in the lower profile is mainly due to the asymmetric secondary particle shower combined with geometric effects in the detector-wire set-up. The contribution from multiple scattering is small compared to these effects.

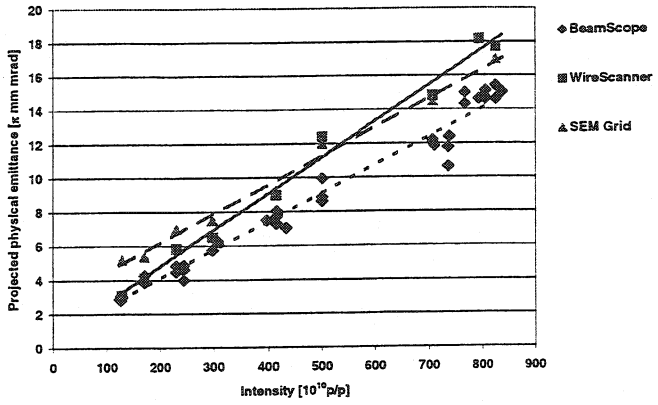

FIGURE 7: Emittance as a function of intensity at 1 GeV measured with the BeamScope, the Wire scanner and the SEM-grid.

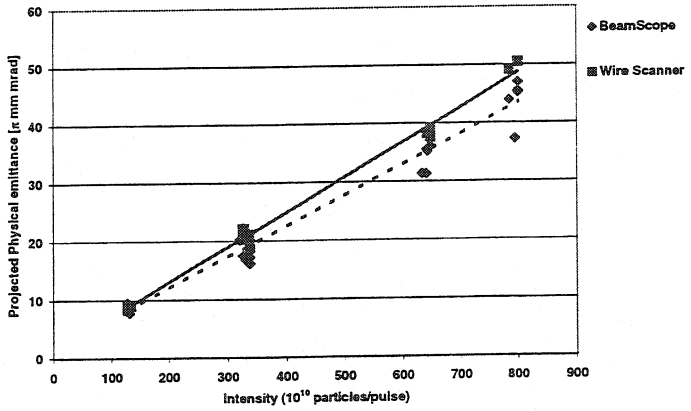

FIGURE 8: Emittance as a function of intensity at 200 MeV measured with the BeamScope and the Wire scanner.

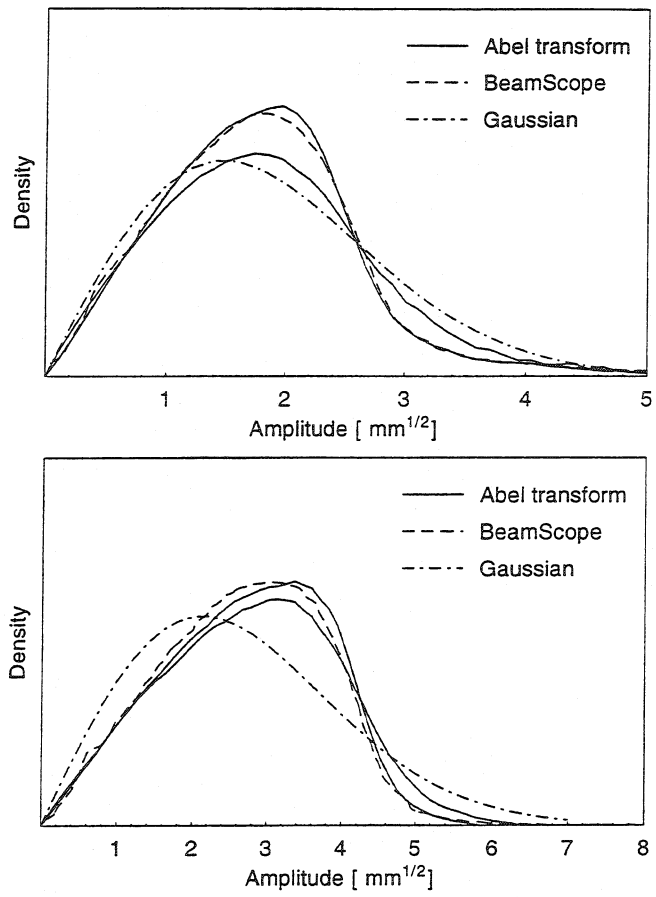

FIGURE 9: Comparisons of amplitude densities at a 200 MeV flat top. The solid lines are obtained from the wire scanner measurements via an Abel type transform using the two different half-profiles. The dashed lines are directly measured with the BeamScope. The dash-dot line shows the amplitude density for a Gaussian beam of approximately the same emittance. The upper figure is for a low intensity beam and the lower figure for a high intensity beam.

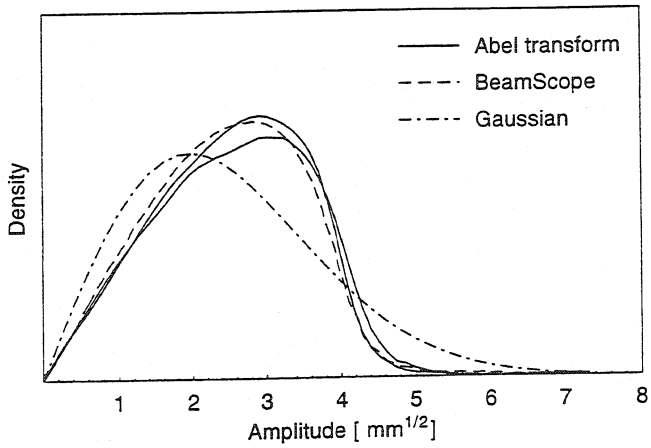

FIGURE 10: Comparison of amplitude densities at a 1 GeV flat top.

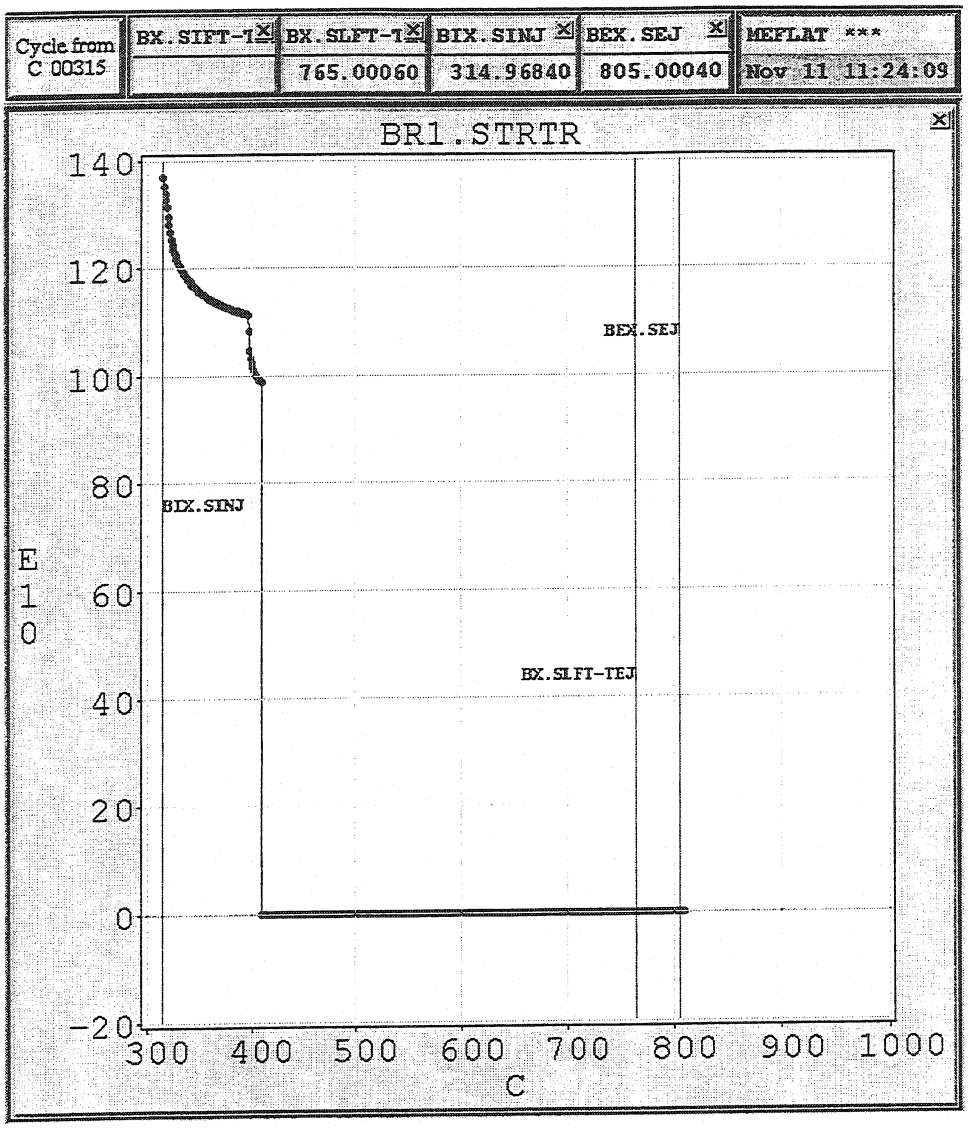

FIGURE 11: Screen capture of a beam current transformer measurement involving a wire scanner measurement (ϵ = 42.4 $\pi\, mm\, mrad$) followed by a BeamScope measurement (ϵ = 32.2 $\pi\, mm\, mrad$) at 50 MeV. On the x-axes the time in units of ms, starting at a fixed machine cycle reference point (called the 'C-train') is plotted and on the y-axes the intensity in units of 10^{10} *protons/pulse* is plotted. Observe that the wire scanner measurement at C=400 induces losses at 50 MeV. The sequential BeamScope measurement at C=415 is inheritly destructive.

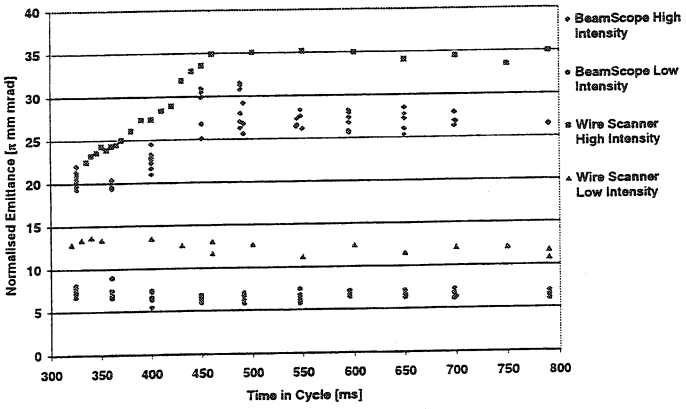

FIGURE 12: Emittance as a function of energy, at low and high intensity, measured with the BeamScope and the Wire scanner.

TABLE 1: Definitions of greek and roman symbols used in this paper

Symbol	Description	Definition
β_L	Relativistic β Lorentz factor	
γ_L	Relativistic γ Lorentz factor	
β	Lattice (Twiss) parameter	
α	Lattice (Twiss) parameter	
γ	Lattice (Twiss) parameter	
ϵ	Physical 2σ emittance	$(2\sigma)^2/\beta$
ϵ^*	Normalised 2σ emittance	$\beta_L\gamma_L\epsilon$
σ_β	One standard deviation of projected betatron distribution	
σ_a^2	Second moment of amplitude distribution	
σ_{profile}	One standard deviation of measured projected beam	
$\sigma^2_{\text{scraped}}$	Second moment of measured amplitude distribution	
ρ_i	Transverse beam distribution function at data point i	
θ	Average scattering angle	
c	velocity of light	
D	Transverse dispersion function	
n_p	Density function in $\delta p/p$	
$\delta p/p$	1σ momentum spread	
τ_0	Revolution time at $\beta_L = 0$	
Q	Charge state	
x_i	Physical position corresponding to data point i	
X_0	Radiation length	
z_{vft}	Equivalent foil thickness of a wire sweeping through the beam	

TABLE 2: Measurements of the projected physical beam emittance at 50 MeV with the BeamScope and the Wire scanner. The BeamScope measurement was either done on the next beam pulse or the same beam pulse. In the case that the measurements were done in the same pulse the BeamScope measurement was done after the wire scanner measurement. All the emittances in units of π mm mrad.

Wire scanner:		**BeamScope:**	
SEM signal	Scintillator signal	In next pulse	In the same pulse
42.9		27	
42.3		26	
42.4			32.2
41.1		26.7	
	38.7	26.2	
	40.8	26.3	
	37.6		28.4
	40.1		31.9